



**VYSOKÉ UČENÍ TECHNICKÉ V BRNĚ**

BRNO UNIVERSITY OF TECHNOLOGY

**FAKULTA STAVEBNÍ**

FACULTY OF CIVIL ENGINEERING

**ÚSTAV STAVEBNÍ MECHANIKY**

INSTITUTE OF STRUCTURAL MECHANICS

**NUMERICAL STUDY OF THIN HPC OVERLAY FOR  
ORTHOTROPIC BRIDGE DECK**

NUMERICAL STUDY OF THIN HPC OVERLAY FOR ORTHOTROPIC BRIDGE DECK

**DIPLOMOVÁ PRÁCE**

DIPLOMA THESIS

**AUTOR PRÁCE**

AUTHOR

**Bc. Petr Miarka**

**VEDOUCÍ PRÁCE**

SUPERVISOR

**doc. Ing. STANISLAV SEITL, Ph.D.**

**BRNO 2017**



# VYSOKÉ UČENÍ TECHNICKÉ V BRNĚ FAKULTA STAVEBNÍ

STUDIJNÍ PROGRAM	N3607 Stavební inženýrství
TYP STUDIJNÍHO PROGRAMU	Navazující magisterský studijní program s prezenční formou studia
STUDIJNÍ OBOR	3608T001 Pozemní stavby
PRACOVISŤE	Ústav stavební mechaniky

## ZADÁNÍ DIPLOMOVÉ PRÁCE

DIPLOMANT	<b>Bc. Petr Miarka</b>
NÁZEV	<b>Numerical study of thin HPC overlay for orthotropic bridge deck</b>
VEDOUCÍ DIPLOMOVÉ PRÁCE	doc. Ing. Stanislav Seitl, Ph.D.
DATUM ZADÁNÍ	30. 8. 2016
DATUM ODEVZDÁNÍ	13. 1. 2017

V Brně dne 30. 8. 2016

.....  
prof. Ing. Drahomír Novák, DrSc.  
Vedoucí ústavu

.....  
prof. Ing. Rostislav Drochytka, CSc., MBA  
Děkan Fakulty stavební VUT

## PODKLADY A LITERATURA

Bencardino, F., Rizzuti, L., Spadea, G., & Swamy, R. N. (2008). Stress-Strain Behavior of Steel Fiber-Reinforced.

Yang, J., & Fisher, G. (2006). Investigation of the fiber bridging stress-crack opening relationship of fiber reinforced cementitious composites.

RILEM. (2002). RILEM TC 162-TDF : TEST AND DESIGN METHODS FOR STEEL FIBRE.

RILEM. (2003). Stress-strain design method- Final recommendation.

Naaman, A. E., & Reinhardt, H. W. (2005). Proposed classification of HPFRC composites based on their.

## ZÁSADY PRO VYPRACOVÁNÍ (ZADÁNÍ, CÍLE PRÁCE, POŽADOVANÉ VÝSTUPY)

-Vypracujte stručný přehled o deskách používaných pro mostní konstrukce, a způsobech jejich zatěžování.

-Navrhne numerický model v software ABAQUS s uvážením různých druhů vláknově vyztužených materiálů se zaměřením na přechodový koncentrátor napětí. Provede podrobnou analýzu napětí v okolí koncentrátoru a následně zhodnotí jaký má vliv použití různých vláknově vyztužených materiálů na koncentraci napětí.

-Na základě rozboru dosažených výsledků parametrické studie uvede základní doporučení pro použití.

## STRUKTURA BAKALÁŘSKÉ/DIPLOMOVÉ PRÁCE

**VŠKP vypracujte a rozčleňte podle dále uvedené struktury:**

1. Textová část VŠKP zpracovaná podle Směrnice rektora "Úprava, odevzdávání, zveřejňování a uchovávání vysokoškolských kvalifikačních prací" a Směrnice děkana "Úprava, odevzdávání, zveřejňování a uchovávání vysokoškolských kvalifikačních prací na FAST VUT" (povinná součást VŠKP).
2. Přílohy textové části VŠKP zpracované podle Směrnice rektora "Úprava, odevzdávání, zveřejňování a uchovávání vysokoškolských kvalifikačních prací" a Směrnice děkana "Úprava, odevzdávání, zveřejňování a uchovávání vysokoškolských kvalifikačních prací na FAST VUT" (nepovinná součást VŠKP v případě, že přílohy nejsou součástí textové části VŠKP, ale textovou část doplňují).

.....  
**doc. Ing. Stanislav Seitl, Ph.D.**

Vedoucí diplomové práce

## **ABSTRAKT**

Diplomová práce porovnává tři různé betonové směsi pro celkové ztužení ortotropní mostovky a zkoumá jejich vliv na redukci napětí ve zvoleném svarovém přípoji. Práce uvažuje se standartní zatěžovací situací mostu, ale také situaci s přetížením mostu. Byla také provedena parametrová studie různých materiálových modelů použitého betonu pro zachycení vlivu napětí ve svarovém přípoji.

## **KLÍČOVÁ SLOVA**

Únava, Ortotropní ocelová mostovka, Vysokohodnotný vlákno beton, Metoda Hot-spot

## **ABSTRACT**

This Master Thesis compares three various concrete materials for stiffening orthotropic bridge deck plate and investigates stress reducing factors in selected weld joints. The thesis investigates the standard load situation and also overloaded situation. A parameter study with different material inputs has been done to see how it affects stress in weld joints.

## **KEYWORDS**

Fatigue, Orthotropic steel deck plate, High-Performance Fibre-Reinforced Concrete, Hot-spot method



## **BIBLIOGRAFICKÁ CITACE VŠKP**

Bc. Petr Miarka *Numerical study of thin HPC overlay for orthotropic bridge deck*. Brno, 2017. 89 s., 0 s. příl. Diplomová práce. Vysoké učení technické v Brně, Fakulta stavební, Ústav stavební mechaniky. Vedoucí práce doc. Ing. Stanislav Seitl, Ph.D.

## **PROHLÁŠENÍ**

Prohlašuji, že jsem diplomovou práci zpracoval(a) samostatně a že jsem uvedl(a) všechny použité informační zdroje.

V Brně dne 12.1. 2017

---

Bc. Petr Miarka  
autor práce

# PROHLÁŠENÍ O SHODĚ LISTINNÉ A ELEKTRONICKÉ FORMY VŠKP

## PROHLÁŠENÍ

Prohlašuji, že elektronická forma odevzdané diplomové práce je shodná s odevzdanou listinnou formou.

V Brně dne 12.1. 2017

---

Bc. Petr Miarka  
autor práce

## **ACKNOWLEDGEMENT**

This master thesis has been partly written during my stay at Ghent University as an exchange student on the Erasmus+ program. It was a very challenging, practical and valuable experience which helped me to improve my knowledge in structural design, finite element modelling and English language. This lifetime experience will never be forgotten.

My thanks go to many people who encouraged me to finish this thesis and helped me during my stay in Gent. Big thanks has to go especially to my promoters prof. Wouter De Corte, who had useful and valuable remarks during our discussion on results from FE models and to dr. Arne Jansseune who had very practical remarks about modelling and calculations in FE software Abaqus. A special thanks has to go to my Czech promoter assoc. prof. Stanislav Seitzl, who had useful remarks on total appearance of this thesis, which helped me to finish this thesis.

The author acknowledges the support of Czech Sciences foundation project No. 15-07210S and No. 16-18702S. This thesis has been carried out under the project No. LO1408 "AdMaS UP – Advanced Materials, Structures and Technologies", supported by Ministry of Education, Youth and Sports under the „National Sustainability Programme I”.

Special thanks has to go to my parents and my sister who supported me during my stay abroad and also during my studies. Without their support it would be almost impossible to finish this important chapter of my life.

## TABLE OF CONTENTS

Introduction .....	11
1. Orthotropic Bridge Deck .....	12
1.1 Orthotropic Steel Bridge Deck .....	12
1.2 Common Dimensions of Components .....	12
1.3 Fatigue Damage Phenomenon .....	13
1.3.1 Cracks in the Deck Plate .....	14
1.3.2 Cracks in the Longitudinal Weld .....	15
1.3.3 Crack in Trough Splice Joint .....	16
1.3.4 Cracks in the Connection Between Trough Profile and Crossbeam .....	16
1.4 Renovation Techniques for Fatigue Damage .....	17
1.5. Hot-Spot Method .....	19
2. Concrete Overlay as a Renovation Technique .....	22
2.1 Reinforced Concrete Overlay .....	22
2.2 Fibre Reinforced Concrete Overlay .....	22
2.2.1 Types of Fibres for FRC and UHPFRC .....	24
2.2.2 Mechanical behaviour of UHPFRC .....	26
2.2.2.1 Material Response to Tensile Load .....	26
2.2.2.2 Material Response to Compressive Load .....	29
2.2.2.3 Material Response to Cyclic Load .....	30
2.3 Composite Behaviour of Overlay and Steel Deck Plate .....	34
2.4 Three Point Bending Test – Crack Mouth Open Displacement Measurement .....	36
3. Numerical Model .....	40
3.1. Dimensions .....	40
3.2. Material Characteristics .....	42
3.2.1. Material Characteristics Used for Bridge Parts .....	42
3.2.2. Concrete .....	42
3.2.2.1 Uniaxial Compressive Behaviour .....	43
3.2.2.2. Uniaxial Tensile Behaviour .....	45
3.2.2.3. Uniaxial Cyclic Behaviour .....	47
3.3. Boundary Conditions and Load .....	47
3.4. Mesh .....	50
4. Results of Numerical Study and Discussion .....	53
4.1. Results from Single Crossbeam Model .....	53

4.2. Results from Double Crossbeam Model .....	58
4.3. Results from Overloaded Model .....	65
4.4. Results from Parameter Study.....	71
Conclusion .....	75
References .....	76
List of Abbreviations.....	79
List of Symbols .....	80
List of Figures .....	82
List of Graphs .....	84
List of Tables.....	86
Curriculum Vitae .....	87
Author's Publications.....	89

## **Introduction**

Increased automobile and train transportation on orthotropic steel bridges in recent years has led to a serious fatigue damage. This damage has to be eliminated and the renovation technique should be sustainable. The current solution is the application of a reinforced high strength concrete overlay. This renovation method is labour intensive, time consuming and has some issues with sustainability. These facts have led, in recent years to the application of the fibre reinforced concrete overlay as a renovation technique.

### ***AIM***

This thesis investigates the stress reduction effects of three various types of fibre reinforced concrete materials. Each of these concrete materials differ in types of fibres, tensile and compressive strength limit and post-crack behaviour. Finite element (FE) software Abaqus has been used for the investigation of stress reducing effect of concrete overlay on the steel deck plate. Two different models of the bridge deck were modelled in the software Abaqus. Models for investigation had one or two transversal crossbeams. Investigation of the stress was in the weld joint connecting longitudinal rib and steel deck plate. For evaluation of the stress in weld a Hot-spot method has been used. Three different paths were used for evaluation of the stress in the deck plate. The bridge deck was loaded with standard wheel load caused by a truck and it was also overload to understand the behaviour of damaged concrete overlay in overloaded situation.

# 1. Orthotropic Bridge Deck

## 1.1 Orthotropic Steel Bridge Deck

To accomplish further numerical simulations of the orthotropic bridge deck plate, it is necessary to have a small description of its structural concept. The whole concept of this kind of bridge consists of a deck plate, where a traffic load is applied. The deck plate is stiffened by welded longitudinal ribs, which are supported by two stiffeners at each end. This is shown in Figure 1.

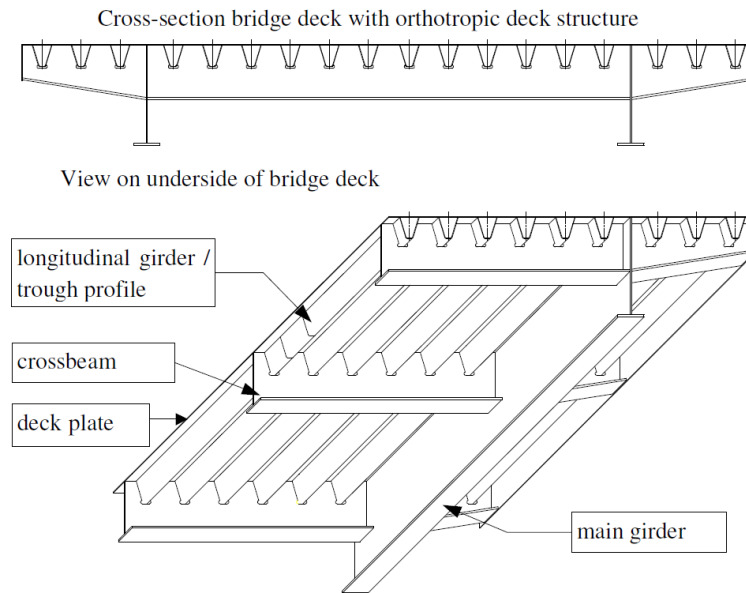


**Figure 1:** Main components of orthotropic steel bridge deck <sup>[1]</sup>

The load is distributed from the deck to the closed longitudinal rib a.k.a a trough. The ribs carry out transversal stiffener/crossbeam and finally main girder/longitudinal beam supports crossbeam. The longitudinal beam is held up by supports at each end. The deck plate is usually covered with a thick layer of asphalt. The whole concept is named orthotropic because of the stiffness ratio in a transversal and longitudinal direction, whereby elastic behaviour of the deck plate is different in two orthogonal directions. These types of structures increase the ratio of nonpermanent/self-weight load in comparison with another types of bridges.

The orthotropic steel bridge decks are used around the world mainly for:

- Plate girder bridges and box girder bridges,
- Arch bridges and truss bridges
- Cable stayed bridges and suspension bridges
- Moveable bridges.

## 1.2 Common Dimensions of Components

The steel deck plate usually has a thickness from 9 mm to 15 mm, this depends on spacing between through walls and acceptable deflection of steel deck plate under the applied wheel load. In the most cases, a steel plate is used with thickness of 12 mm.

The ribs are generally categorised as an open-rib or closed-rib system. The closed-rib system has a better torsion stiffness and is more effective in a lateral distribution of the local wheel load, than the open-rib system. The closed-rib is regularly made by bended



steel sheet into the wanted shape. Thickness of this part differs from 5 to 10 mm. Common steel profiles or single steel plates are used for the open-rib system. Figure 2 shows common shapes of longitudinal ribs.

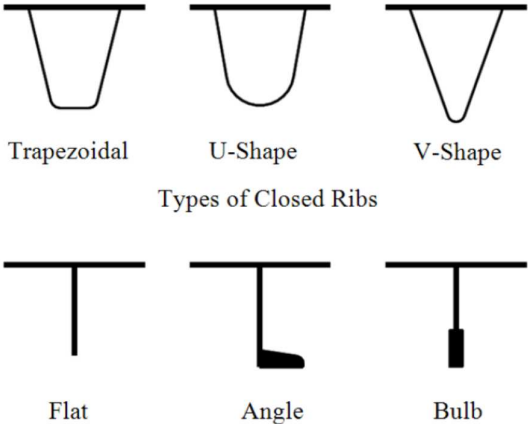


**Figure 2:** Types of longitudinal ribs [2]

The transversal stiffeners usually have a cross section of half I-profile or two steel plates welded together into the shape of a reversed letter T. In this part, there are usually cut outs for welded connection of longitudinal ribs. The main girders are made from common I profiles or half of I profiles.

**1.3 Fatigue Damage Phenomenon**

Fatigue has been recognised as a specific failure mechanism in the early nineteenth century, with the fast development of a rail transportation it has received the major interest of researchers. Fatigue is the weakening of a material caused by repeatedly applied load. The damage caused by fatigue is mostly progressive and localised. There are many failure mechanisms which lead to failure of a structure, but the fatigue is the most dangerous one, because it shows a very little or no warning at all. The value of maximum stress that causes this type of damage is much less than the ultimate strength, below the yield point of the metal material and below the acceptable static load of the structure. The fatigue can be divided into three categories: Low-cycle, High-cycle and Super-high-cycle fatigue. This separation shows Table 1.

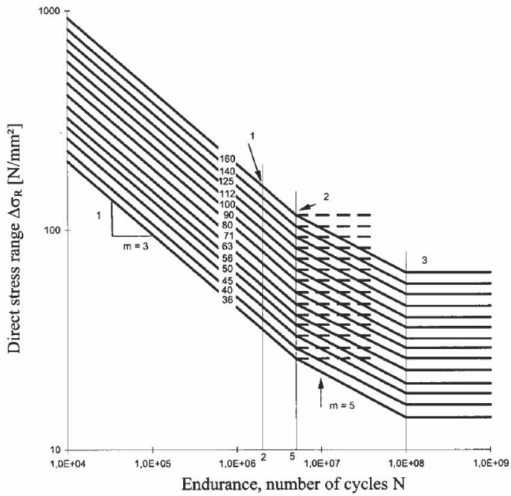
**Table 1:** Separation of load cycles applied on structure [3]

Low-cycle fatigue			High-cycle fatigue				Super-high-cycle fatigue		
1	10 <sup>1</sup>	10 <sup>2</sup>	10 <sup>3</sup>	10 <sup>4</sup>	10 <sup>5</sup>	10 <sup>6</sup>	10 <sup>7</sup>	10 <sup>8</sup>	10 <sup>9</sup>
Structures subjected to earthquakes			Airport pavements and bridges		Highway and railway bridges, highway pavements		Mass rapid transit structures		Sea structures

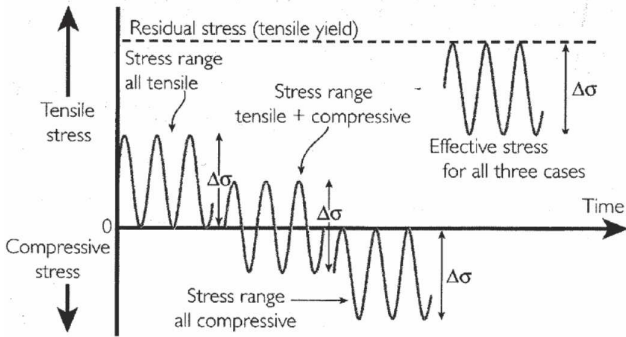
This division of fatigue into fatigue categories is made by a number of cycles, where the load is applied on a structure. Reliability of fatigue life of the structure has been made into the Wöhler’s curve or S-N curve. Graph 1 shows  $S(\Delta\sigma)$ , applied stress range, against  $N$ , the number of cycles. This approach in the fatigue investigation has a major disadvantage in deriving stress range, meaning it is very difficult to get an exact value of the stress range.

Graph 2 shows different types of stress ranges in weld connection. It has to be noticed that, even if the applied stress range is entirely compressive and there is apparently no

fluctuating tensile stress to cause a crack to form and grow, the effect of welding residual stress is to make the structure susceptible to fatigue failure. [4]



**Graph 1: Fatigue strength curves for direct stress ranges** [5]



**Graph 2: Effective stress and residual stress applied on structure** [4]

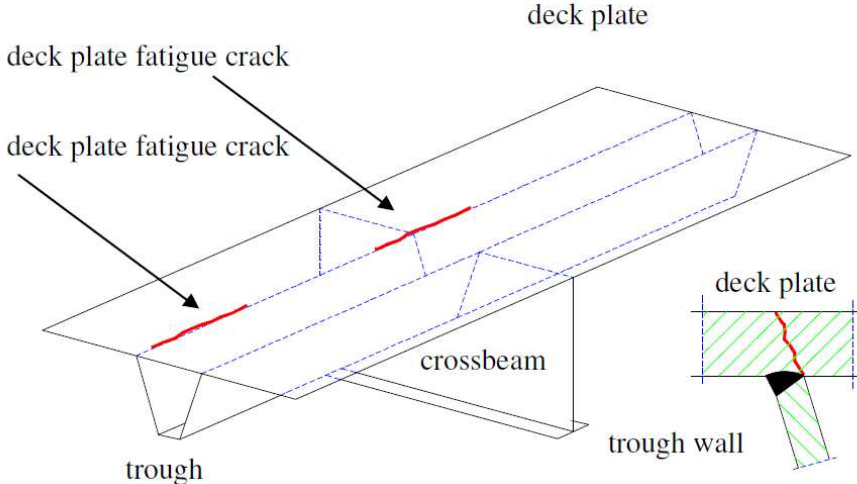
The orthotropic bridge deck structural concept has to carry mainly own weight and non-permanent loads such as automobile or train transportation. Recent years have shown an increase of these traffic loads and this became the main reason for the presence of fatigue cracks. These cracks occur after large number of load cycles. In the past this fact has not been taken into account and some structural details suffer from the fatigue damage cracking problem. The main crack can occur at different locations such as:

- Cracks in the deck plate
- Cracks in the longitudinal weld between deck plate and trough
- Cracks in the trough splice joint
- Cracks in the connection between trough profile and crossbeam. [1]

**1.3.1 Cracks in the Deck Plate**

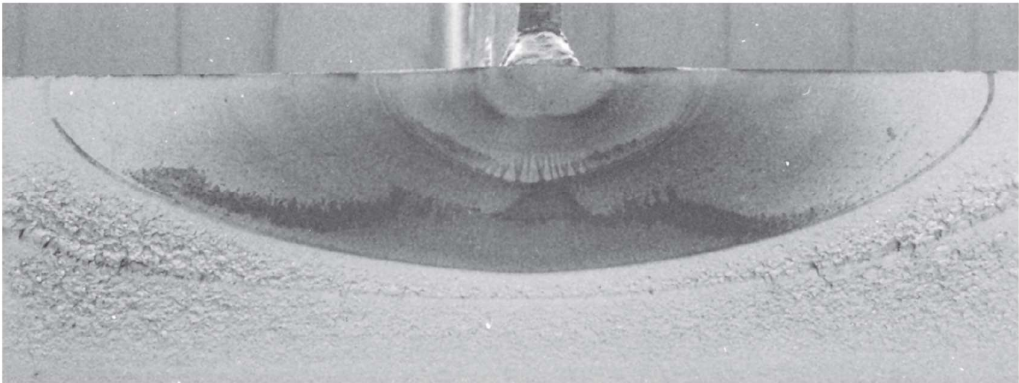
The cracks are mostly located at the deck, where the transversal stiffener crosses the longitudinal rib. This is shown in Figure 3. This kind of cracks have basically three stages. The first stage is crack initiation at the root of a longitudinal weld. The weld connects deck plate and trough. In the second stage the crack starts to grow in a vertical direction from the bottom to the top surface of the deck plate. In the third stage crack starts to grow in a longitudinal direction.

Figure 3 also shows another position of crack in the deck plate. The crack can be found also between the crossbeams instead of intersection. The crack between crossbeams has only two stages. The first one is initiation of the crack and the second stage the crack grows simultaneously in a vertical and horizontal direction. The length of these cracks can be up to 500 mm.



**Figure 3:** Fatigue crack propagation in deck plate [1]

These cracks are caused by a local wheel load, which is positioned directly in the middle of the rib. This position of the load causes deflection of the deck plate. The rib is welded to deck plate and deflection of the deck plate causes high clamping moment with a high local bending stress. Due to this welding connection and clamping, fatigue crack at the deck plate will appear. Figure 4 shows propagation of fatigue crack.



**Figure 4:** Typical elliptical surface of fatigue cracks [4]

**1.3.2 Cracks in the Longitudinal Weld**

These cracks can appear in any position of the welded connection between the longitudinal rib and deck plate. The crack initiates at the root of this weld on outer surface of the deck plate. After the phase of initiation the crack starts to grow out from the surface of trough and grows in a longitudinal direction. Figure 5 shows different damage at this welded connection.

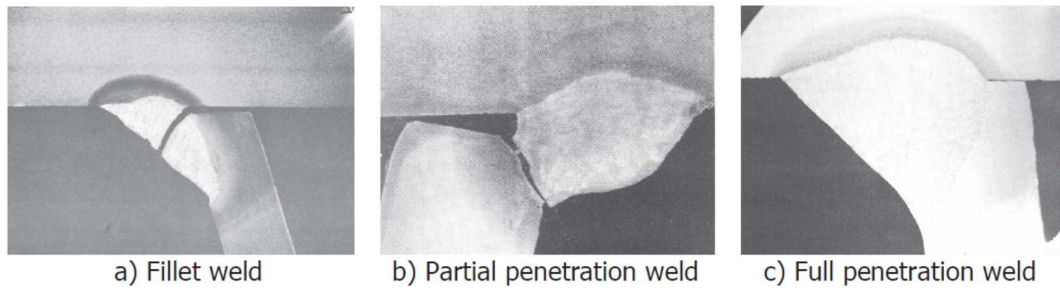


**Figure 5: Macro section of different to deck plated welds <sup>[4]</sup>**

The deck plate behaves like girder beam with multiple supports. The wheel load located at mid span of the ribs causes downward deflection of deck plate and other areas of the deck plate deflect upwards. The closed ribs are not rigid supports, they behave more likely as an elastic spring and they deflect as well. The deflection of the rib is caused by the limited bending stiffness of rib the profile. Deflection depends on the distance between two transversal stiffeners. The bending moments in the deck plate arise and result into the high stresses in the longitudinal weld.

### 1.3.3 Crack in Trough Splice Joint

The crack appears in the welded connection of two longitudinal ribs. This connection is made for the rib with a small length which is fitted between two ribs, which are in their position from the factory. The weld has usually a small backing steel strip. Figure 6 shows two different locations of a crack initiation. The crack can occur either in a fully penetrated weld, which connects two troughs together or it can occur at the weld connecting the backing steel strip with rib.

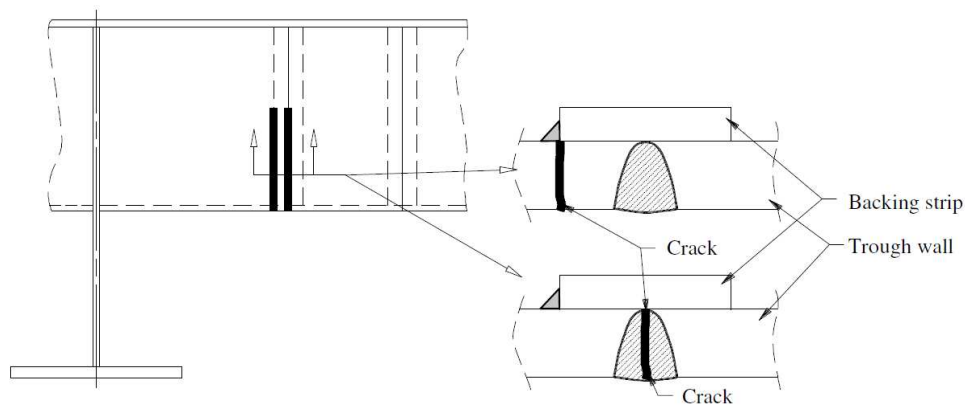


**Figure 6: Crack in trough splice joint <sup>[1]</sup>**

Passing vehicles cause significant bending moment in a trough profile. This moment results in a considerable longitudinal bending stress. The position of splice joints are normally chosen in a location with the lowest bending moment range. However this stress range, along with a combination of misalignment causes high stress concentration. The concentration of stress results in the initiation of the fatigue crack at this splice joint.

### 1.3.4 Cracks in the Connection Between Trough Profile and Crossbeam

Cracks in the connection between trough profile and crossbeam usually grow on the weld connection those two parts together. Figures 7-9 show position of cracks in this

joint. Cracks can appear in the rib and crossbeam as well. These cracks can be suppressed by cut-out in the crossbeam section.

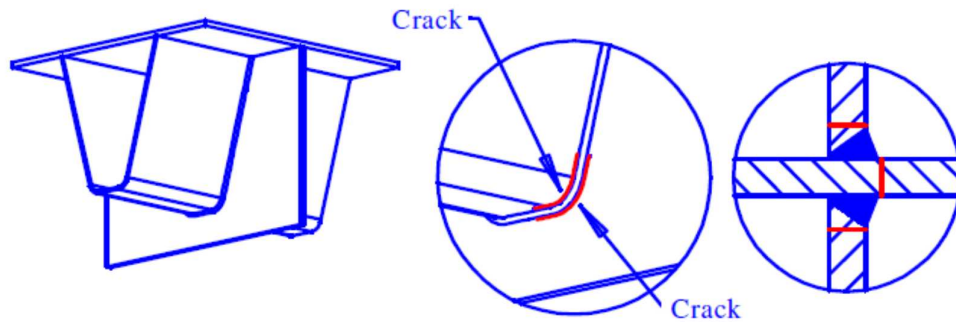


**Figure 7:** Fatigue crack trough-crossbeam connection, (trough fitted between crossbeams) <sup>[1]</sup>

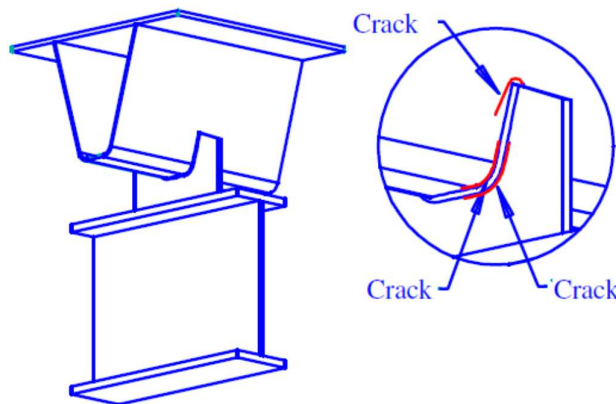


**Figure 8:** Fatigue crack trough-crossbeam connection, (floating deck structure) <sup>[1]</sup>

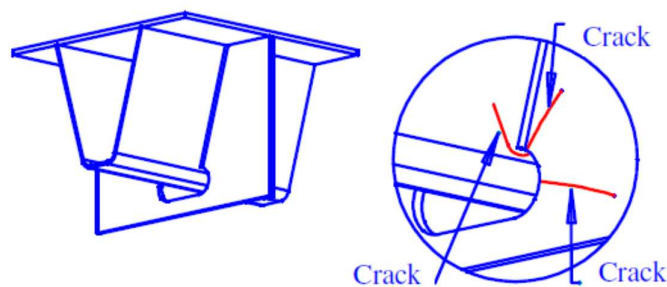


**Figure 9:** Fatigue crack trough-crossbeam connection, (with cut-outs) <sup>[1]</sup>

#### 1.4 Renovation Techniques for Fatigue Damage

As mentioned in the previous section, there are some structural details which suffer from fatigue damage. To extend the lifetime of the bridge, reparation of a fatigue damage has to be done. The demands on the renovation technique vary from bridge to bridge and the owner of the bridge has the last word of a chosen technique. In the past there were a lot of studies developing optimal technique of the renovation. The initial technique was to switch traffic lines, however this solution was not fixing existing cracks and was mostly used to gain time before actual renovation started.

The most of past renovations have been done by welding existing cracks together. Cracks were welded by a classic arc welding or submerged arc welding. The submerged arc welding were used more. This welding technique is under a layer of welding powder in which the weld is automatically performed. The crack is heated by an electric plasma arc, so the material melts and flows together. This welding technique is very quick can be applied only from the top surface of the deck plate and also the shrinkage of the weld is relatively small. Another ways of renovation were using: a cut-out of the damaged area of deck plate and replacing it with a new steel sheet or were welding a new small steel plate on the top surface of the deck plate.

Nevertheless those techniques fixed only existing cracks and did not prevent the new ones to appear or the old ones to reappear again. The sustainable solutions can be found in the study of Netherland civil engineer F.B.P De Jong 2007 <sup>[1]</sup>.

**Table 2: Renovation techniques <sup>[1]</sup>**

Parameter	A	B	C	D	E
Old Surfacing	50 mm traditional mastic asphalt	7 mm epoxy surfacing			
Existing fatigue cracks	Not repair the cracks	Repair the cracks			
Material	Steel	(High strength) concrete	Wood	Aluminium	Fibre reinforced plastic
Form	Board / planks	Extruded profiles	Poured layer	Plate material	Sandwich Panels
Connection	Welding	Bolting	Bonding	Vulcanization of rubber	
Connection Technology	0 % composite action	100 % composite action	Vertical connection at distances of 300 mm	Vertical support of the deck plate	

Table 2 shows an overview of general renovation methods separated into a table by following parameters: Old surfacing, existing fatigue cracks, material of renovation and connection technology. Basically all these parameters can be combined with each other. De Jong chose for paper a meaningful combinations of these parameters for further research:

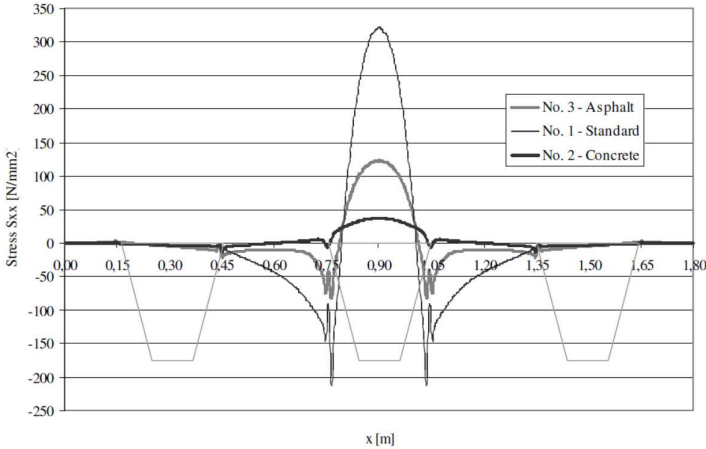
- Glued wooden boards
- Bolted wooden planks
- Bolted aluminium shelves
- Glued aluminium shelves
- Formed steel sheet
- Pre-formed steel sheet
- Bonded extruded aluminium profiles
- Connected steel plate with rubber layer
- Connected steel plate with a layer of polyurethane
- Prefabricated sandwich panel
- A second steel sheet glued above existing deck plate
- Filled troughs
- Classical reinforced concrete overlay.

The bolted connections are not recommended, because they have lower sustainability and they are more predisposed to corrosion. The other methods of renovation were avoided because of a suspicion that the steel deck corrosion problems could show up. The gluing second steel plate on the existing bridge deck is only recommended for a moveable bridges, because this technique does not add weight to the bridge. Filling



of longitudinal ribs is also possible more advantageously without a disruption in traffic on the bridge.

De Jong in his paper compared different types of materials for additional overlay renovation technique. The materials were asphalt and concrete. The results were compared to model without any overlay and it is clearly visible that this kind of renovations has positive influence on stress reduction in the steel plate. The stress reduction effect of this materials used as an overlay can be found in Graph 3. In Graph 3 there are three stress curves: No.1 – Standard – stress in steel plate without any overlay, No.2 – Concrete – stress in steel plate with concrete overlay, No.3 – Asphalt – stress in the steel plate with asphalt overlay. Dimensions of FE model can be found in Figure 10. Stress was acquired from path in transversal X-direction also mentioned in Figure 10.



**Graph 3: Comparison of stress in X-direction [1]**

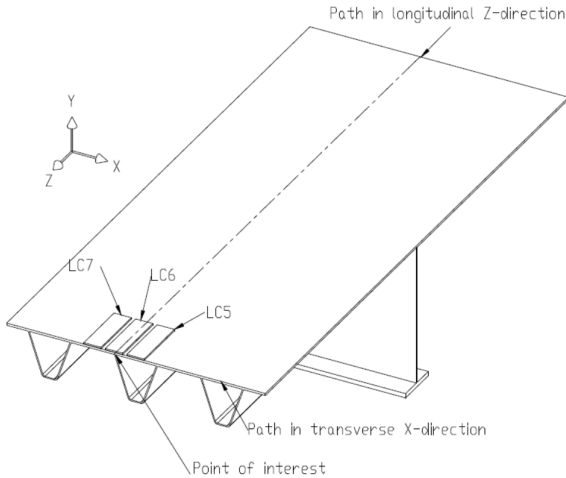


**Figure 10: De Jong's sketch of numerical model [1]**

**1.5. Hot-Spot Method**

In subsection 1.3 of this thesis, the classical approach of fatigue design of structures is mentioned. This approach is not very efficient, because it has some problems with evaluating the stress range  $S(\Delta\sigma)$  applied to the structure. A new approach in structural survey of welded joints has been developed. This method is called "Hot spot stress method" (HSM) and it was proposed by International Institute of Welding (IIW) in

December 2008. IIW recommends to use this method in cases where the stress range is not clearly defined or where the structural detail is not comparable to other typical detail mentioned in this recommendations.

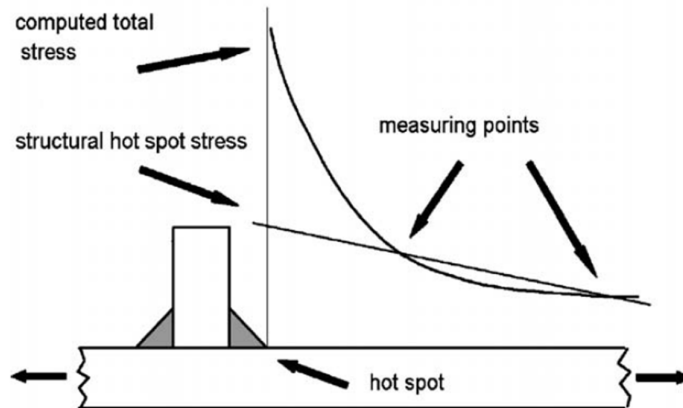


**Figure 11:** Definition of the hot-spot method <sup>[6]</sup>

The hot-spot stress is calculated by using reference points for extrapolating stress at the weld toe. Firstly, it is necessary to establish the reference points and then determine the structural hot spot stress. This is shown in Figure 11. Determination of the structural hot spot stress is made by an extrapolation to the weld toe from the calculated stresses at these reference points. Positions of reference point are shown in Figure 13. Depending on the method of the extrapolation, there are two or three of these reference points. Calculations of the stresses at the reference points are done by finite element analysis (FEA). For the solid elements, IIW recommends to use 20-node elements with the mid side nodes at the edge in the locations with steep stress, which allows only one element to be arranged in the plate thickness.

The hot spots are also classified by a position in the structure:

- Hot-spot type a: Weld toe on plate surface
- Hot-spot type b: Weld toe at plate edge.

In this case the investigated weld can be classified as a “type a”. Types of Hot-spots are shown in Figure 12.

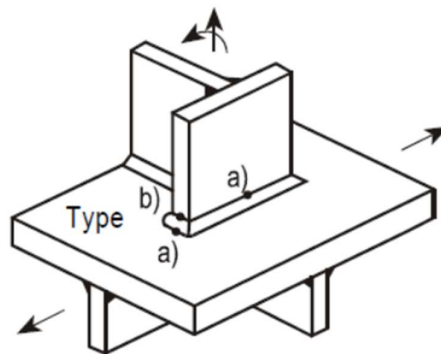


**Figure 12:** Hot-spot types <sup>[7]</sup>

Based on the length and types of used elements around the hot spot, the position of the reference points can vary. The reference point can be in a distance  $0.4t$  from hotspot in model with fine mesh or in the distance  $0.5t$  from the hotspot, where the  $t$  is thickness of investigated steel plate. The hotspot does not have to be necessary



on the same position as nodes of elements. To get the value in needed location a linear interpolation can be used.

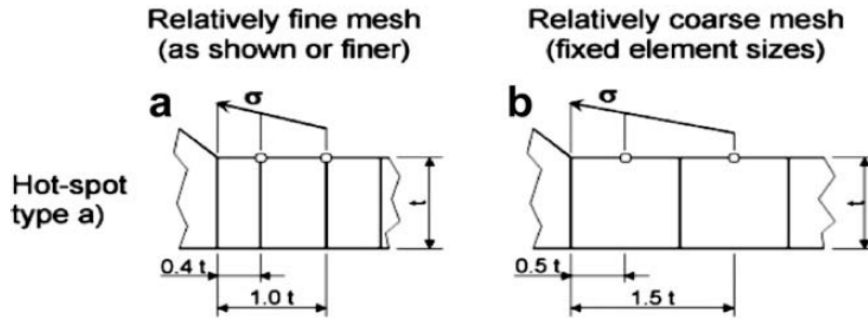


Figure 13: Position of reference points [6]

In this study the mesh is relatively coarse and the values of the stresses at the reference points were linearly interpolated from calculated nodal values. According to IIW recommendation the following formula was used for  $\sigma_{hs}$  stress extrapolation:

$$\sigma_{hs} = 1.5 \cdot \sigma_{0.5t} - 0.5 \cdot \sigma_{1.5t} , \quad (1)$$

where:  $\sigma_{hs}$  is extrapolated stress in the hot-spot,  $\sigma_{0.5t}$  is calculated stress in reference point at distance  $0.5t$  from weld toe,  $\sigma_{1.5t}$  is calculated stress in reference point at distance  $1.5t$  from weld toe and  $t$  is thickness of steel deck plate.

The three different paths were defined to extrapolate stress values from the FE models results. The position of the hot spot is on the underside of the steel deck plate where the middle longitudinal rib is connected by welded joint to deck plate. The first path gets stress values from the outside of the trapezoidal rib at  $X = 750$  mm, the reference points are at  $X = 732$  and  $744$  mm. The second one extrapolates stress from the inside of the rib in the position  $X = 755$  mm with reference points at  $X = 761$  and  $773$  mm. The third path is on the inner side of the longitudinal rib. The hot-spot is located at the end of the rib, where it is connected to the deck plate i.e. in coordinates of rib  $X = 0$  mm and reference points are at  $X = 2.5$  and  $7.5$  mm. Figure 14 shows investigated hot-spot and paths for stress extrapolation.

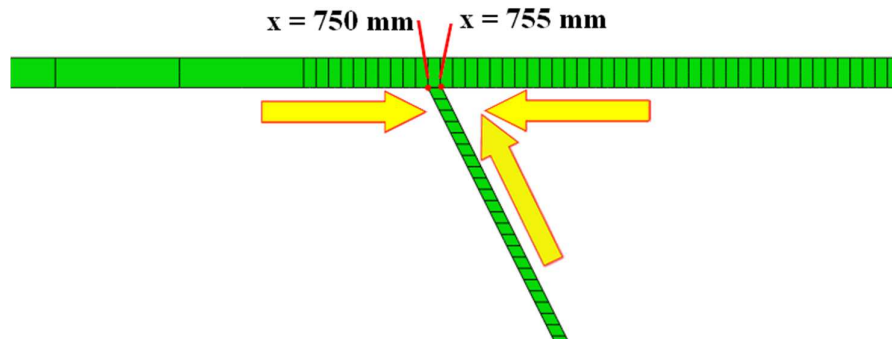


Figure 14: Paths for stress extrapolation at hot-spot

## 2. Concrete Overlay as a Renovation Technique

### 2.1 Reinforced Concrete Overlay

Concrete overlay as a renovation technique for fatigue damage of orthotropic bridge has its main advantage in the stiffening of the bridge. The stiffening is done by additional concrete overlay on the top surface of steel deck plate. This solution greatly reduces stress in the most of the details mentioned in 1.3 of this thesis.

To achieve good connection between the steel and the overlay, asphalt or epoxy layer is usually applied on the steel plate. Reinforcement bars are mostly embedded into the concrete overlay. After the application of concrete overlay it is necessary to have a technological break to achieve demanded material properties of used concrete. This whole application process is very time consuming and labour intensive. The reinforcement is used to carry out tension stresses in the overlay. The tension stresses can be caused by wheel load or environmental loads such as shrinkage and changing temperature. The dense reinforcement mesh can cause bad compaction of concrete mixture in some areas. Badly compacted concrete can cause cracking in concrete and more damage can show up after repeatedly applied wheel load. Damaging of concrete overlay can be caused also by bad stacking of reinforcement. These negative effects are shown in Figure 15.



*Figure 15: Dense reinforcement and badly compacted concrete [1]*

The shrinkage of concrete is determined by the water/cement ratio of the fresh concrete mixture. The shrinkage is caused by drying water out of the mixture from the exposed surface. This behaviour causes shortening of concrete material, which bends the overlay and causes compressive and tensile stresses in it. The solution for this negative effect is to use a steel L-profile welded on the edge of the bridge deck. This solution and shrinkage behaviour can be found in Figure 16.

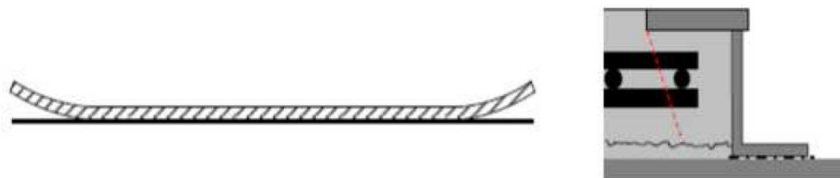


*Figure 16: Shrinkage of overlay and edge detail [8]*

### 2.2 Fibre Reinforced Concrete Overlay

The reinforced concrete overlay for the orthotropic steel bridges has its advantages, which cannot be neglected. The increased stiffness leads to a reduction of the stresses in the steel deck plate, which results in an extended lifetime of the bridge. Unfortunately,

some problems can occur in cases using reinforced concrete overlay (section above). In order to solve these problems, it would be advantageous to achieve a concrete overlay without a traditional reinforcement. This reason led in a recent years into research and deployment in using the ultra-high performance fibre reinforced concrete (UHPFRC) as a material for overlay on the orthotropic steel bridge concepts for the fatigue damage renovations. This new material brings following advantages:

- Faster time of renovation
- Shorter period in disruption of traffic
- Less intensive for labour
- Less risky to problems with sustainability.

The following sections focus mainly on mechanical properties and classification of the fibre reinforced concrete. The other concern is, if this new material can be used as an equal replacement of the classical reinforced overlay renovation technique.

The longitudinal ribs work as a support for the steel deck plate. This structural behaviour causes negative bending moments above the supports (longitudinal ribs). These negative bending moments cause tensile stresses on the top surface of the concrete overlay. The classical concrete has a low tensile strength, therefore the steel reinforcement is used to carry out the tension stresses. If the tensile stresses are greater than the tensile strength limit of used concrete, the concrete overlay cracks and the opening of the cracks expose the reinforcement. The exposed reinforcement suffers to a corrosion, which results in more damage to the concrete, because the corrosion of the steel has greater volume than the steel bars without corrosion, therefore new cracks in the concrete can appear or old ones can grow even more. This disadvantage can be neglected by using fibre reinforced concrete as a material for the overlay. The fibre reinforced concrete is type of a material, which belongs into the class of engineered cementitious composites (ECC) with discrete (discontinuous) fibres dispersed in a cement matrix. The ECC materials were developed in a last five decades. The main characteristics of ECC materials are a high ductility, toughness and energy absorbing under the direct impact. The described problem with cracks opening and corrosion of the reinforcement cannot be taken into account any more, because of the mechanical behaviour of the fibre reinforced concrete. The tension stresses mentioned above are now carried out by fibres and not by steel reinforcement.

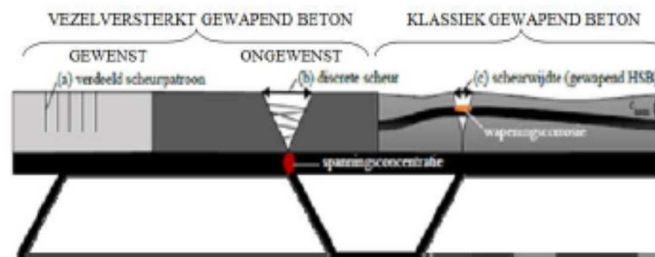


**Figure 17:** Difference between reinforced overlay and HPC overlay <sup>[8]</sup>

In Figure 17: “Vezelversterkt gewapend beton” means fibre reinforced overlay vs “Klassiek gewapend beton” means concrete reinforcement with steel bars.

The distribution of the fibres in the concrete mainly leads to a lot of micro-cracks. These small cracks are the characteristic and the most important mechanical response of the fibre reinforced concrete. Micro-cracking indicates a good structural behaviour of fibre reinforced concrete. Basically more micro-cracks are sustainable, than one major macro cracks. This behaviour is described in the subsection below (2.2.2).

## 2.2.1 Types of Fibres for FRC and UHPFRC

The fibres and their properties are main component of the fibre reinforced concrete (FRC) and ultra high performance fibre reinforced concrete (UHPFRC) and have direct influence on the mechanical and structural behaviour of this kind of material. The classical concrete material fails in a brittle behaviour, thus adding this small needle like fibres into a cementitious matrix, highly improves material properties. In the first development of the ECC were only used steel fibres, but in recent years there were several studies on a synthetic (polymeric, glass, Kevlar or carbon) fibres. The studies have also dealt with shape design of fibres. The fibres can vary in a cross sectional shape, length, surface deformation and endings.

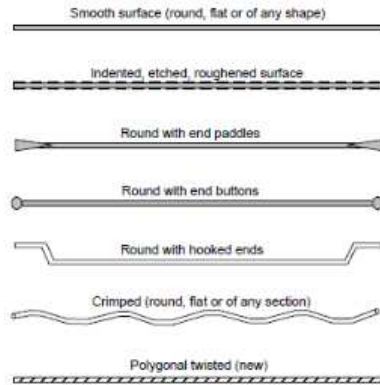


**Figure 18:** Geometries of fibres used in concrete <sup>[9]</sup>

The variation in geometry of the fibres is shown in Figure 18. The fibres can have different modifications on surface, mostly they are smooth without any protrusions on them or can be twisted and crimped. The ends of fibres can also have some modification such as end paddle, end button or hooked end, instead of having a straight end. The cross section can have a round, square or flat rectangular shape. The steel fibres have common diameter in range from 0.4 to 0.8 mm and synthetic fibres can have diameter from 10  $\mu\text{m}$  up to 0.8 mm. The length of these fibres can also vary from 25 to 60 mm. The difference in cross sections shape of the fibres is shown in Figure 19 and Figure 20.

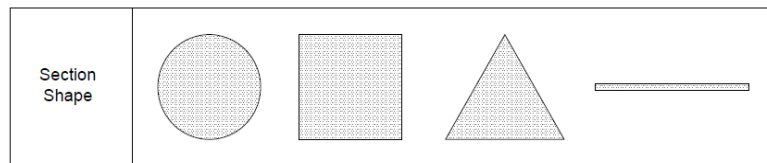


**Figure 19:** Cross sectional area of fibres used in concrete <sup>[9]</sup>

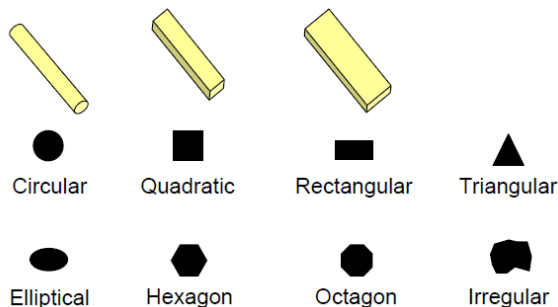


**Figure 20:** Cross sectional area of fibres used in concrete <sup>[10]</sup>

These geometrical characteristics have a main influence in total strength of the UHPFRC. Whole composites are affected directly by these characteristics: mechanical properties of used fibres such as modulus of elasticity  $E_f$ , tensile strength  $\sigma_{fu}$  and the coefficient of the thermal expansion  $\alpha_t$ . The bond between fibres and cementitious matrix also has a significant influence on the ductility of structure.

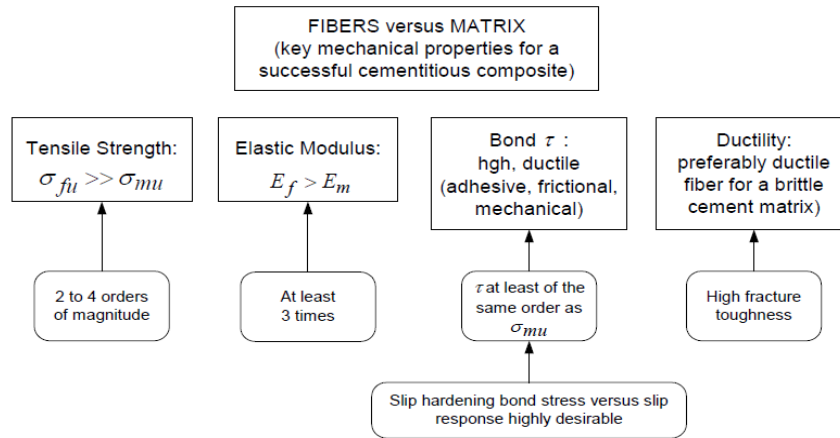


Figure 21: Fibres vs cementitious matrix properties [9]

Figure 21 sums up demanded properties of the fibres and shows an optimal difference between fibres and cementitious matrix. The tensile strength should be  $10^2$  to  $10^4$  times greater, than the strength of the matrix, this can be achieved by using a high quality steel or using a synthetic material with  $\sigma_{fu} > 1500$  MPa.

The common tensile strength of the matrix  $\sigma_{mu} < 12$  MPa. The modulus of elasticity  $E_f$  should be at least three times greater that the  $E_m$ . This could be easily fulfilled, because the concrete has a modulus of elasticity less than 50 GPa and common steel has modulus of elasticity greater than 190 GPa. However the bond between matrix and fibres, can be improved by geometry variations mentioned above. Table 3 shows various materials used for fibres.

Table 3: Comparison of different materials used for fibres in concrete mixture [10]

Type of Fibre	Diameter [ $\mu$ m]	Specific gravity [g/cm <sup>3</sup> ]	Tensile strength [MPa]	Elastic modulus [GPa]	Ultimate elongation [%]
<b>Metallic</b>					
Steel	5-1 000	7.85	200-2 600	195-210	0.5-5
<b>Glass</b>					
E glass	8-15	2.54	2 000-4 000	72	3.0-4.8
AR glass	8-20	2.70	1 500-3 700	80	2.5-3.6
<b>Synthetic</b>					
Acrylic (PAN)	5-17	1.18	200-1 000	14.6-19.6	7.5-50.0
Aramid (e.g. Kevlar)	10-12	1.4-1.5	2 000-3 500	62-130	2.0-4.6
Carbon (low modulus)	7-18	1.6-1.7	800-1 100	38-43	2.1-2.5
Carbon (high modulus)	7-18	1.7-1.9	1 500-4 000	200-800	1.3-1.8
Nylon (polyamide)	20-25	1.16	965	5.17	20.0
Polyester (e.g. PET)	10-8	1.34-1.39	280-1 200	10-18	10-50
Polyethylene (PE)	25-1 000	0.96	80-600	5.0	12-100
Polyethylene (HPPE)	-	0.97	4 100-3 000	80-150	2.9-4.1
Polypropylene (PP)	10-200	0.90-0.91	310-760	3.5-4.9	6-15.0
Polyvinyl acetate (PVA)	3-8	1.2-2.5	800-3 600	20-80	4-12
<b>Natural - organic</b>					
Cellulose (wood)	15-125	1.50	300-2 000	10-50	20
Coconut	100-400	1.12-1.15	120-200	19-25	10-25
Bamboo	50-400	1.50	350-50	33-40	-
Jute	100-200	1.02-1.04	250-350	25-32	1.5-1.9
<b>Natural - inorganic</b>					
Asbestos	0.02-25	2.55	200-1 800	164	2-3
Wollastonite	25-40	2.87-3.09	2 700-4 100	303-530	-

Another factor that affects structural behaviour is a volume of the fibres  $V_f$  used in the concrete mixture. The volume of fibres has a major influence on the total tensile and compressive strength and ease of processing of the concrete mixture. The volume of fibres is also used as a parameter for classification of the fibre reinforced cementitious materials. Table 4 shows classification based on fibre volume.

**Table 4:** Classification of fibre reinforced concrete based on volume of fibres [11]

Material	Range of $V_f$	Remark
FRC – Fiber Reinforced Concrete	$V_f \leq 2\%$	Fibers are premixed with the concrete matrix. Finer aggregates may be needed.
HPFRCC – High Performance Fiber Reinforced Cement Composites	$V_f \begin{cases} \geq (V_f)_{critical} \\ \geq 1\% \end{cases}$	Strain hardening and multiple cracking characteristics in tension. With proper design, critical $V_f$ can be less than 2%.

**2.2.2 Mechanical behaviour of UHPFRC**

Adding fibres to brittle cementitious matrix greatly improves, the mechanical behaviour and changes it into a relatively ductile material. The following sections describe different material behaviour and material model of ultra-high performance fibre reinforced concrete.

**2.2.2.1 Material Response to Tensile Load**

The most significant influence of the fibres is, when this kind of composite is exposed to a tensile or bending load. The response of these materials to the tensile or bending load, has basically two possible outcomes. The concrete test sample cracks, because the tensile stress caused by a load is greater than the tensile strength limit. The whole sample of the composite collapses, because one major macro-crack is opened very wide. The fibres cannot hold this stress, therefore the composite collapses. This behaviour is called post-crack softening. The other possibility is that the several micro-cracks are located in the tested sample. The fibres carry out the tensile stresses in the cracked locations, therefore the whole composite can carry out higher tensile stresses. This behaviour is called post-crack hardening. The limit of the strain hardening is when the fibres cannot carry out the stresses or the bond between the fibres and matrix collapses.

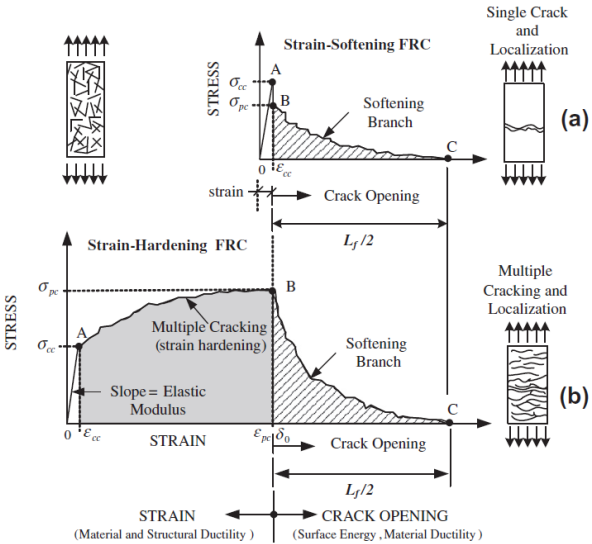
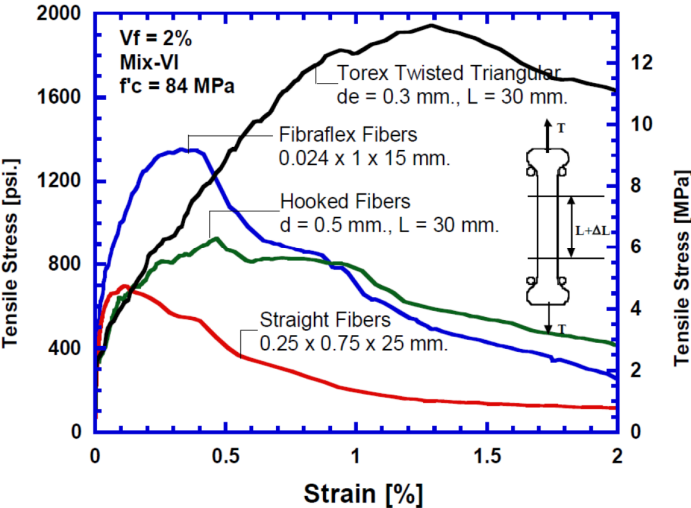


**Figure 22:** Difference between strain hardening/softening of fibre reinforced material [11]

The difference between those two responses is clearly visible in Figure 22. Both curves have a similar shape until crack initiation. This is the point where the first cracks start to appear, because tensile strength limit of the concrete material was reached. Until this point all deformations are elastic. This stress can be calculated by:

$$\sigma_{cc} = E_{cc} \cdot \epsilon_{cc}, \tag{2}$$

where:  $E_{cc}$  is modulus of elasticity and  $\epsilon_{cc}$  is measured elongation of the tested specimen. After this point both curves starts to highly differ and measured elongation is inelastic. In the case with a post-crack strain hardening the curve can reach another peak called post-crack stress  $\sigma_{pc}$ . The micro-cracks start to appear and the fibres can carry more tensile stresses than the matrix itself, therefore this branch is called hardening. After reaching this point major crack starts to initiate and the curve starts to have a decreasing branch also called softening branch and the whole test sample collapses. In the case with a post-crack strain softening the major crack starts to localise almost immediately after reaching the crack initiation point. The curve has its decreasing branch (softening branch). Fibre reinforced concrete materials can have different response to the tension load depending on volume and material of used fibres in the concrete mixture. Graph 4 shows response to tension load with various fibres types in concrete.



**Graph 4:** Difference in material response to tensile load with steel fibres [9]

The difference of stress distribution in a cracked plain concrete and cracked fibre reinforced concrete is shown in Figure 23. In the plain concrete the stress has a steep slope and reaches its limit at the end of the crack, where the stress has value of the tensile strength limit of the cementitious matrix or concrete  $f_t$ . The stress in the fibre reinforced concrete has an almost uniform distribution along the crack. The concrete matrix reached its limit, but the fibres are intersecting the crack and carry out the stress. The steep slope is in the area, where the tensile strength limit  $f_t$  has been reached.



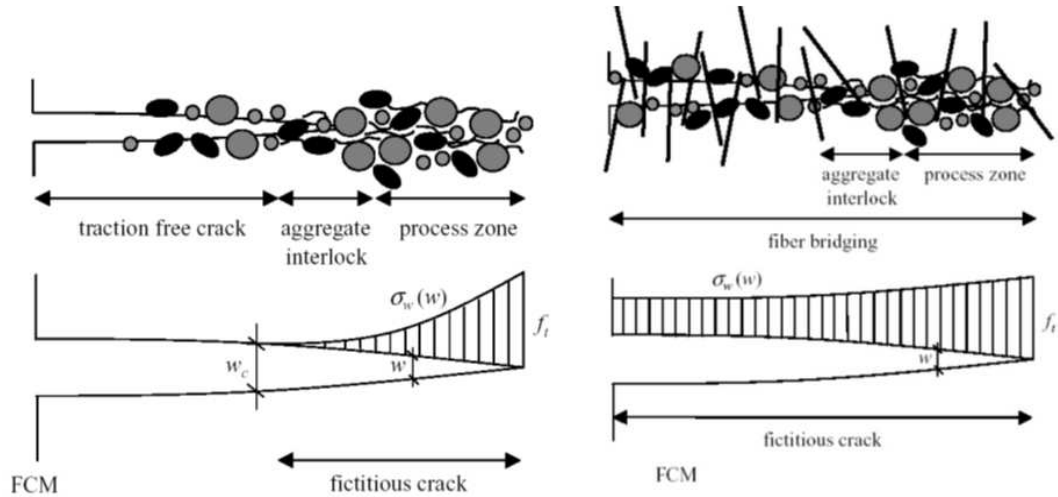


Figure 23: Difference in cracked plain/fibre concrete [12]

The addition of the fibres can improve the fracture energy  $G_f$  of such ultra-high performance fibre reinforced concretes (UHPC) by several orders of the magnitude. The fracture energy is influenced by numerous variables which include the fibre and matrix properties, their bonding behaviour and the average number of the fibres crossing the crack. Assuming steel fibres with a high strength and ductility are used, the fracture energy of UHPC can be enhanced:

- by improving the physico-chemical bond through higher matrix strength and packing density
- by improving the mechanical bond through deformed steel fibres
- by increasing the amount of the fibres.

However the amount of the fibres is limited by the workability of the composite. A low workability may lead to air entrapment and decreased compressive strength, therefore optimisation of various parameters is needed in order to maximise the fracture energy of the composite in tension. Since the compressive failure is induced by splitting tensile cracks in the concrete, the addition of fibres is therefore expected to quell the explosive nature of compression failure of UHPC. [11]

Fracture energy  $G_f$  is defined as an amount of dissipated work  $W$  needed to generate a unit crack with two completely separated crack surfaces ( $A_{Lig}$ ); if the new crack area or fracture area, or ligament area is defined as  $A_{Lig}$  then:

$$G_f = \frac{W}{A_{Lig}} = \frac{\int_{\delta=0}^{\delta=\delta_u} F(\delta) d\delta}{A_{Lig}}, \quad (3)$$

where:  $F$  = load applied in tension;  $\delta$  = crack opening, and  $\delta_u$  crack opening up to complete separation. The evaluation of fracture energy of strain hardening fibre reinforced concrete un-notched specimens under direct tension requires the distinction between the energy dissipated during strain hardening  $G_{f,A,n}$  and the energy dissipated during softening  $G_{f,B}$  per unit ligament area. Figure 24 and Figure 25 show definition of fracture energy and its calculation.



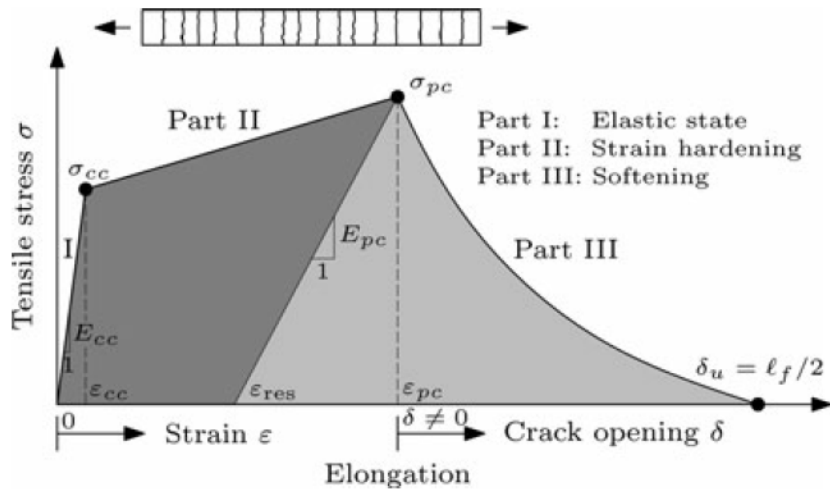


Figure 24: Definition of energy per unit volume  $g_f$  and per unit area <sup>[11]</sup>

The energy per unit area  $G_{f,A,n}$  dissipated during strain hardening depends on the gauge length  $L_g$  used in measuring strain, and represents the energy needed to generate  $n_{cr}$  cracks with a permanent crack opening,  $\delta_{pc}$ . The ratio  $L_g/n_{cr}$  defines the average crack spacing,  $s_{cr}$ , assuming that within  $L_g$  an evenly distributed crack pattern is generated for a given composite. Thus the relative fracture energy  $g_f$  per unit gauge length can be defined as described below. This type of energy per unit volume is only related to strain hardening materials and allows an objective comparison of the strain hardening performance of different composites. Reaching the peak stress or post-cracking strength,  $\sigma_{pc}$ , initiates the crack opening of one major crack, defined as the critical failure crack, and leads to the softening behaviour of the material. A determination of residual strain  $\varepsilon_{res}$  as well as stiffness at peak load  $E_{pc}$  is needed to calculate the energy  $G_{f,B}$ , which represents the energy per ligament area to separate the major crack starting from a residual crack opening of  $\delta_{pc}$  <sup>[11]</sup>.

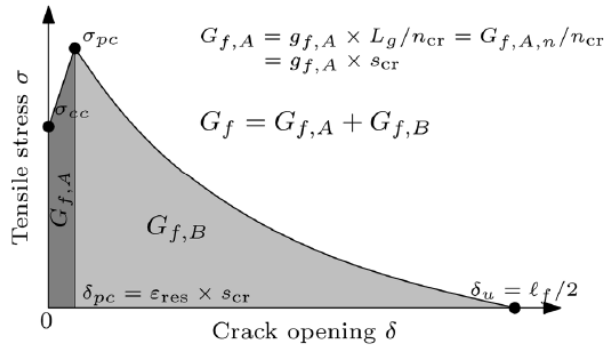
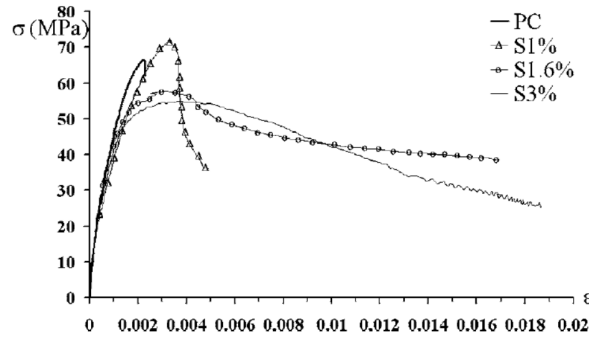


Figure 25: Definition of fracture energy  $G_f$  <sup>[11]</sup>

### 2.2.2.2 Material Response to Compressive Load

Ultra-high performance concretes (UHPC) are characterised by a very high packing density. This leads to ultra-high compressive strength, which results in an explosive failure in compression, and a very brittle failure in tension <sup>[10]</sup>. Classical plain concrete does not have a compressive strength limit  $f_c$  greater than 50MPa. The UHPC can have a compression strength limit more than 100 MPa depending on selected mixture and fibres properties.

Compressive tests of this type of material also show strain hardening and softening behaviour. The strain hardening is not very significant as it is in tensile response. This is caused by the fact that fibres are compressed and shortened, but they help to overcome cracking of concrete in another direction. The typical failure of material in uniaxial compression is caused by Poisson's effect. Specimen starts to crack in lateral direction to applied load and therefore it collapses or explodes. The fibres can carry out the lateral tensile stresses, therefore tested sample can show a small hardening or the compressive strength limit can have a higher value.

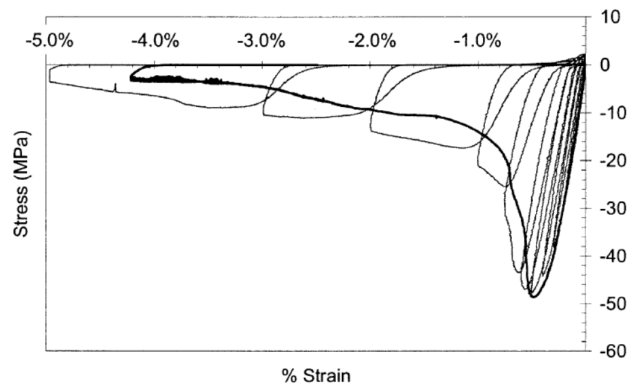


**Graph 5:** Difference in stress-strain curve for plain and fibre concrete <sup>[13]</sup>

Graph 5 shows different stress-strain curves of cylindrical specimens with and without fibres. Graph 5 also shows the response to compressive stress with different volume of fibres in the concrete mixture. PC means plain concrete and S1% - S3% mean volume of steel fibres in the concrete mixture.

### 2.2.2.3 Material Response to Cyclic Load

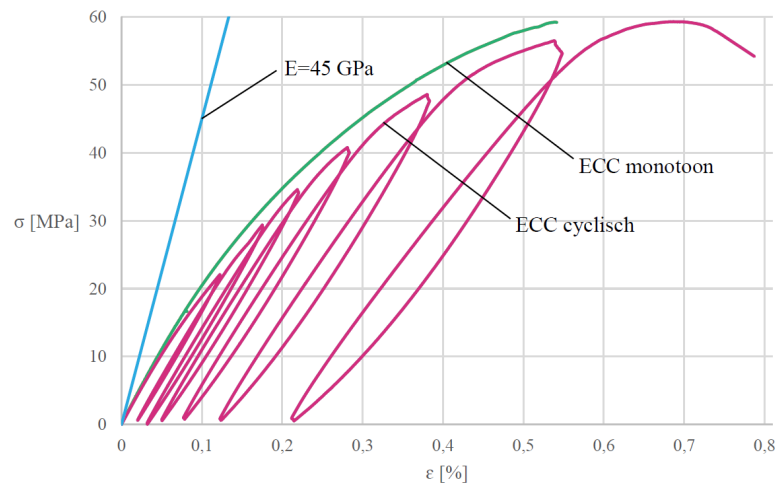
Cyclic load is a repetitive load applied on a structure. The cyclic load can have same magnitude or magnitude can change itself during the applied time period. Bridges are mainly exposed to the traffic load, which are caused by passing vehicles. The passing vehicles are loading and unloading the structure in cycles. These cycles can expose the structure to tensile and compressive stresses during one cycle, therefore it should be taken a closer look on a material response to this kind of the load. The material response to a monotonic compressive load was mentioned in subsection 2.2.2.2. The response to a cyclic compression is different, but some similarities can be found in a stress-strain diagram. Comparison of these two different loading schemes was done by K. E. Kesner and S. L. Billington <sup>[14]</sup> and G. Dilsiz <sup>[8]</sup>.



**Graph 6:** Monotonic and cyclic response of UHPFRC <sup>[14]</sup>

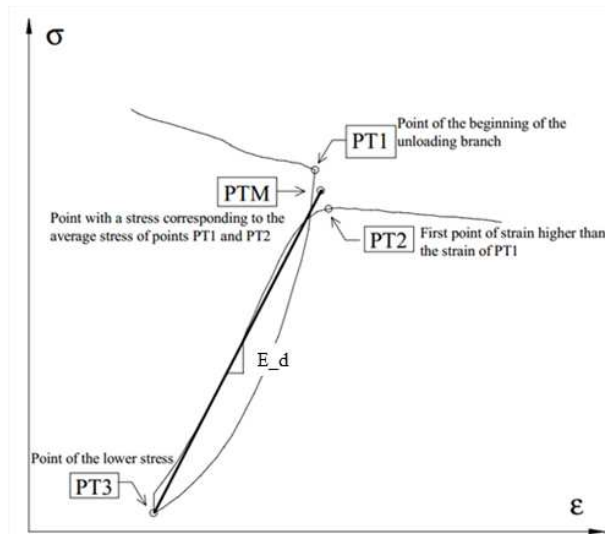
When the tested specimen is exposed to the monotonic load, the stress-strain curve has continuous shape. The measured strain grows constantly during the test until total collapse of the specimen. The cyclic stress-strain curve shows cycles of reloading during the test. The residual strain is clearly visible after a first cycle. This residual strain depends on a loading scheme and gets higher values after reaching higher compressive stress in the specimen. In study [14] by K. E. Kesner and S. L. Billington the cyclic compressive testing involved loading and reloading to strain levels from 0.1 to 5 %. The tested specimens were cylinders with a 50 mm diameter and 100 mm height. The stress-strain curve shows linear unloading until reaching compression peak. After reaching this point the unloading showed the parabolic shape. The parabolic unloading is consequence of the permanent deformation that occurred while the material was softening in compression. This response of reloading can be found in Graph 6.

The Graph 6 shows monotonic and cyclic load scheme. The tensile stress was necessary to reach strain 0% after a compressive load. The same comparison for cyclic and monotonic was made by G. Dilsiz. The test samples were prisms with dimensions 40 mm × 40 mm × 160 mm. The measured force was divided by cross sectional area to obtain stress. The strain was derived by dividing measured elongation with original length of LVDT. Dilsiz compares his monotone and cyclic results to a referent curve with modulus of elasticity  $E = 45$  GPa. Both curves starts to have a nonlinear behaviour after reaching stress around 20 MPa. The results of tests are shown in Graph 7. In Graph 7 are three curves of material behaviour: blue –  $E = 45$  GPa as a reference curve, green – ECC response to monotone load and red – ECC response to cyclic load.



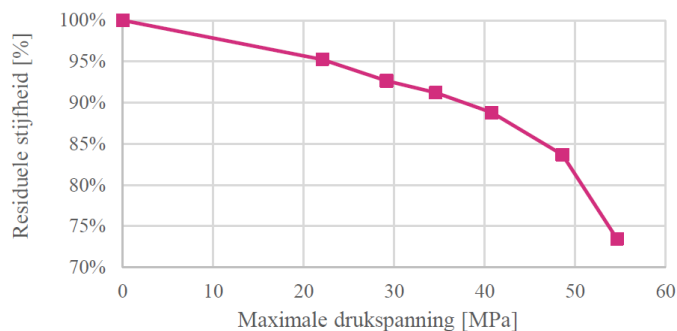
**Graph 7:** Comparison of monotone, cyclic and reference stress-strain curve <sup>[8]</sup>

The test results reflect the residual strain that greatly increase with stress close to the compression strength limit. Dilsiz in his study measured damaged modulus of elasticity  $E_d$  and found relationship between residual stiffness and maximal compressive stress applied on a tested specimen. The residual stiffness is damaged modulus of elasticity  $E_d$  divided by elastic modulus of elasticity  $E$ . The damaged modulus of elasticity was calculated from a cyclic stress-strain curve. The calculation of the  $E_d$  can be found in Graph 8.



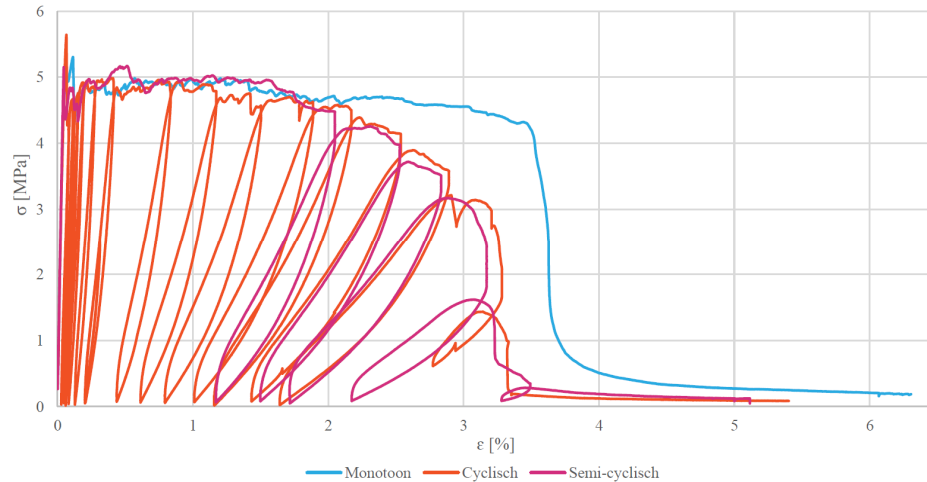
**Graph 8:** Calculation of damaged modulus of elasticity  $E_d$  [8]

Graph 9 shows curve of residual stiffness. The residual stiffness  $E_d/E$  decreases with increasing compressive stress. The curve for a residual stiffness starts at 70 % not at 0 % this should be noticed for a right interpretation of results. In Graph 9 "Residuele stijfheid" means residual stiffness and "Maximale drukspanning" means maximum compressive stress.



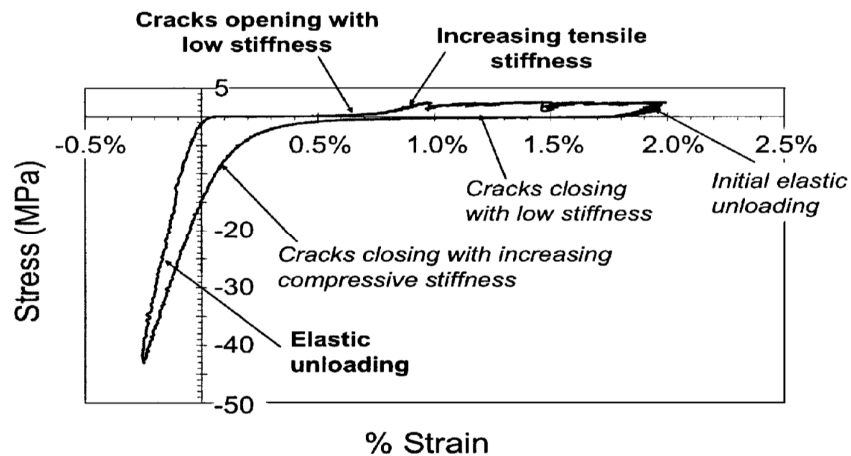
**Graph 9:** Relationship between residual stiffness and compressive stress [8]

Material response in a cyclic tensile test is similar to monotone tensile test. The tested samples had shape of a dog bone with cross sectional area  $20 \times 50 \text{ mm}^2$ . Four LVDT's were used to measure elongation of a specimen. The strain was calculated as an average elongation divided by original length of LVDT. Results from the cyclic tensile test also showed the strain hardening behaviour and tested sample collapsed after major crack initiation. The cyclic tensile test had also the residual strain. The residual strain gets higher value after a crack formation in strain hardening region. The residual stiffness of the tested specimen is also clearly visible and decreases with number of cycles. The same procedure of calculation of the damaged modulus of elasticity was preserved as in the compressive cyclic test. Stress-strain curves of cyclic ("Cyclish"), semi-cyclic ("Semi-Cyclish") and monotone ("Monoton") tensile test can be found in Graph 10. Cyclic curved showed linear unloading for a noticeable number of cycles. Both curves of cyclic and semi-cyclic response showed a smaller fracture capacity than the monotone response. This fact is caused by repeatedly stretched fibres.



**Graph 10: Comparison of monotone, cyclic and semi-cyclic test** [8]

When a tested specimen is exposed to one complete cycle (from compressive to tensile stresses or reversely see Graph 11) the fibres in cracked area are stretched. All fibres want to return to their original length with whole specimen. The stretched fibres after couple of cycles cannot return into the original length, if the specimen reached critical strain. This is caused by permanent in-elastic elongation of the specimen and fibres. This effect can be called as residual strain. The whole specimen starts to act more likely as springs connected in series than as a compact sample. This physical explanation of this material behaviour can be found in Figure 26. Following equation shows strain calculation of cracked concrete sample.



**Graph 11: One complete cyclic of cyclic loading** [14]

$$\varepsilon = \frac{\Delta l}{l} = \frac{n \cdot w + \frac{n \cdot F \cdot w}{E_f \cdot A_f} + \frac{F \cdot l}{E_c \cdot A_c}}{l} \quad (4)$$

$n \cdot w$  is residual strain of fibers

$\frac{n \cdot F \cdot w}{E_f \cdot A_f}$  is elastic strain of fibers

$\frac{F \cdot l}{E_c \cdot A_c}$  is elastic strain of un-cracked (concrete) cross section

where:

- $\varepsilon$ : is total strain
- $F$ : is force applied on test sample
- $l$ : is original length of sample
- $\Delta l$ : is difference in length(measured elongation)
- $n$ : number of (micro) cracks
- $w$ : is stable crack width
- $E_f \cdot A_f$ : is a centric stiffness of fibers in cracked cross section
- $E_c \cdot A_c$ : is a centric stiffness of uncracked (concrete) cross section

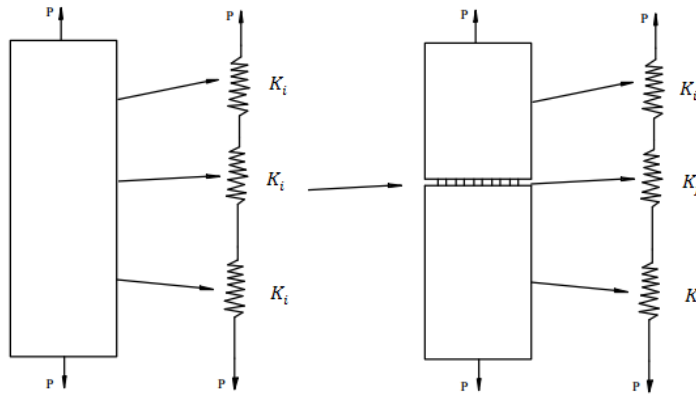


**Figure 26:** Physical explanation of material behaviour <sup>[9]</sup>

### 2.3 Composite Behaviour of Overlay and Steel Deck Plate

The stress reduction of the concrete overlay applied on the deck plate is very noticeable, but to be able to achieve this effect the composite connection between steel plate and concrete overlay has to be achieved. Composite behaviour between concrete overlays and steel deck plates is in most cases achieved by conventional mechanical fasteners. These fasteners can cause a stress concentration around them in the concrete overlay. These stress concentrations can cause cracking of the concrete overlay. The fabrication of fasteners the renovated bridge is time consumable and labour intensive. Therefore in recent years many studies had investigated the composite joint by adhesion. This behaviour was investigated by R. Walter <sup>[15]</sup>.

Walter, in his paper, describes mechanical behaviour of this kind of composite. In this paper the negative bending test was performed with three different kinds of fibre reinforced materials: steel-FRC with  $V_f = 1\%$  steel end hooked fibres, steel-FRD with  $V_f = 2\%$  steel and ECC with  $V_f = 2\%$  and PVA fibres. The negative bending moment was chosen because of structural behaviour of the orthotropic bridge. Test set up was a composite beam turned upside down and subjected to three point bending test. The composite beam consisted of a steel plate and cement-based overlay with a notch at the mid span, because the beams showed cracking in this area. The notch has 1/8 of beam height and is positioned there to be able measure crack opening and to ensure stable crack grow during the test. The cracking in the mid span is caused by bending moment, which reaches its maximum there. Crack opening and debonding between steel and concrete was observed during the tests. Crack width was monitored by microscope with a magnification of 200 times and the debonding was measured by two linear variable differential transformers (LVDT) placed 50 mm on both sides of loading point. The experimental set up can be found in Figure 27 and the real placing of LVDT shows Figure 28.

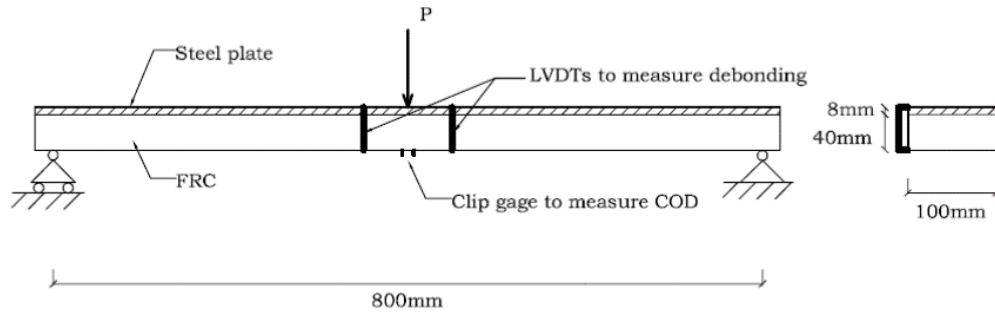


**Figure 27:** Experimental set-up for negative bending test <sup>[15]</sup>

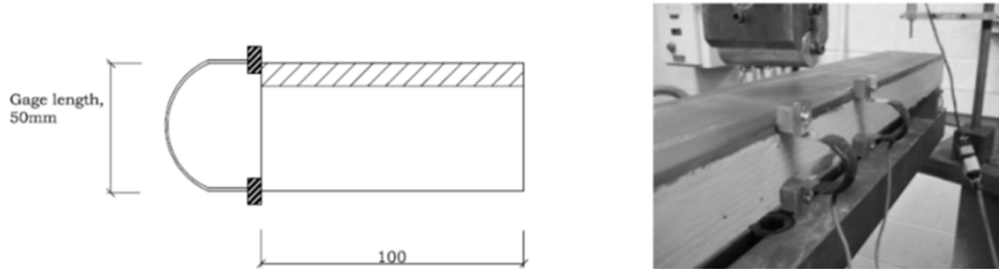


**Figure 28:** Placing of gage and picture of beam <sup>[15]</sup>

Materials ECC and FRD started to crack approximately around 2000 N, FRC had lower cracking limit of around 1000 N. ECC has showed increased load and deflection of tested beam until failure point.

Figure 29 shows test results the from three point bending test. The scale on the Y-axis is different to be able to compare results for all materials. Beam with ECC material showed two different fail mechanisms, localisation of a crack and reaching of the yield strain in the steel plate. Yielding of the steel plate will subsequently cause crack localisation in the ECC. In this study, yielding of the steel plate is the major failure mode and is taken into account. <sup>[15]</sup>

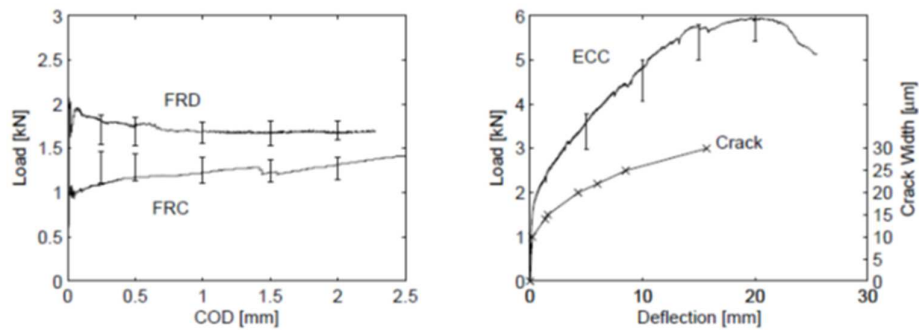


**Figure 29:** Experimental results from composite beam tests <sup>[14]</sup>

The first few cracks have formed at a low load level and as the beam was monitored during the whole experiment. Debonding of the overlay was measured by gages. Figure 29 shows measured debonding of all three tested composited beams. It should be noted the relation between deflection and debonding and that FRC and FRD materials started to debond in early stage of the test, but the ECC-steel connection remained intact until high deflection of the beam. ECC showed more ductile behaviour that FRC and FRD. Figure 29 shows illustrative and actual bending crack/debonding between the steel and the overlay material.

## 2.4 Three Point Bending Test – Crack Mouth Open Displacement Measurement

In the subsection 2.2.2.1, a material response to the tensile load was described. In this subsection the testing mechanism is described. To obtain the main parameters to describe strain softening/hardening behaviour is done by CMOD test. The crack mouth opening displacement measurement (CMOD) is three point bending test, where the crack width or deflection at the mid span of tested specimen are measured. The test is performed on a sample with specific dimensions. The test samples are prisms with a square cross section 150 mm × 150 mm and length from 550 mm to 700 mm. The specimen has also 25 mm notch in the mid span to ensure that the crack starts to grow, where measurement apparatus is placed. The test set up is shown in Figure 30.

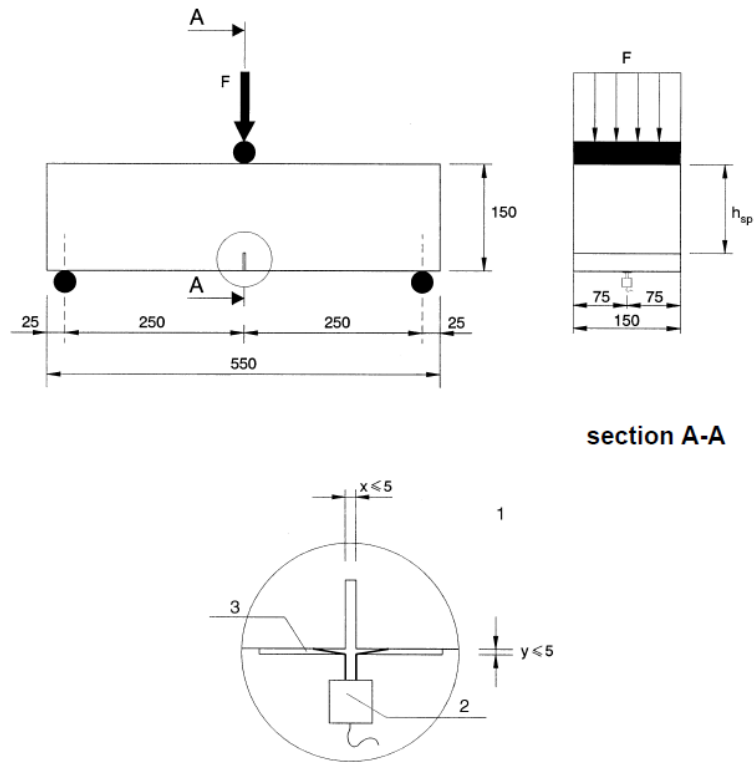


**Figure 30:** Three point bending test and detail of CMOD measurement set up <sup>[16]</sup>

The specimen is loaded with a force/load in the middle, which should produce a constant rate of the displacement. In this test two values can be measured: crack opening or deflection of the specimen. Crack opening is measured by clip gage at the bottom of the specimen. The clip gage measures the opening of the crack in a longitudinal direction. The deflection of the specimen has to be measured by tools, which can exclude deformations of the testing machine.

The standard for the CMOD test describes load rate for a controlled test. In case of a testing machine with controlling the increasing rate of CMOD, the machine should be operating on the constant rate with 0.05 mm/min. When CMOD = 0.1 mm, the machine changes constant rate to 0.2 mm/min. If the testing machine controls the rate of increasing deflection, the above testing procedure shall be applied provided that the CMOD related parameters are transformed into deflection related parameters.

The relation between CMOD and deflection  $\delta$  can be approximately calculated:

$$\delta = 0.85 \cdot CMOD + 0.04, \quad (5)$$



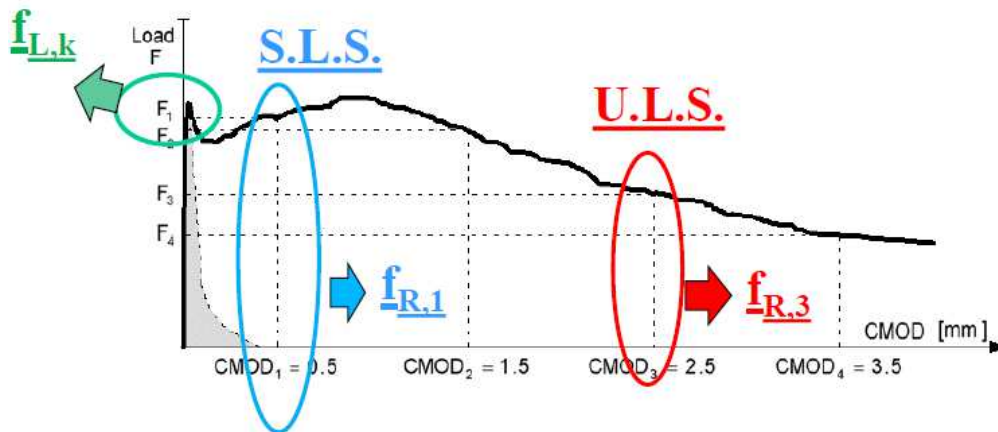
The output of the CMOD test done can be a Load-CMOD diagram or Load-Deflection diagram depending on chosen measurement procedure during the test. These graphs have to be transformed into constitutive law and therefore get important values for numerical simulations or design of structure. From these measured values (force  $F$  and deflection  $\delta$ ), equivalent stress values are calculated at important points of  $F$ -CMOD graph and results are transformed into Stress-CMOD diagram. The stress values of the important points are marked on Graph 12 and can be calculated by following equation:

$$f_{R,j} = \frac{3 \cdot F_j \cdot l}{2 \cdot b \cdot h_{sp}^2}, \quad (6)$$

where:

- $f_{R,j}$  is the residual flexural tensile strength corresponding with  $CMOD = CMOD_j$
- $F_j$  is the load corresponding with  $CMOD = CMOD_j$
- $l$  is span of tested specimen [mm]
- $b$  is the width of tested specimen [mm]
- $h_{sp}$  is the distance between the notch tip and the top of the specimen [mm].

The important points where the stress is calculated are: " $f_{L,k}$ " which is limit of proportionality, " $f_{R,1}$ " which is stress limit, where a major crack starts to form itself, this point is at  $CMOD = 0.5$  and " $f_{R,3}$ " is the ultimate tensile stress limit of tested specimen. In the CEB-FIB model code 2010 there is fully described procedure of derivation of the important points from measured values.



**Graph 12:** CMOD test output with marked important points <sup>[12]</sup>

These calculated equivalent stresses, for each important point mentioned in Graph 12, are fictitious and therefore they have to be transferred into constitutive law in tension. Transformation is done for three points mentioned in Graph 12 i.e.  $f_{L,k}$ ,  $f_{R1,k}$  and  $f_{R3,k}$ . The meaning of transformation is described in Graph 13. Based on the results of transformation the behaviour of material can be characterised as a post crack-softening or hardening.

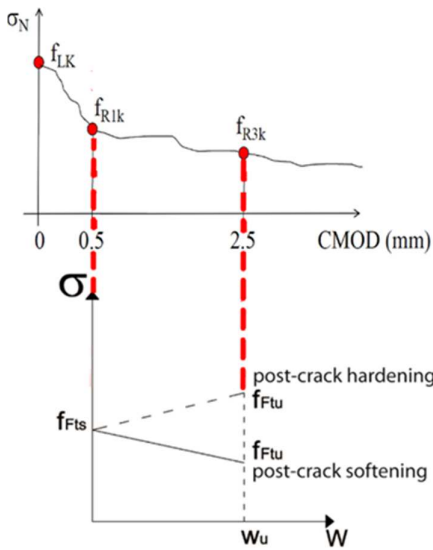
The following equations show transformation according to CEB-FIB model code 2010:

$$f_{ct} = 0.42 \cdot f_{L,k} \quad (7-9)$$

$$f_{Fts} = 0.45 \cdot f_{R1}$$

$$f_{Ftu} = 0.5 \cdot f_{R3} - 0.2 \cdot f_{R1}$$

In Graph 13 value  $w_u$  represent maximum crack opening for ULS – ultimate limit state in tension. These values of  $f$ - $w$  curve can be used in the most FE software. Most types of software and standards use stress-strain diagrams and therefore the final transformation of measured values has to be done. The strain of the tested specimen is important value, which shows accurate deformation of the specimen and is obtained from rotational equilibrium. The calculation of strain is shown in Figure 31.



**Graph 13:** Transformation from  $f$ - to constitutive law <sup>[12]</sup>

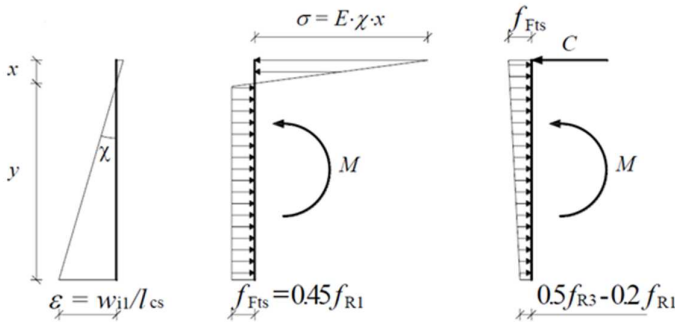


**Figure 31:** Simplified model for ULS in uniaxial tension <sup>[12]</sup>

The total strain in tension of the specimen is calculated by:

$$\varepsilon_{tot} = \frac{w_{il}}{l_{cs}} \text{ where } l_{cs} = \min\{s_{rm}, y\}, \tag{10}$$

where:

- $\varepsilon_{tot}$  is total strain of specimen
- $w_{il}$  is measured crack opening in important points
- $s_{rm}$  is distance between cracks in specimens with steel reinforcement
- $y$  is height of the crack (from edge of specimen to the end tip of the crack)

Explanation of the equation 10 can be found in Figure 32.

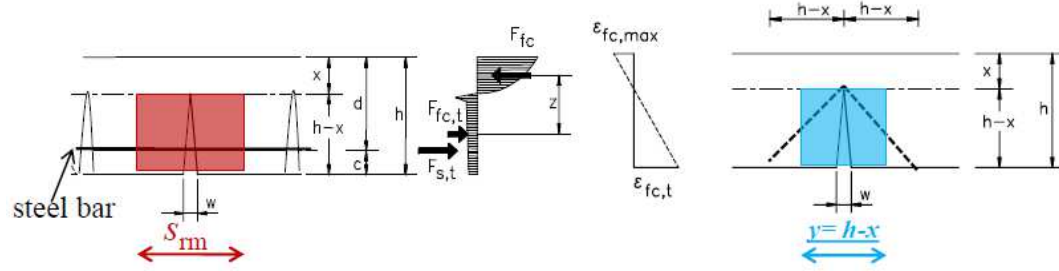


Figure 32: Explanation of the calculation of strain <sup>[12]</sup>

### 3. Numerical Model

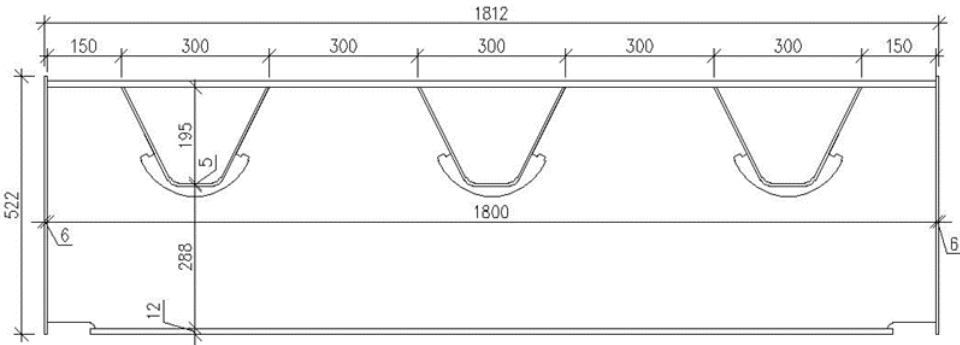
A finite element (FE) model has been made to be able investigate the influence of different types of HPC overlays on the stress reduction effect in the steel deck plate of an orthotropic bridge deck. The numerical model is made in a commercial FE software Abaqus/CAE version 6.14. This software is a very efficient tool for monitoring, diagnosing and visualising advanced analyses. The intuitive interface integrates modelling, analysis and results visualisation into an easy-to-use environment. Users can create geometry, import CAD models for meshing, or integrate geometry-based meshes that do not have associated CAD geometry.

The open customisation toolset of Abaqus/CAE provides a powerful process automation solution, enabling specialists to deploy proven workflows across the engineering enterprise. Abaqus/CAE also offers comprehensive visualisation options, which enable users to interpret and communicate the results of any Abaqus analysis.

#### 3.1. Dimensions

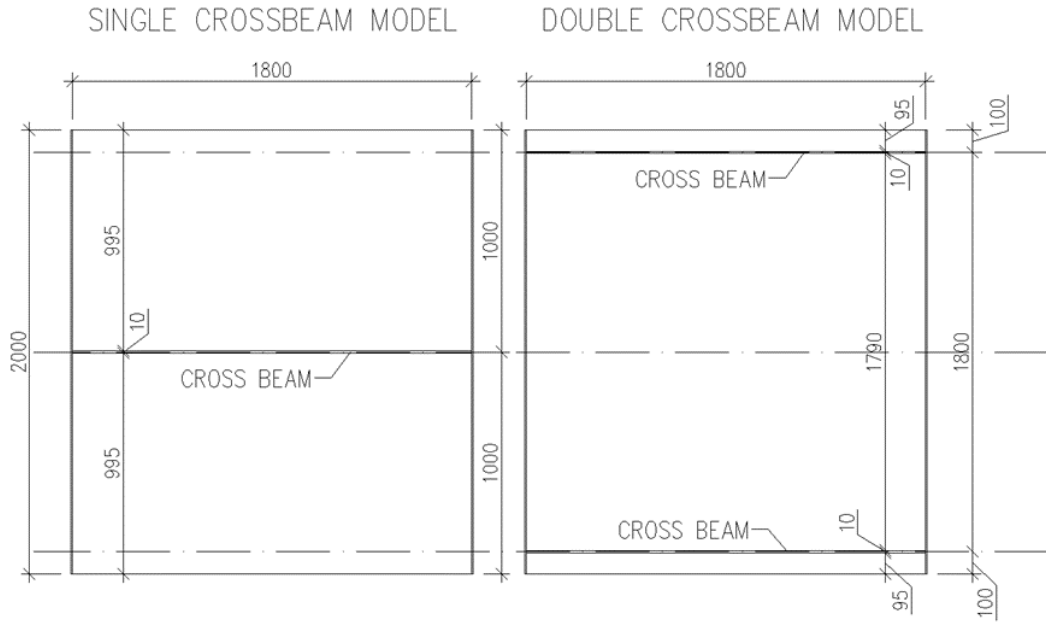
As mentioned in the sections 1.2, the transversal stiffeners are welded to the deck plate in distance from 1.5 m to 3 m. The stress value under the local wheel load has different values, when wheel load is in the position above the stiffener, respectively in the middle position between two transversals stiffeners. This has been taken into account and two numerical models were made. Results from both of them were compared. Both models have same dimensions of each part, but differ in number of the stiffeners.

The studied bridge decks are 1.8 m wide and 2.0 m long with a deck plate with a thickness 12 mm. Models have three trapezoidal longitudinal troughs. The troughs are 300 mm wide and 200 mm height with wall thickness 5 mm. The crossbeams have cross section of half I-profile with a thickness 10 mm and they are connected in the middle of the deck plate (single crossbeam model), respectively in range of 1.8 m between them (double crossbeam model). The supporting girders have dimensions 6 mm × 522 mm and they are connected to the deck plate and to crossbeams.



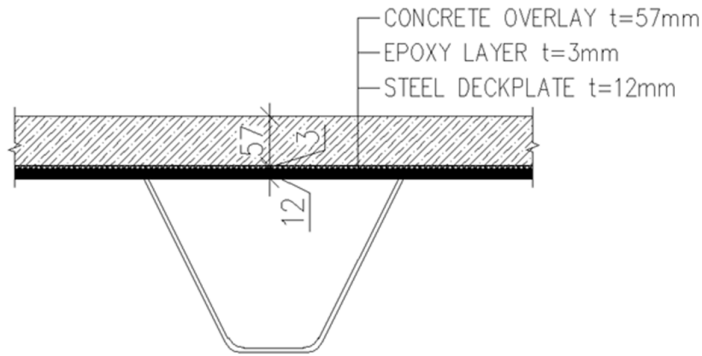
**Figure 33:** Cross section of studied bridge deck

Figure 33 shows the dimensions of each part and cross section of studied bridge deck, which are same for both models. The differences in the models are shown in Figure 34. The cross beam is connected exactly in the middle of the deck plate in single crossbeam model. The first crossbeam is connected to the deck plate at position 100 mm from the edge on both opposite sides in the double crossbeam model. The distance between them is 1800 mm.



**Figure 34:** Difference between single and double crossbeam model

Both variations of numerical models were calculated with and without HPC overlay. On the top of the steel deck plate an epoxy layer with a thickness 3 mm was applied. The concrete overlay with thickness 57 mm was applied above the epoxy layer. This is shown in Figure 35. The overlay differs in a material properties. The epoxy layer is applied on the steel deck plate to provide composite connection between the steel deck plate and the concrete overlay.



**Figure 35:** Cross section of deck plate

Reinforcement mesh has been also modelled in the concrete overlay to find out, if the reinforcement has some influence on the stress reduction in the investigated weld joint. The mesh of reinforcement is made from steel bars with a diameter 12 mm, with a distance 75 mm × 75 mm. The total area of reinforcement in transversal direction  $A_{s,x} = 1526,85 \text{ mm}^2/\text{m}^2$  and in longitudinal direction  $A_{s,y} = 1445,16 \text{ mm}^2/\text{m}^2$ . The reinforcement is used for both models and for every type of the overlay.

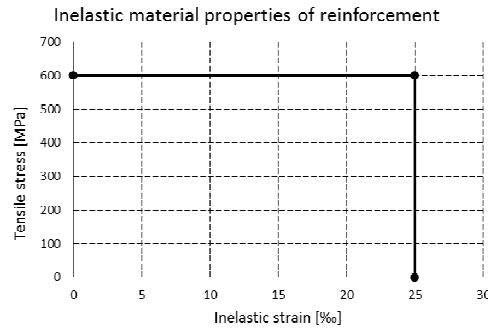
## 3.2. Material Characteristics

### 3.2.1. Material Characteristics Used for Bridge Parts

Steel parts of the bridge have a linear-elastic behaviour, because it is assumed that, the stress in steel parts of the bridge is not higher than the yield stress of the steel used. The difference in behaviour between structural and reinforcement steel has been taken into account. Value of E-modulus for steel parts is 210 GPa, Young's modulus for reinforcement has value 200 GPa. Steel for reinforcement embedded in concrete overlay has a standard behaviour of steel for the reinforcement defined as a bilinear-elastic with a plastic branch. The input material parameters are summed up in Table 5 and the bilinear behaviour of reinforcement steel is shown in Graph 14.

**Table 5:** Linear elastic behaviour of used materials

Material	Young's modulus [MPa]	Poisson's ratio [-]
Steel	210 000	0.3
Reinforcement	200 000	0.3
Epoxy	2 000	0.45



**Graph 14:** Inelastic behaviour of reinforcement steel

### 3.2.2. Concrete

In section 3.1 are mentioned three different materials used for concrete overlay. In FE software Abaqus, input of linear elastic behaviour is made by Poisson's ratio and Young's modulus. Material PAV360 has Young's modulus  $E = 17$  GPa and both CONTEC and REFOR materials had same modulus of elasticity  $E = 35$  GPa. All these concrete material has same value of Poisson's ratio which is 0.2. Table 6 sums up linear elastic mechanical behaviour of used concrete materials.

**Table 6:** Linear elastic material properties of used concrete <sup>[18]</sup>

Material	Young's modulus [MPa]	Poisson's ratio [-]
PAV360	17 000	0.2
CONTEC	35 000	0.2
REFOR	35 000	0.2

The concrete for overlay had three various types of high performance concrete: PAV360, CONTEC and REFOR. Material characteristics of each concrete were determined from test samples in master thesis "Studie van verschillende types hoogperformante vezelversterkte betonoverlagingen voor bestaande dunne stalen rijvloeren 2015" written by Jan Bekaert and Bert Vanthournout <sup>[18]</sup>. Material PAV360 has polyvinyl alcohol (PVA) fibres with total volume of fibres in mixture  $V_f = 1.5\%$ , CONTEC has steel fibres with total

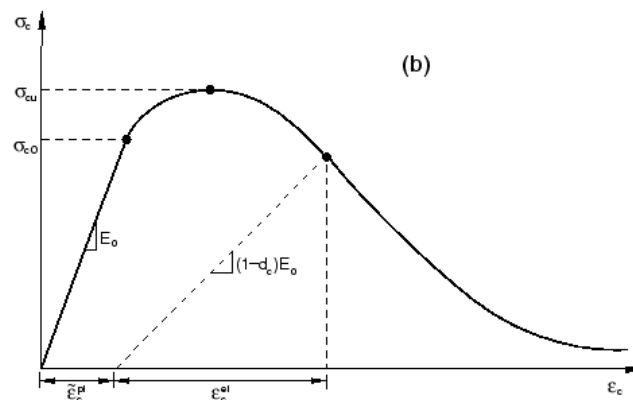
volume of fibres in mixture  $V_f = 3.0 \%$  and REFOR has PVA fibres with total volume of fibres in mixture  $V_f = 4.6 \%$ .

These types of materials are characterised by post crack hardening. Various material models can be used to simulate this material behaviour of the concrete with strain hardening or softening. In this study it was used a material model called Concrete Damaged Plasticity in the finite element software Abaqus. Two main failure mechanism are expected: crushing of concrete in compression and cracking of concrete in tension. The concrete damaged plasticity model in Abaqus can be described with following properties:

- provides a general capability for modelling concrete and other quasi-brittle materials in all types of structures (beams, trusses, shells, and solids);
- uses concepts of isotropic damaged elasticity in combination with isotropic tensile and compressive plasticity to represent the inelastic behaviour of concrete;
- can be used for plain concrete, even though it is intended primarily for the analysis of reinforced concrete structures;
- can be used with rebar to model concrete reinforcement;
- is designed for applications in which concrete is subjected to monotonic, cyclic, and/or dynamic loading under low confining pressures;
- consists of the combination of non-associated multi-hardening plasticity and scalar (isotropic) damaged elasticity to describe the irreversible damage that occurs during the fracturing process;
- allows user control of stiffness recovery effects during cyclic load reversals;
- can be defined to be sensitive to the rate of straining;
- requires that the elastic behaviour of the material be isotropic and linear. [17]

### 3.2.2.1 Uniaxial Compressive Behaviour

Under uniaxial compression the response is linear until the value of initial yield stress  $\sigma_{c0}$ . In the plastic regime the response is typically characterised by stress hardening followed by strain softening beyond the ultimate stress  $\sigma_{cu}$ . This representation, although somewhat simplified, captures the main features of the response of concrete [17].



**Graph 15: Response of concrete in uniaxial compression** [17]

Graph 15 shows response of concrete in uniaxial tension, and shows inelastic strain which is reached after appearing of first crack in concrete.  $\sigma_{cu}$  is value obtained from compression test. Graph 15 also shows calculation of damaged modulus of elasticity in compression and shows calculation of stress in cracked concrete. Calculation of

damaged modulus of elasticity in compression is done by damage parameter  $d_c$  and can take values from 0 to 1. Zero represents undamaged material and one represent total loss of strength. The damage parameter can be defined as a tabular function of either cracking strain or cracking displacement. The  $E_d$  is calculated by equation:

$$E_d = (1 - d_c) \cdot E_o \quad (11)$$

In the master thesis of J. Bekaert and B. Vanthournout, compressive tests for each type of material used for concrete overlay has been performed. Compressive tests have been performed on a cube with dimensions 150 mm × 150 mm × 150 mm with three samples of each material. From these three tests experimental values were obtained. The experimental values have been interspersed with best-fit curve to get an average value of the modulus of elasticity. Measured stress and modulus of elasticity has been compared with product sheet. Hooke's law equation was used to calculate modulus of elasticity.

$$\sigma = E \cdot \varepsilon \Rightarrow E = \frac{\sigma}{\varepsilon}, \quad (12)$$

where  $\sigma$  is measured compressive stress [MPa] and  $\varepsilon$  is measured elastic strain [‰].

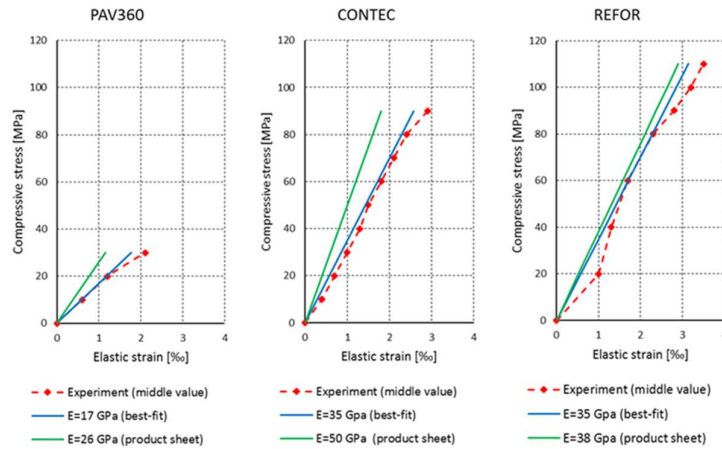


**Figure 36:** Comparison of compressive behaviour <sup>[18]</sup>

Figure 36 compares all three compressive tests and show the difference in declared material characteristics by producer and measured values of each material. It also shows that the PAV360 has the lowest modulus of elasticity only 17 GPa. Both CONTEC and REFOR have same values of the E-modulus 35 GPa.

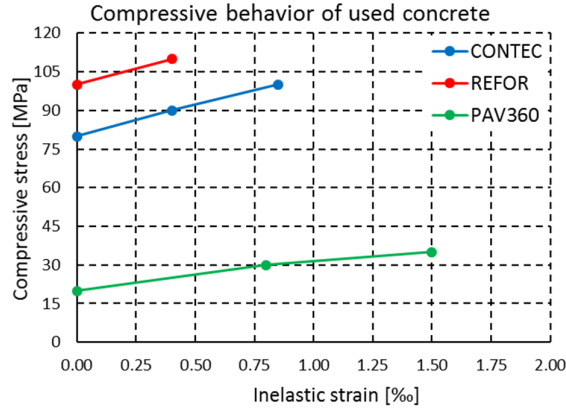
These compressive tests were done to obtain modulus of elasticity and maximal compressive stress. The software Abaqus needs input of an inelastic compressive behaviour of a concrete. The inelastic strain is calculated as a difference between an experimental measured strain and calculated theoretical strain. Table 6 shows input values for inelastic compressive behaviour of concrete in software Abaqus.

**Table 7:** Abaqus input files of compressive behaviour <sup>[18]</sup>

PAV360			CONTEC			REFOR		
Compressive stress [MPa]	Inelastic strain		Compressive stress [MPa]	Inelastic strain		Compressive stress [MPa]	Inelastic strain	
	[-]	[‰]		[-]	[‰]		[-]	[‰]
20	0.00000	0	80	0.00000	0.00	100	0.00000	0.00
30	0.00080	0.8	90	0.00040	0.40	110	0.00040	0.40
35	0.00150	1.5	100	0.00085	0.85			

Difference of inelastic compressive behaviour is shown in Graph 16.

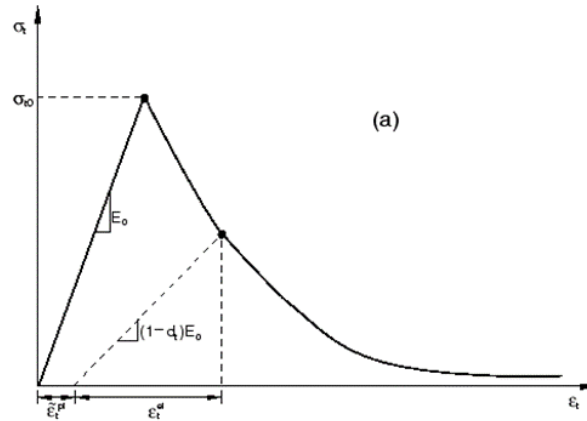




**Graph 16:** Comparison of inelastic compressive behaviour <sup>[18]</sup>

### 3.2.2.2. Uniaxial Tensile Behaviour

Under uniaxial tension the stress-strain response follows a linear elastic relationship until the value of the failure stress,  $\sigma_{(t,0)}$  is reached. The failure stress corresponds with the onset of micro-cracking in the concrete material. Beyond the failure stress the formation of micro-cracks is represented macroscopically with a softening stress-strain response, which induces strain localisation in the concrete structure. <sup>[17]</sup>



**Graph 17:** Response of concrete to uniaxial tension <sup>[16]</sup>

Graph 17 shows response of concrete in uniaxial tension, and shows inelastic strain which is reached after appearing of first crack in concrete.  $\sigma_{(t,0)}$  is value obtained from the CMOD-test. Graph 17 also shows calculation of damaged modulus of elasticity in tension and shows calculation of stress in cracked concrete. Calculation of damaged modulus of elasticity in tension is done by damage parameter  $d_t$  and can take values from 0 to 1. Zero represents undamaged material and one represent total loss of strength. The damage parameter can be defined as a tabular function of either cracking strain or cracking displacement. The  $E_d$  is calculated by the equation:

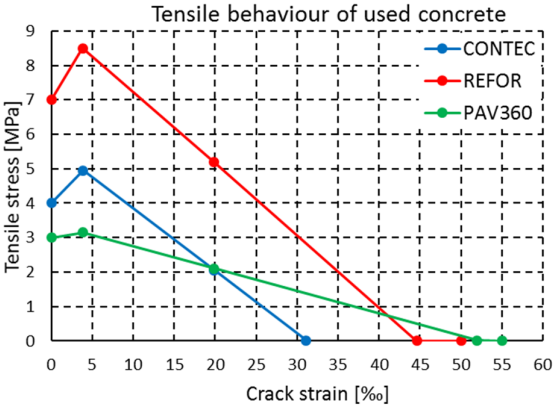
$$E_d = (1 - d_t) \cdot E_o \quad (13)$$

The tensile characteristics and post crack behaviour has been obtained from a CMOD test. Tested samples had dimensions 150 mm × 150 mm × 600 mm with 25 mm notch in the mid span of tested specimens. The test was performed as an opposite three point bending test. A non-moveable support was in the middle and two supports at the ends were moving against the middle support with constant speed. The important values has been calculated as it is mentioned in subsection 2.4 Three Point Bending Test – Crack

Mouth Open Displacement Measurement. Table 8 sums up material input for software Abaqus and Graph 18 compares strain-hardening behaviour of concrete in tension.

**Table 8:** Abaqus input values of tensile behaviour [18]

PAV360			CONTEC			REFOR		
Tensile stress [MPa]	Crack strain		Tensile stress [MPa]	Crack strain		Tensile stress [MPa]	Crack strain	
	[-]	[%o]		[-]	[%o]		[-]	[%o]
3.00	0.0000	0	4.00	0.00000	0.00	7.00	0.00000	0.00
3.15	0.0039	3.9	4.95	0.00390	3.90	8.50	0.00382	3.82
2.10	0.0199	19.9	2.05	0.01990	19.90	5.20	0.01982	19.82
0.01	0.0520	52	0.02	0.03110	31.10	0.0075	0.04462	44.62
0.00	0.0550	55				0.00	0.05000	50.00

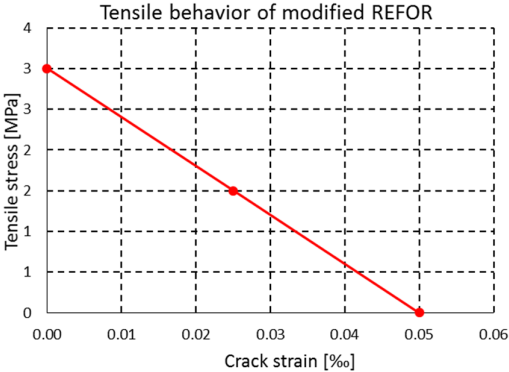


**Graph 18:** Difference of inelastic tensile behaviour [18]

To investigate the influence of concrete material without hardening branch, REFOR has been chosen. Modified REFOR material has material properties like plain concrete. REFOR material has been changed to have ultimate tensile strength only  $f_{ct} = 3 \text{ MPa}$  and not  $f_{ct} = 7 \text{ MPa}$ , this change has been done, because there is lower value of applied wheel load. Input values for software Abaqus can be found in Table 9 and in Graph 19.

**Table 9:** Input values of modified REFOR material

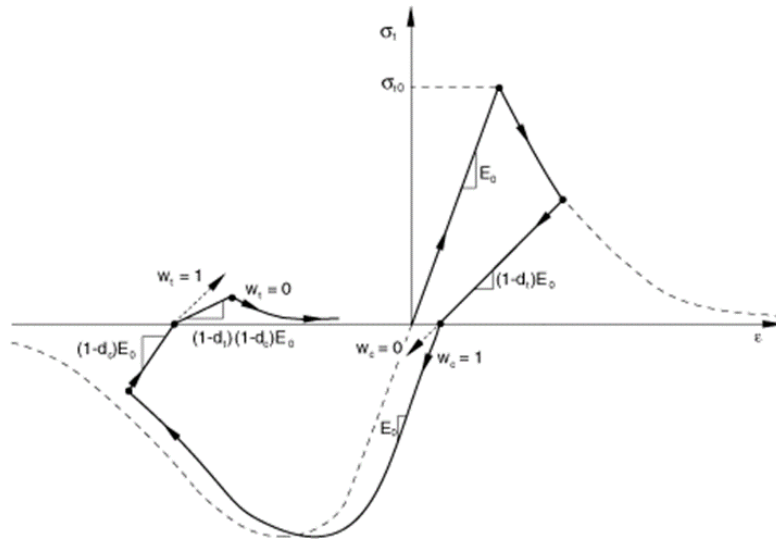
Modified REFOR		
stress [MPa]	Crack strain	
	[-]	[%o]
3.00	0.00E+00	0.00
1.50	2.50E-05	0.03
0.00	5.00E-05	0.05



**Graph 19:** Material behaviour of modified REFOR material

### 3.2.2.3. Uniaxial Cyclic Behaviour

Under uniaxial cyclic loading conditions the degradation mechanisms are quite complex, involving the opening and closing of previously formed micro-cracks, as well as their interaction. Experimentally, it is observed that there is some recovery of the elastic stiffness as the load changes sign during a uniaxial cyclic test. The stiffness recovery effect, also known as the “unilateral effect,” is an important aspect of the concrete behaviour under cyclic loading. The effect is usually more pronounced as the load changes from tension to compression, causing tensile cracks to close, which results in the recovery of the compressive stiffness. The concrete damaged plasticity model assumes that the reduction of the elastic modulus is given in terms of a scalar degradation variable  $d$  as where is the initial (undamaged) modulus of the material. [16]



**Graph 20: Uniaxial cyclic response of concrete** [17]

Graph 20 describes behaviour of material model under uniaxial cyclic behaviour. It should be noted when the cycle goes back and material is damaged by compression or tension the calculation of damaged modulus of elasticity  $E_d$  take into account both damage parameters  $d_c$  and  $d_t$ . The  $E_d$  is calculated by equation:

$$E_d = (1 - d_c)(1 - d_t) \cdot E_0 \quad (14)$$

### 3.3. Boundary Conditions and Load

The boundary conditions of the models were chosen to simulate real behaviour of the bridge deck. Models are supported by two linear boundaries in Z-direction, which has to simulate the support from the main girder. It is also supported in X and Y-direction, which has to prevent the model from moving or deforming in the direction of X and Y axis. The boundary conditions constrain only a displacement in each axis. The rotations were allowed. Boundary conditions can be found in Figure 37-39.

VIEW IN X-AXIS

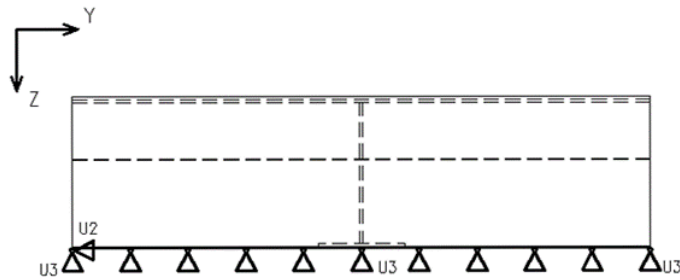


**Figure 37:** Boundary conditions of bridge deck model, view in X-axis

VIEW IN Y-AXIS

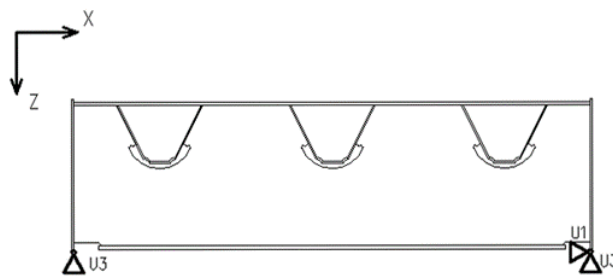


**Figure 38:** Boundary conditions of bridge deck model, view in Y-axis

VIEW IN Z-AXIS

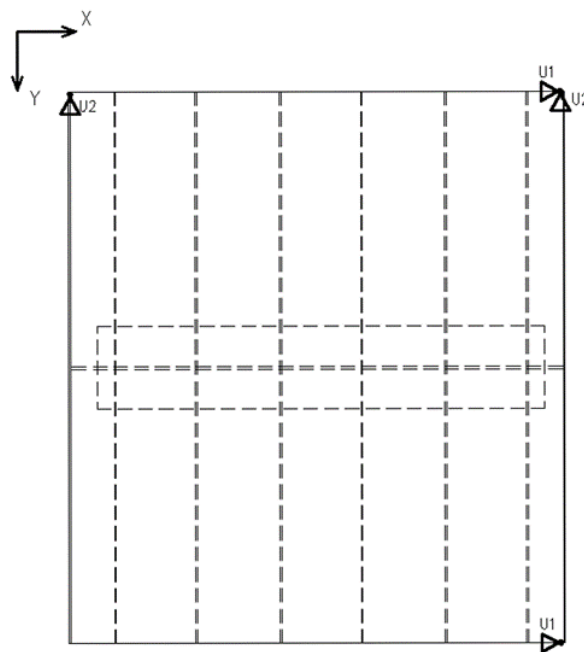


**Figure 39:** Boundary condition of bridge deck model, view Z-axis

All models were loaded with a same load, which represents one wheel from a truck. The load is changing position from the left to the right side of the bridge deck. The load of one wheel has magnitude 5 000 kg which is approximately 50 kN and it is applied on

a square area  $250 \times 250 \text{ mm}^2$ . 29 load cases were modelled in total. Load positions are showed in Figure 40 and in Figure 41.

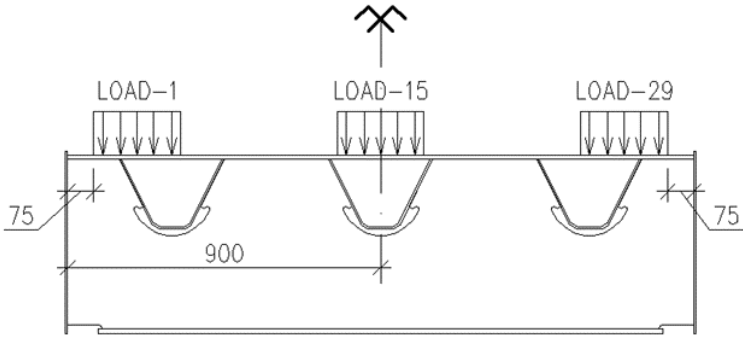


**Figure 40:** Load cases

The first one (LOAD-1) starts at position 75 mm from the edge, so distance to the centre of the load is 200 mm. The central position of each load case changes every 50 mm and load case 15 (LOAD-15) is exactly in the middle of the bridge deck, which is 900 mm from the edge to the centre of the load. The last load case (LOAD-29) has same position as LOAD-1, but on the opposite edge of the bridge deck, which is 75 mm from the edge and distance to the centre of the load is 200 mm.

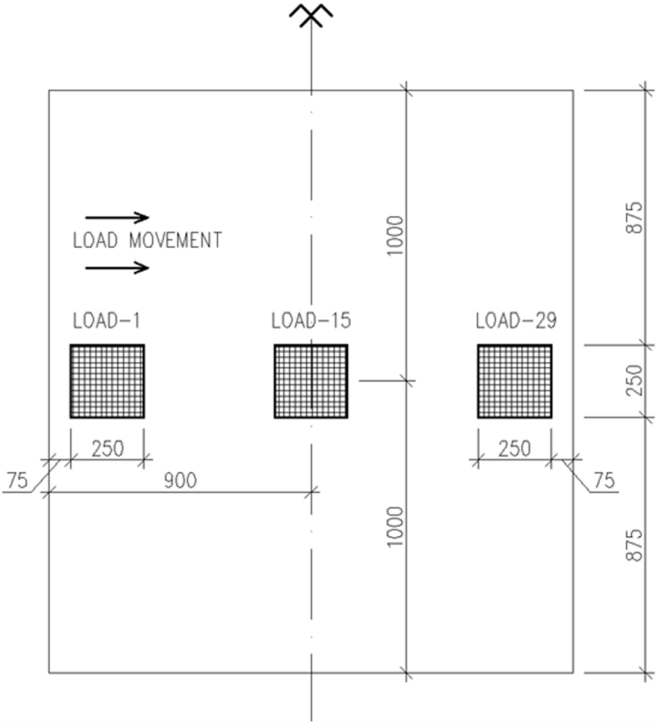


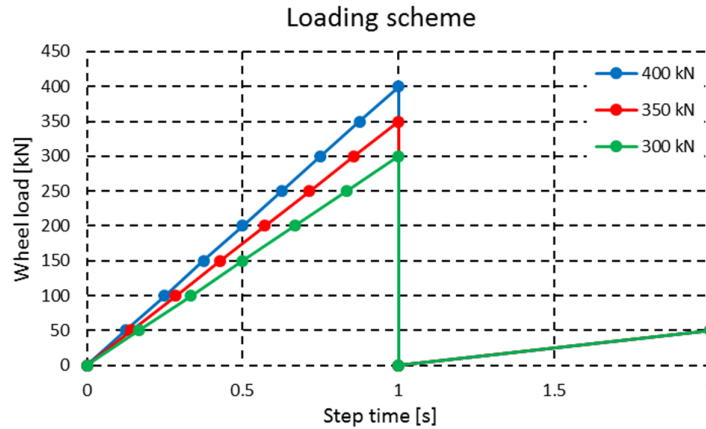
**Figure 41:** Position of load cases on the deck plate

Load cases are applied in the middle of each model and they are moving only in a transversal direction. These load cases were selected as a worst case scenario for the bridge. In reality the load from wheel can be on every position, but it is impossible to simulate an every available load position on the structure.

To simplified application of load on the model, it was used a shell strip, with length 1650 mm and width 250 mm, which is exactly same area where the load is moving. This part

has thickness 0.1 mm and has same material characteristic as steel for of the bridge deck.

Model was overloaded to see behaviour of the bridge deck with cracked overlay. In this case the load was applied at middle i.e. LOAD-15. To see influence of damaged overlay on the stress in the deck plate, model was loaded with following scheme: Overloaded, no load on the bridge and again normal/usual wheel load – 50 kN. Model was overload with 300 kN, 350 kN and 400 kN as an alternative for wheel load. Loading scheme is shown in Graph 21. In Graph 21 step time shows loading history and wheel load, which was divided into 50 kN increments to be able to investigate stress in equal increments of load for each load scheme.



**Graph 21:** Loading scheme for overloaded model

In all calculated models, only static loads were used. Environmental loads such as shrinkage or changing temperature have not been taken into account.

### 3.4. Mesh

The Software Abaqus offers many ways of meshing each part, depending on a chosen geometry and analysis. Meshing divides each part into a smaller elements. The selected mesh and its finest determines quickness of calculation and accuracy of results. There are several types of elements which can be divided into three categories: 1D - wire elements, 2D - planar elements and 3D - solid elements. Figure 42 shows commonly used element types based on geometry and analysis type.

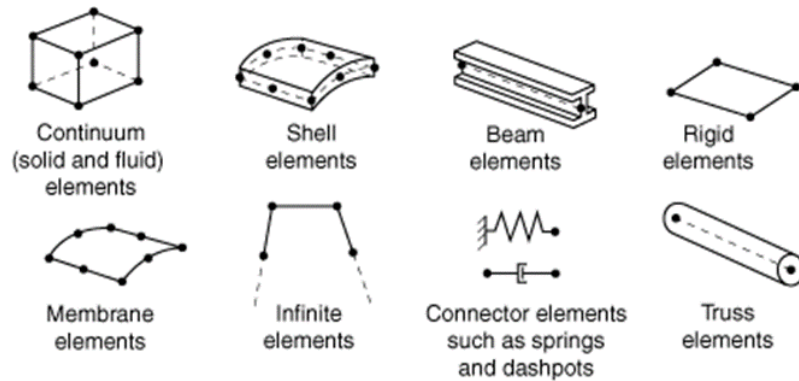


**Figure 42:** Different types of element in FE software ABAQUS/CAE <sup>[17]</sup>

The deformations, stresses and other parameters are calculated in each node of a chosen element. The magnitude of chosen parameter at other place in one element are

interpolated from nodal magnitude. For example the solid geometry: The user can choose linear element. Linear element has 8 nodes (on each vertex of brick), where parameters are calculated they using linear interpolation to obtain value at another point in the element. The second way is to use 20 nodes element, the node is also in the middle of the edge of the brick. To obtain values elsewhere, it is used quadratic interpolation and these types of elements are called quadratic. Lastly the user can choose custom tetrahedral elements with 10 nodes and midpoints. These elements use also quadratic interpolation. Figure 43 shows various types of elements.

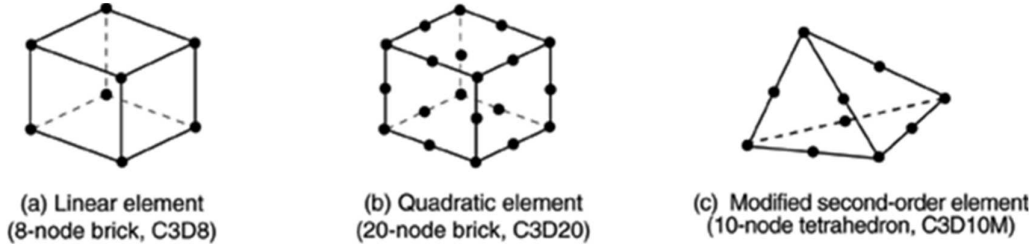


Figure 43: Various types of elements for solid geometry [17]

The modelled bridge decks were meshed with the C3D20R element type - solid 20 node second order 3D brick element with reduced integration. Reduced integration elements were used to reduce the time of the calculations, because there are more than 500 000 nodes in each model. For the reinforcement was used truss second order element, which were embedded into the concrete overlay. The component for load application is meshed with 10 node second order shell element with a thickness 0.1 mm.

The elements have size of 5 mm and 50 mm, where the stress in the deck plate was investigated a mesh of 5 mm was adopted. It is in the zone under the load with width 250 mm and in the connection of middle rib to the deck plate. 50 mm length elements were used elsewhere. This solution also reduces time of the calculation, because it reduces the total number of elements from 2.5 mil (only 5 mm length elements in the model) to 50 thousands. Mesh properties are shown in Figure 44 and axonometric view can be found in Figure 46 and in Figure 47. The mesh with these parameters provide accurate values of the stress in the steel deck plate. The concrete overlay was meshed with a two elements along the thickness.

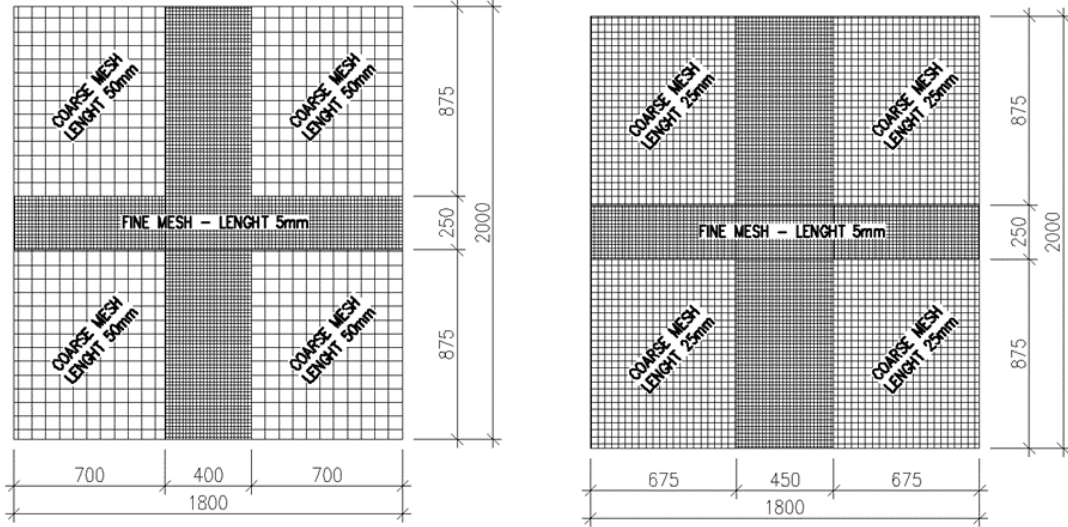
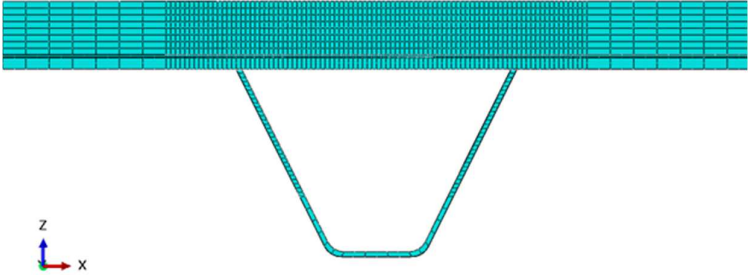


Figure 44: Mesh properties of standard and overloaded model



The investigation of the overloaded model and its influence of cracked concrete on stress in the deck plate, was meshed with elements of length 25 mm. Mesh properties are shown in Figure 45. The concrete overlay was meshed with 8 elements along the thickness, because 2 elements along the thickness were not enough to provide accurate values of inelastic strain. This meshing increased total number of elements, however the model was loaded only with three load cases.



**Figure 45:** Mesh properties of overloaded model

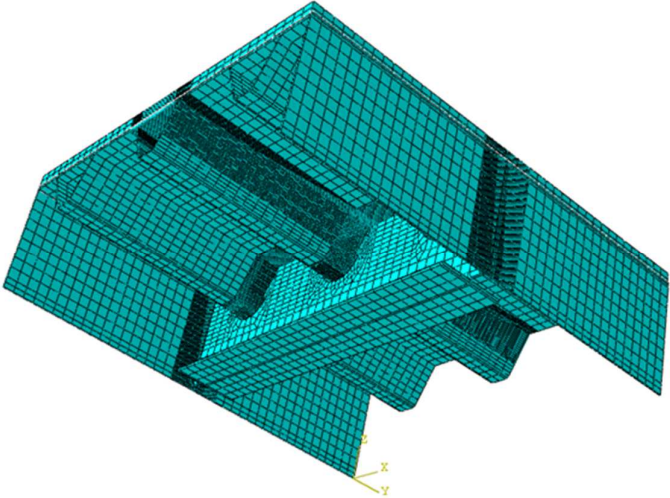


**Figure 46:** Axonometric view of meshed single crossbeam model

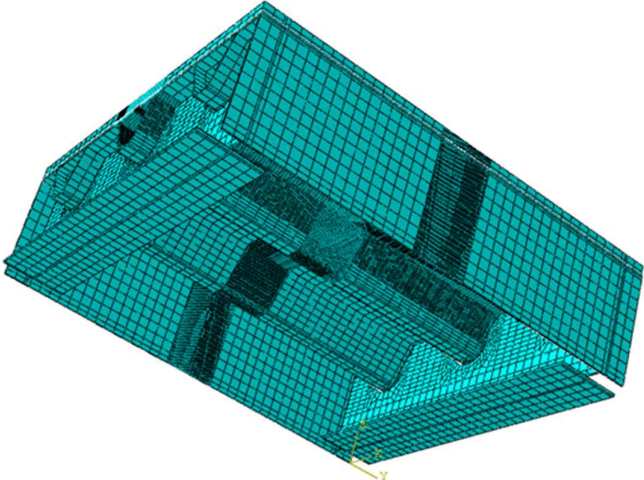


**Figure 47:** Axonometric view of meshed double crossbeam model



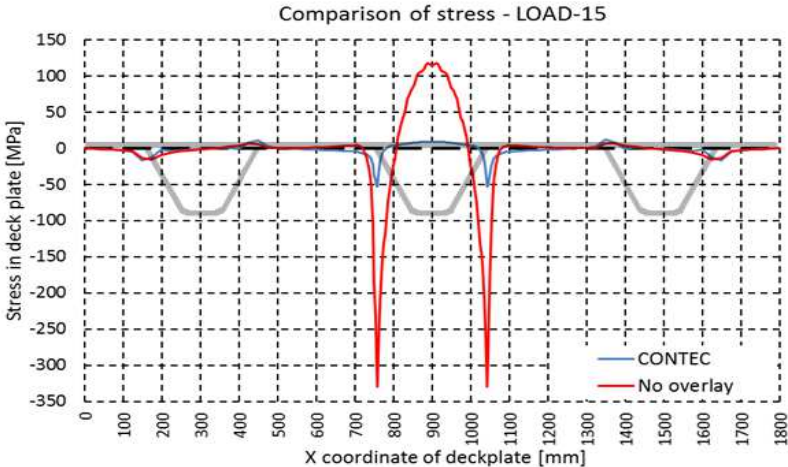
## 4. Results of Numerical Study and Discussion

Structural concept of the orthotropic bridge deck suffers to fatigue damage in the several construction details. This problem has been fully described in sections 1.3. One detail has been selected for further investigation on all numerical models. The detail is on the rib to deck plate weld joint. The main focus of this study is on the influence of HPC overlay and its stress reducing actions in this detail. In total 14 models were calculated: one of each of the models without the concrete overlay, three of each of the models with different types of the overlay material and three with reinforcement in the overlay. The results can be found in section 4.1, 4.2 and 4.3 of this study. In results all Graphs and Figures show stress  $S_{11}$  which is stress in X - direction obtained from FE software Abaqus and  $PE_{11}$  which is inelastic strain obtained from FE software Abaqus also.

- Single and double model – without concrete overlay
- Single and double model – with PAV360 concrete overlay
- Single and double model – with CONTEC concrete overlay
- Single and double model – with REFOR concrete overlay
- Single and double model – with PAV360 overlay with bars  $\text{Ø}12\ 75 \times 75\ \text{mm}$
- Single and double model – with CONTEC overlay bars  $\text{Ø}12\ 75 \times 75\ \text{mm}$
- Single and double model – with REFOR overlay with bars  $\text{Ø}12\ 75 \times 75\ \text{mm}$
- Overloaded model up to 300, 350 and 400 kN wheel load

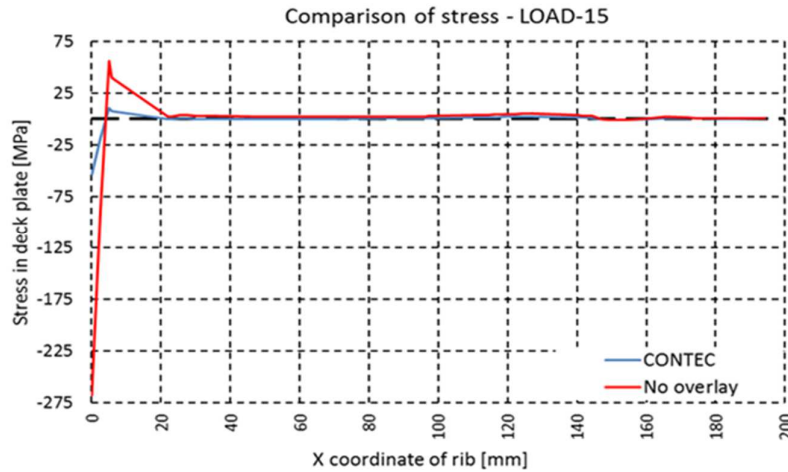
### 4.1. Results from Single Crossbeam Model

For the right interpretation of the extrapolated stress from the hot-spot, it has to be shown structural behaviour of the bridge deck. This structural behaviour of the deck can be shown by shape of stress  $S_{11}$  curve along the deck plate. The stress shown in Graph 22 is taken from underside of the deck plate for LOAD-15 which cause highest stress magnitude in the deck plate. Peaks of the stress curve are caused by high bending moment above the longitudinal rib which works as a support. Graph 22 shows stress from model without the overlay and with CONTEC overlay. This is just for an illustration of the stress development in the deck plate.



Graph 22: Stress  $S_{11}$  on underside of steel deck plate

The stress from inner side of the rib wall is shown in Graph 23.



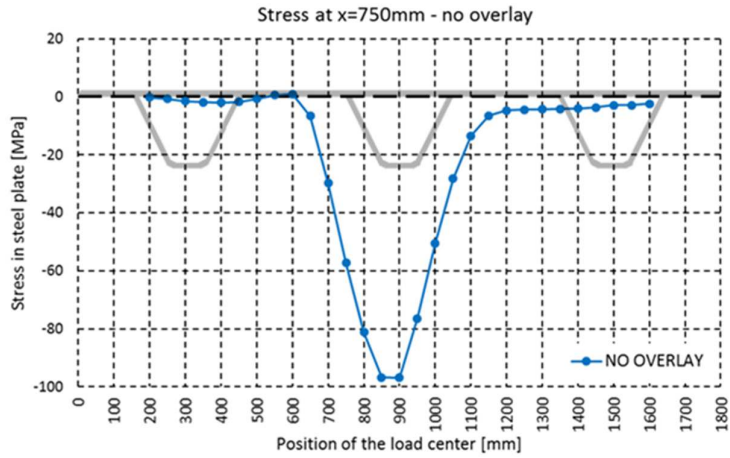
**Graph 23:** Stress  $S_{11}$  on inner side of rib wall

The results of the stresses at the critical points mention above were extrapolated for hotspot at the deck plate at  $X = 750$  mm and hotspot at the rib at  $X = 0$  mm.

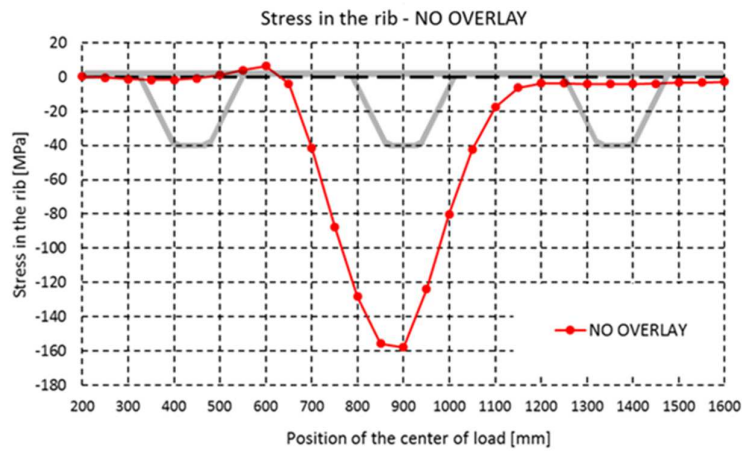
The results of extrapolated stress are shown in the Graph 24-33. Scale of the results is same on all Graphs to show reducing factor of the concrete overlay. The maximum stress values at the investigated critical points are, when the load is located exactly in the middle between two supporting walls of the longitudinal rib i.e.  $X = 900$  mm which is LOAD-15. Another high values are at position  $X = 850$  and  $950$  mm for LOAD-14 and LOAD-16. The longitudinal rib works as a support for the steel deck plate. These loads cause negative bending moment above the support, therefore the calculated stresses are compressive. The stress curves for both hotspots have almost same shape, but with a difference of the stress magnitude at the hotspots. This is caused by a structural behaviour of the bridge deck. The steel plate is generally deforming in one direction, because the transversal crossbeam works as a support in the middle of the deck plate. The deck plate deforms itself only between the spaces of the longitudinal ribs, therefore the stress curves have almost the same shape.

The stress in the single model without the concrete overlay has magnitude nearly  $-160$  MPa at the hot spot placed on the longitudinal rib and  $-100$  MPa at the deck plate. The results from all models with applied concrete overlay have clearly visible stress reducing effect. The stress is reduced by 71% by PAV360 and 77% by CONTEC and REFOR.

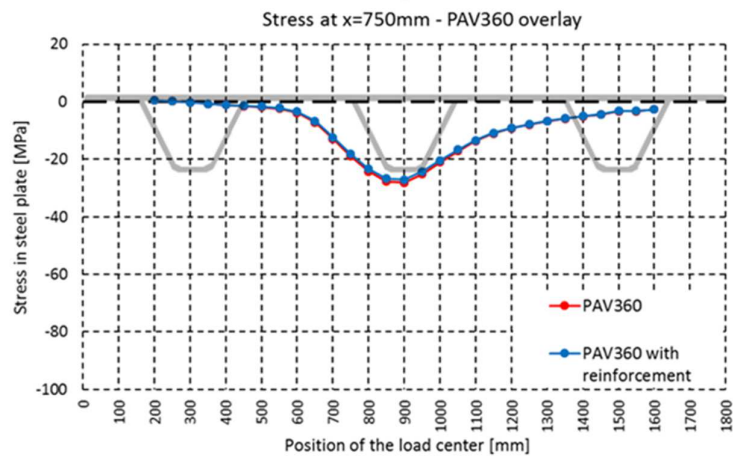
The results for the CONTEC and REFOR are identical, because both materials have same modulus of elasticity  $E = 35$  GPa. The stress in the concrete overlay has a smaller value than the tension strength limit of each material for overlay. This means that the concrete overlay is still in the elastic area. Comparison of stress can be found in Graph 32, 33.



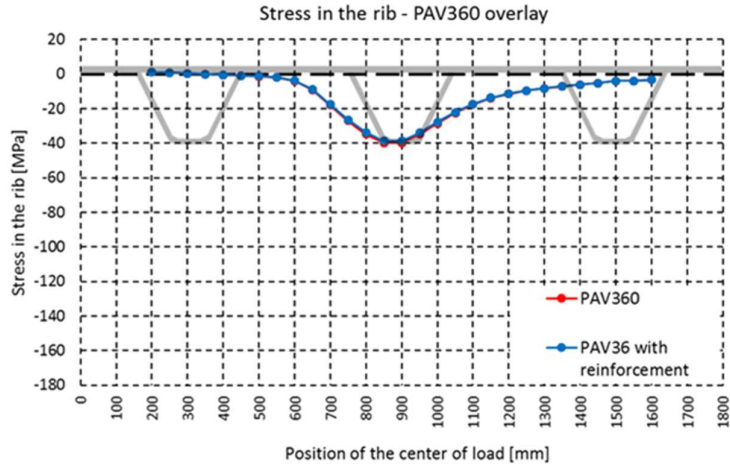
**Graph 24:** Extrapolated stress  $S_{11}$  from steel deck plate without overlay



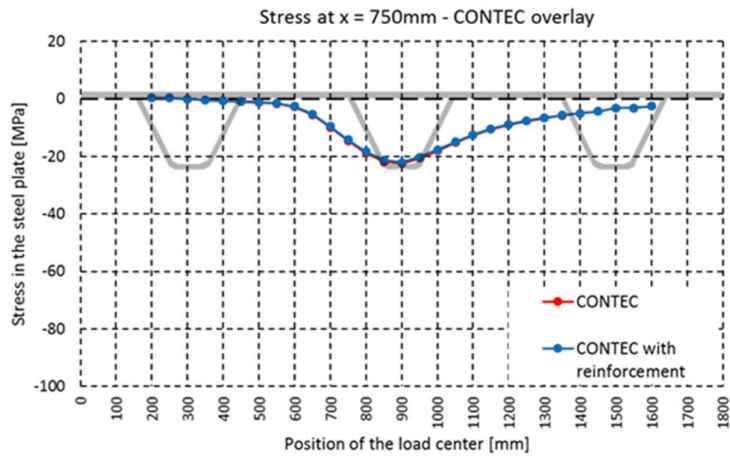
**Graph 25:** Extrapolated stress  $S_{11}$  on inner side of steel rib wall without overlay



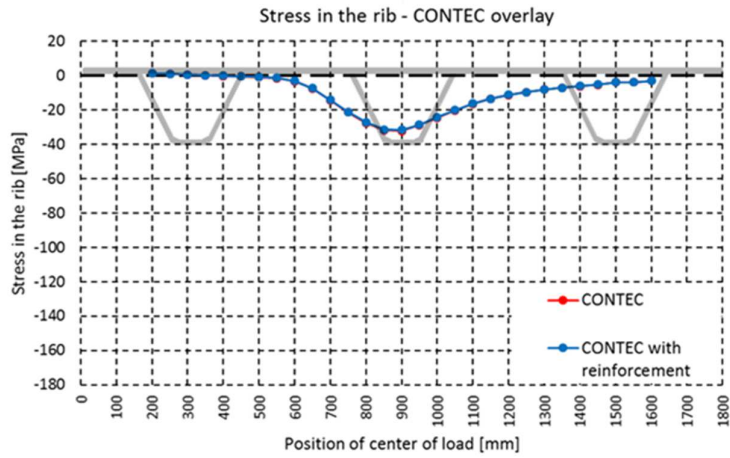
**Graph 26:** Extrapolated stress  $S_{11}$  from steel deck plate with PAV360 overlay



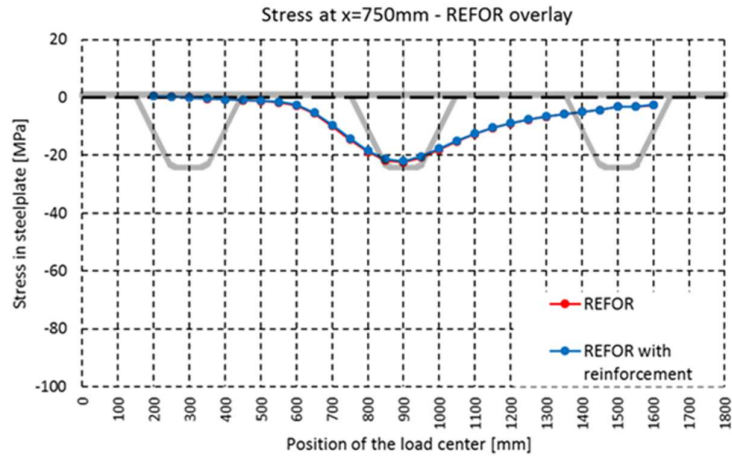
**Graph 27:** Extrapolated stress  $S_{11}$  on inner side of steel rib wall with PAV360 overlay



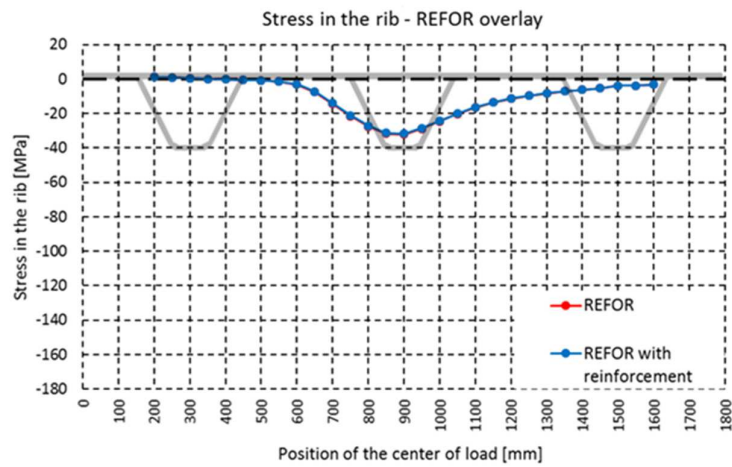
**Graph 28:** Extrapolated stress  $S_{11}$  from steel deck plate with CONTEC overlay



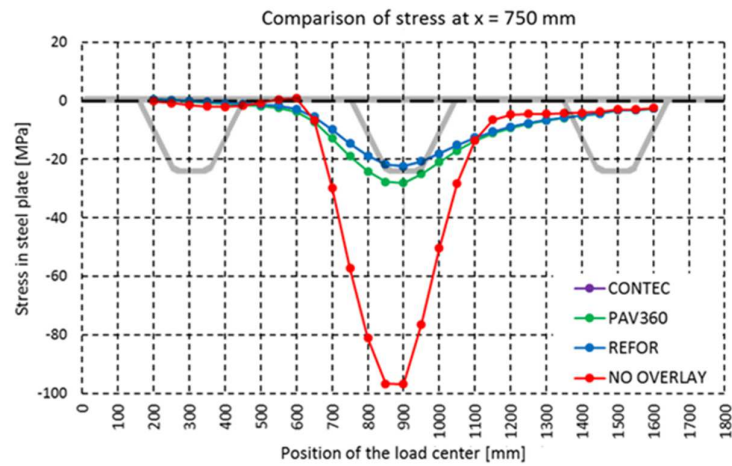
**Graph 29:** Extrapolated stress  $S_{11}$  on inner side of steel rib wall with CONTEC overlay



**Graph 30:** Extrapolated stress  $S_{11}$  from steel deck plate with REFOR overlay

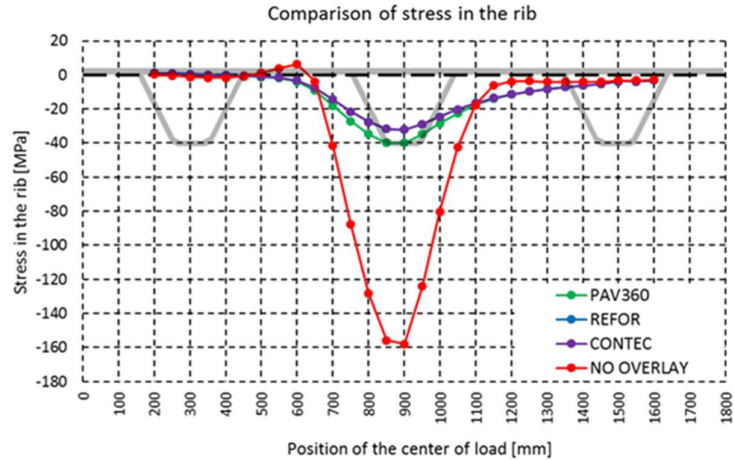


**Graph 31:** Extrapolated stress  $S_{11}$  on inner side of steel rib wall with REFOR overlay



**Graph 32:** Comparison of extrapolated stress  $S_{11}$  from underside steel deck plate

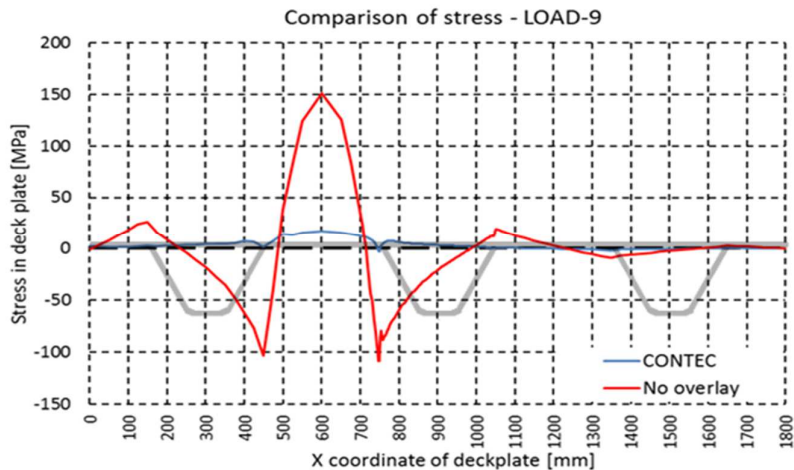




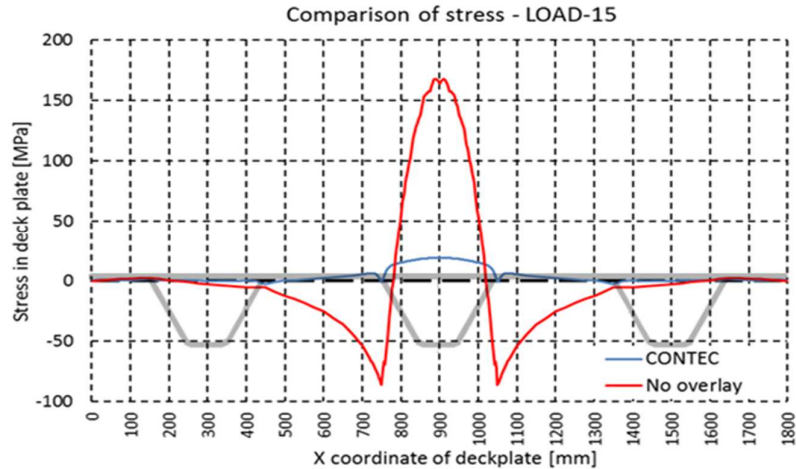
**Graph 33:** Extrapolated stress  $S_{11}$  on inner side of steel rib wall with concrete overlay

#### 4.2. Results from Double Crossbeam Model

For the right interpretation of the extrapolated stress from the hot-spot, it has to be shown structural behaviour of the bridge deck with two transversal crossbeams. This structural behaviour of the deck can be shown by shape of stress curve along the deck plate. The stresses shown in Graph 34 and Graph 35 are also taken from underside of the deck plate, but the maximum stress in this case is caused by LOAD-9. Peaks of the stress curve are caused by high bending moment above the longitudinal rib which works as a support. Graph 34 and Graph 35 show stress from model without the overlay and with CONTEC overlay. This is just for an illustration of the stress development in the deck plate. The shape of stress curve in the rib is same as that of the one with one transversal stiffener.



**Graph 34:** Stress  $S_{11}$  on underside of steel deck plate



**Graph 35:** Stress  $S_{11}$  on underside of steel deck plate

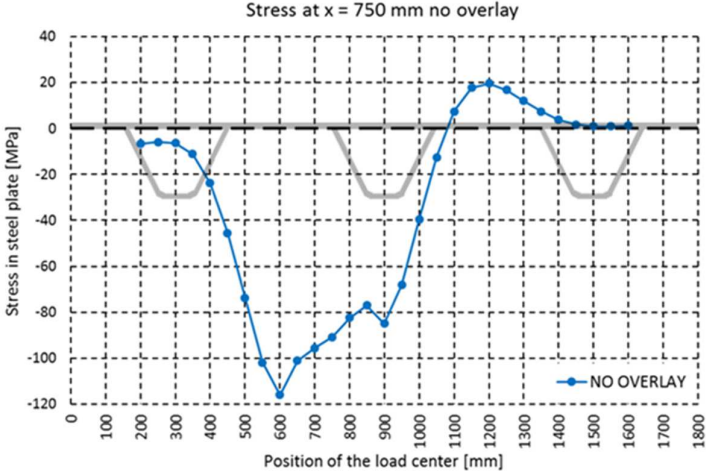
The results for the double model were extrapolated for three hotspots. Two hotspots are located at the deck plate at locations  $X = 750$  and  $755$  mm and third one is situated on the rib at  $X = 0$  mm.

The results for the double model, can be found in the Graph 36-Graph 50. The scale of the results is not same on every Graph, because the results with the concrete overlay have a lower stress and one scale for all Graphs is not very conclusive. The highest values of the stress at the deck plate, are when the load is at position  $X = 600$  mm which is for the LOAD-9 in the case without the overlay. The stress curves for models with an overlay have their peaks in a different location depending on the position of the hot-spot. For the hot-spot on the deck plate at position  $X = 750$  mm stress has its peak with LOAD-8 positioned at  $X = 550$  mm, but for the hot spot located at  $X = 755$  mm stress peak is for the LOAD-12 and LOAD-13. The curves change also their polarity depending on the path of extrapolation. The curve of the stress at the rib has its peak, when the load is at the position  $X = 900$  mm i.e. LOAD-15 for variation without overlay. This curve has also similar shape to results obtained at rib for a single model. The stress curve extrapolated from the rib also changes its polarity from tensile stresses to compressive stresses.

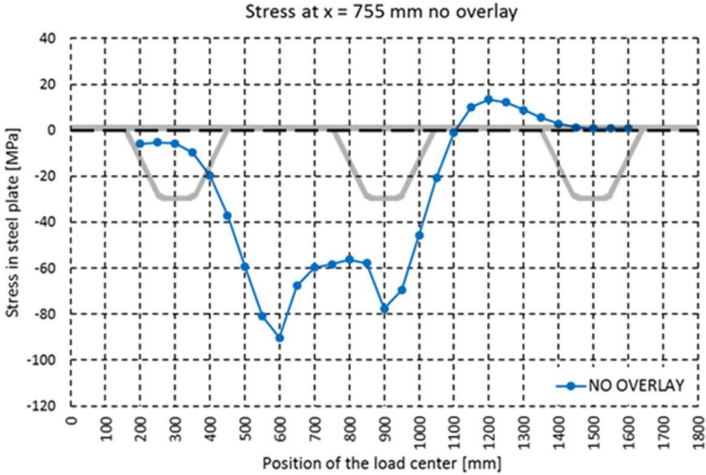
The effects mentioned above, are caused by a structural behaviour of the bridge deck. There is no cross beam which works as a support under the load, therefore the bridge is deforming itself in two directions. When the load is moving from one side to the other one, it causes change in the stress from the tension to the compression. This is caused also by the fact, that the concrete overlay provides an additional stiffness in both directions.

The stress in the double model without concrete overlay has magnitude nearly  $-120$  MPa at hot spots on the deck plate and  $-40$  MPa at the rib. The stress reducing effect in this case is more significant, than in the model with single transversal rib. Results for CONTEC and REFOR overlay material are also identical with results from single model. CONTEC and REFOR reduced stress by 97% to  $-3.0$  MPa. It has to be taken into account, when the overlay is applied on the top of the deck plate, stress is no more compressive, but it is tensile. This effect is for both hot spots for other positions of the load, than for the load case causing peak of the stress magnitude. This is clearly visible in comparison Graph 49. PAV360 reduces stress by 92% to  $-8.0$  MPa and the tensile stress is only for hotspot at position  $X = 755$  mm. Stress reduction effect is clearly visible in comparison Graph 48-50.

Hot spot at the rib has its peak +10 MPa at the tensile zone and -40 MPa in the compression zone of the curve. Concrete overlay from CONTEC and REFOR reduces tensile stresses to 2.2 MPa which makes 78% and by 90% to -4 MPa in the compressive location. The PAV360 reduces the tensile stresses by 70% to +3.0 MPa, and the compressive by 86% to -6 MPa.

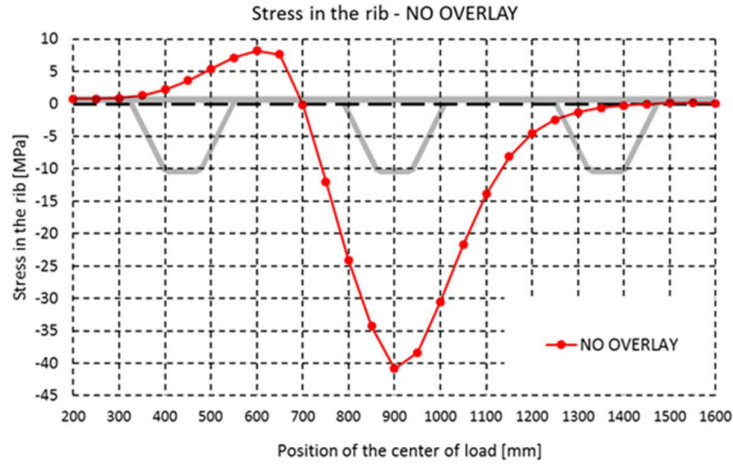


**Graph 36:** Extrapolated stress  $S_{11}$  on steel deck plate at  $X = 750$  mm without overlay

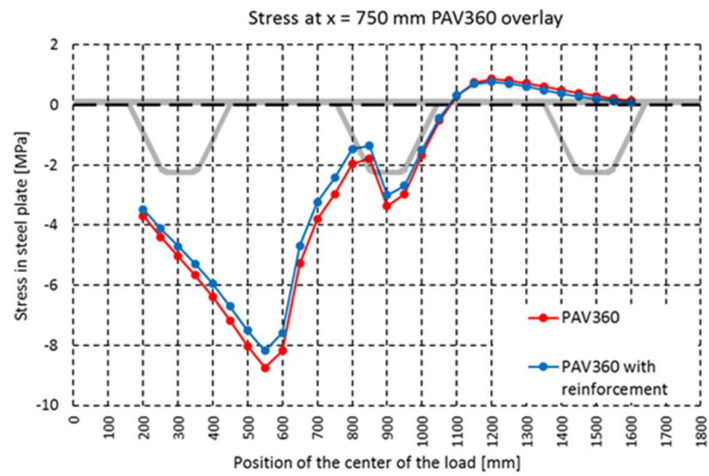


**Graph 37:** Extrapolated stress  $S_{11}$  on steel deck plate at  $X = 755$  mm without overlay

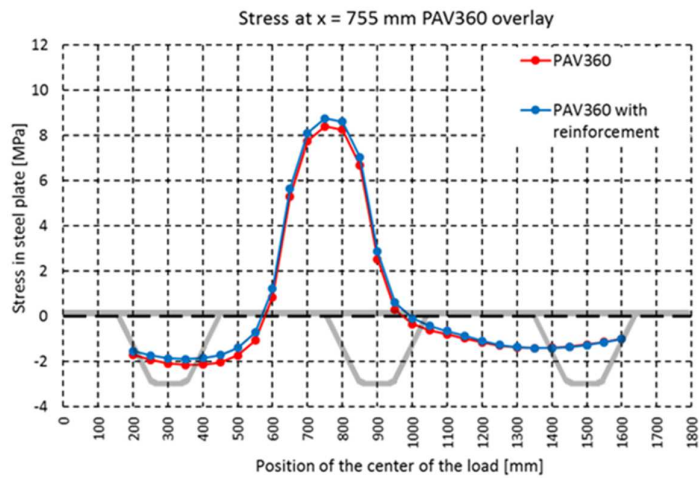




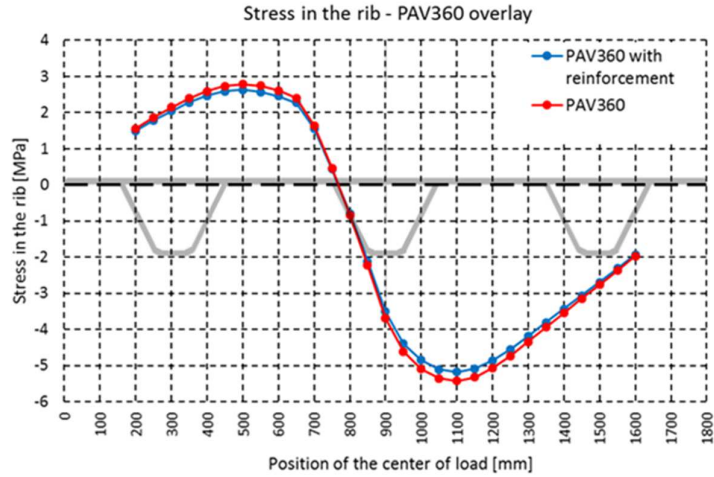
**Graph 38:** Extrapolated stress  $S_{11}$  from inner side of rib wall at  $X = 0$  mm without overlay



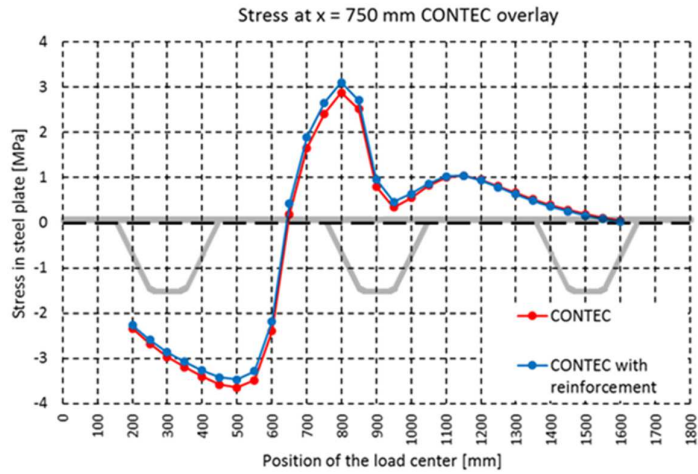
**Graph 39:** Extrapolated stress  $S_{11}$  on steel deck plate at  $X = 750$  mm with PAV360 overlay



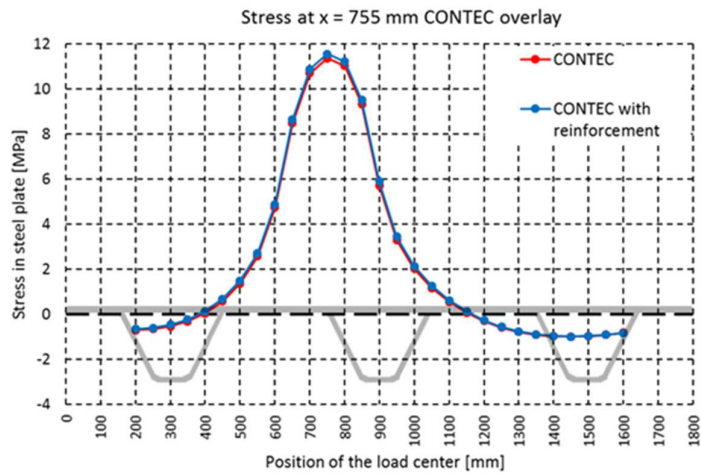
**Graph 40:** Extrapolated stress  $S_{11}$  on steel deck plate at  $X = 755$  mm with PAV360 overlay



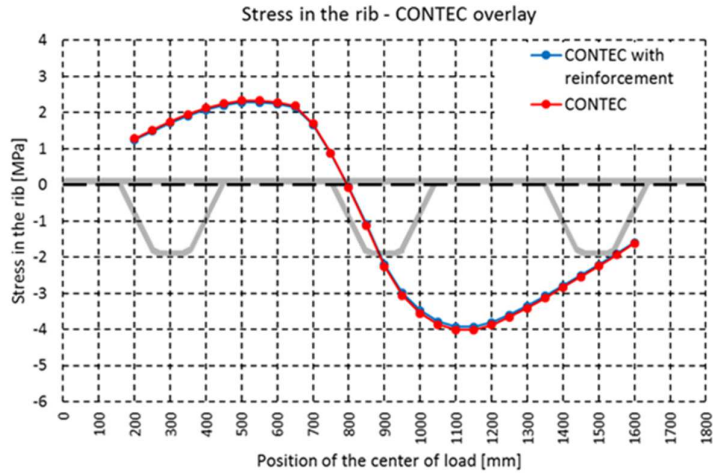
**Graph 41:** Extrapolated stress  $S_{11}$  from inner side of rib wall at  $X = 0$  mm with PAV360 overlay



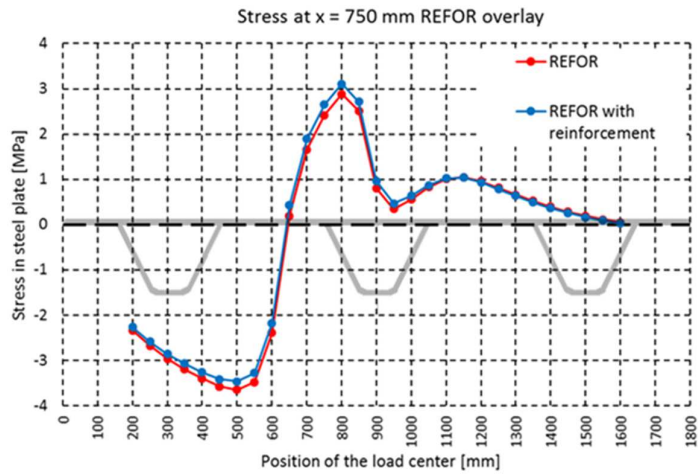
**Graph 42:** Extrapolated stress  $S_{11}$  on steel deck plate at  $X = 750$  mm with CONTEC overlay



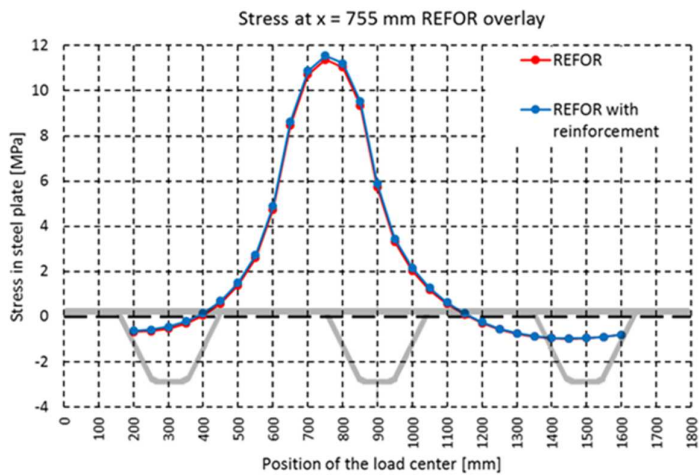
**Graph 43:** Extrapolated stress  $S_{11}$  on steel deck plate at  $X = 755$  mm with CONTEC overlay



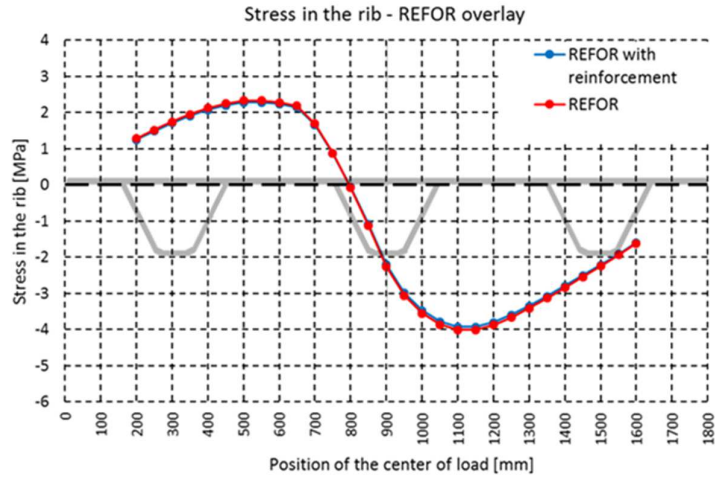
**Graph 44:** Extrapolated stress  $S_{11}$  from inner side of rib wall at  $X = 0$  mm with CONTEC overlay



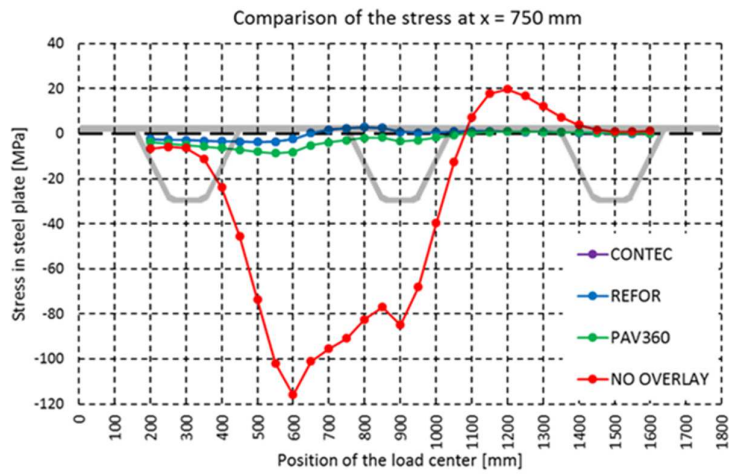
**Graph 45:** Extrapolated stress  $S_{11}$  on steel deck plate at  $X = 750$  mm with REFOR overlay



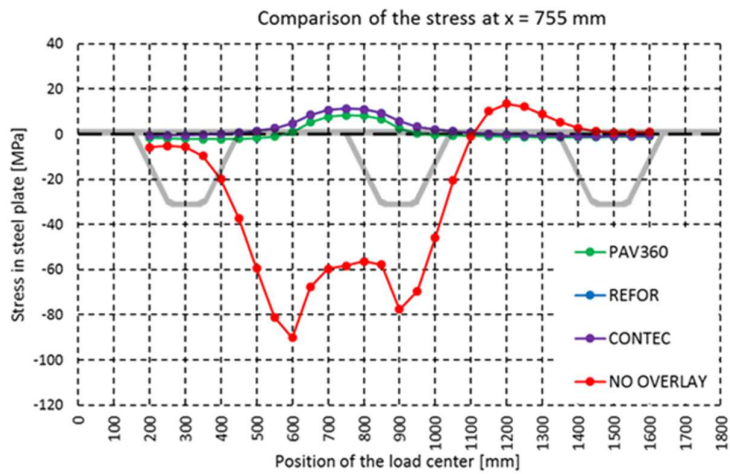
**Graph 46:** Extrapolated stress  $S_{11}$  on steel deck plate at  $X = 755$  mm with REFOR overlay



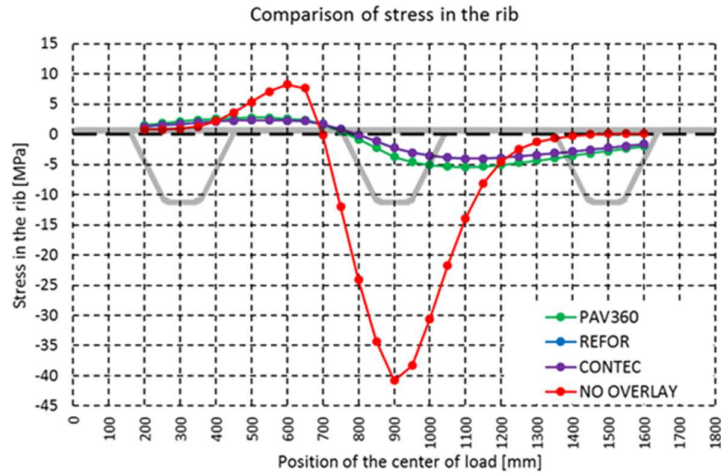
**Graph 47:** Extrapolated stress  $S_{11}$  from inner side of rib wall at  $X = 0$  mm with REFOR overlay



**Graph 48:** Comparison of extrapolated stress  $S_{11}$  on steel deck plate at  $X = 750$  mm



**Graph 49:** Comparison of extrapolated stress  $S_{11}$  on steel deck plate at  $X = 755$  mm



**Graph 50:** Comparison of extrapolated stress  $S_{11}$  from inner side of rib wall at  $X = 0$  mm

### 4.3. Results from Overloaded Model

The single model was selected for overloading with mesh changes mentioned in 3.4 -Mesh of this thesis. Model was overloaded according to scheme in section 3.3 - Boundary condition and Load. This load was applied in load case LOAD-15 which is in the middle of the bridge and causes maximum stresses in the deck plate above the support. Model was overloaded to understand behaviour of cracked concrete overlay and its effects on stress distribution in the steel deck plate. The material for overlay was REFOR, which has a tensile strength limit  $f_{ct} = 7$  MPa, therefore it was necessary to overload the model up to 400 kN applied on same wheel area mentioned in section 3.3 - Boundary condition and Load. Concrete overlay started to crack at 250 kN applied on it. The stress in top thread of steel deck plate, grows with increasing load. However the main interest was on the stress after reloading again with standard 50 kN wheel load after overloading and unloading the deck.

The overlay behaves like high beam (slab) and not behaves as a Bernoulli's beam. Distribution of stress in overlay has shape similar to arch. This arched distribution cause cracking of overlay in the mid span at  $X = 900$  mm, however bending moment above the support cause tensile stresses and the overlay cracks at  $X = 731$  mm (position of the support is at  $X = 750$  mm).

In Figures 48-56, cuts of the bridge deck in the middle are shown. The cuts show the stress distribution in the concrete overlay. It is clearly visible, that the stress distribution for first loads (300 kN - Figure 48, 350 kN - Figure 51, 400 kN - Figure 54) are similar to each other and the maximum tensile stress in the overlay is nearly + 6.9 MPa. However when 50 kN are applied again, the cracked concrete does not carry load anymore see figures 50, 53 and 56. Development of inelastic strain is shown only for case loaded with 300 kN, every other model has same progress until reaching the maximum load. Inelastic strain distribution can be found in Figures 57-62. Scale of Figures 57-62 is chosen to see, other areas of cuts, not only areas above the supports.



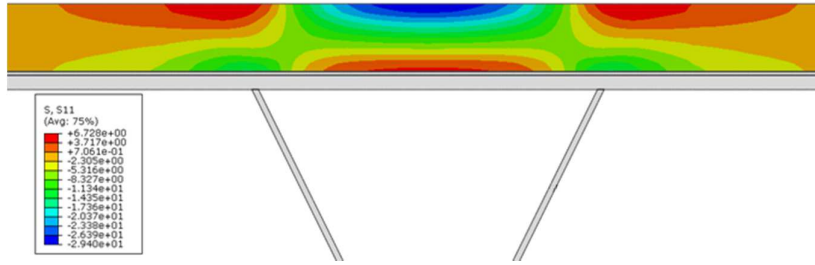


Figure 48: Stress  $S_{11}$  in concrete overlay from 300 kN load case, 300 kN applied on it

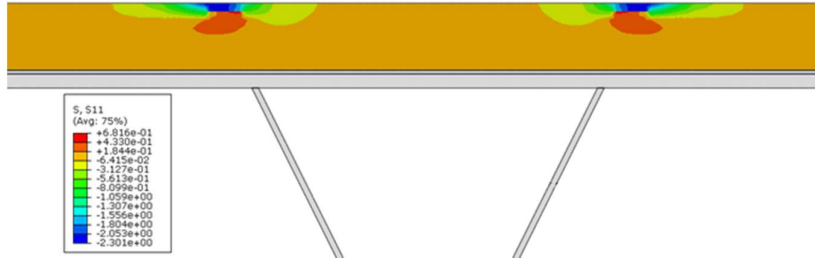


Figure 49: Stress  $S_{11}$  in concrete overlay from 300 kN load case, unloaded to 0 kN

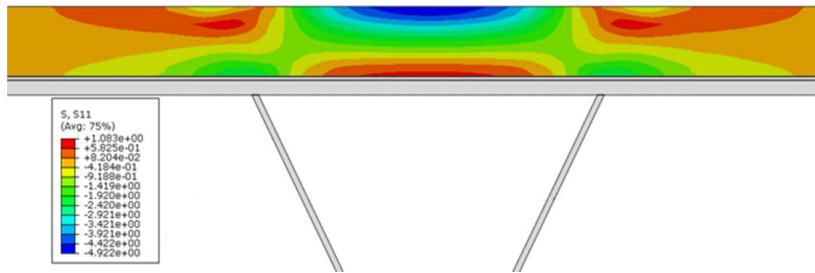


Figure 50: Stress  $S_{11}$  in concrete overlay from 300 kN load case, reloaded to 50 kN

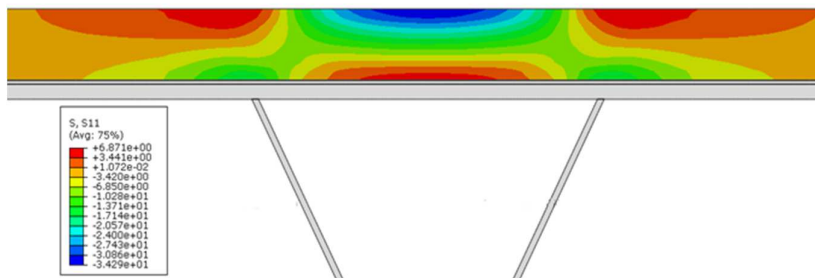


Figure 51: Stress  $S_{11}$  in concrete overlay from 350 kN load case, 350 kN applied on it

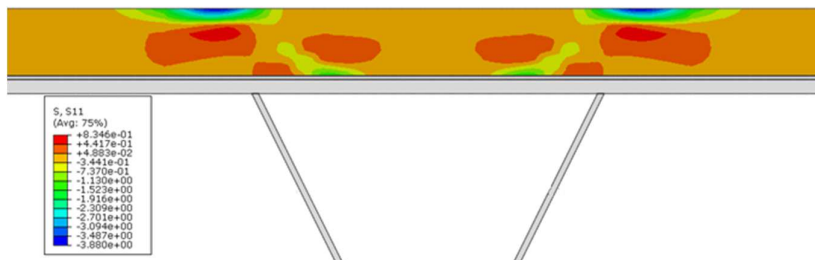


Figure 52: Stress  $S_{11}$  in concrete overlay from 350 kN load case, unloaded to 0 kN

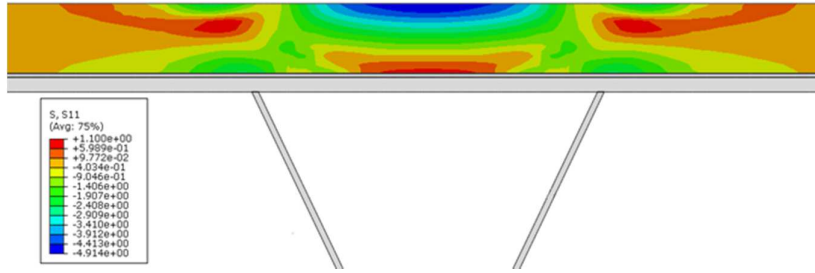


Figure 53: Stress  $S_{11}$  in concrete overlay from 350 kN load case, reloaded to 50 kN

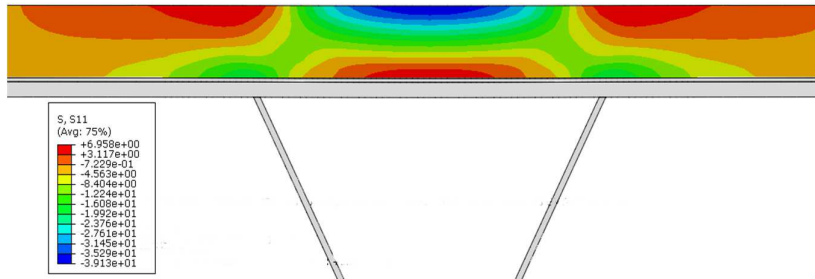


Figure 54: Stress  $S_{11}$  in concrete overlay from 400 kN load case, 400 kN applied on it

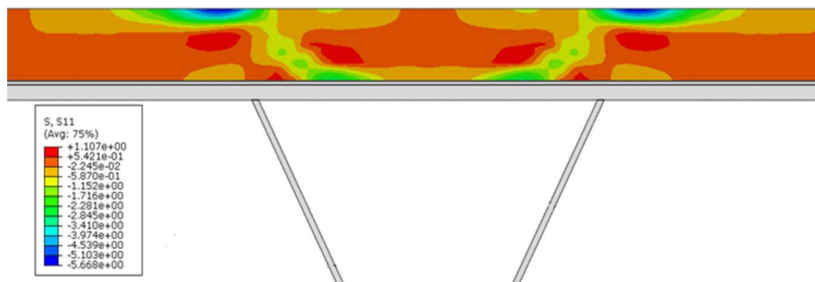


Figure 55: Stress  $S_{11}$  in concrete overlay from 400 kN load case, unloaded to 0 kN

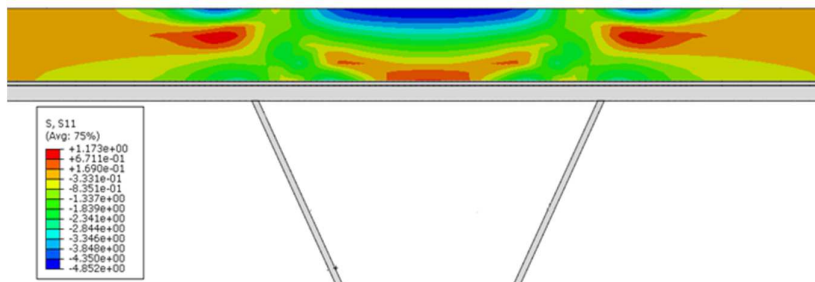


Figure 56: Stress  $S_{11}$  in concrete overlay from 400 kN load case, reloaded to 50 kN

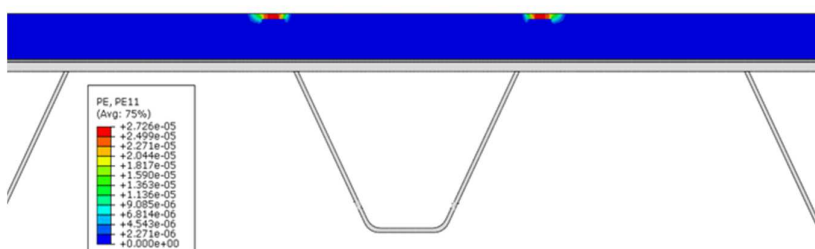


Figure 57: Inelastic strain  $PE_{11}$  from 300 kN load case - 250 kN applied on it

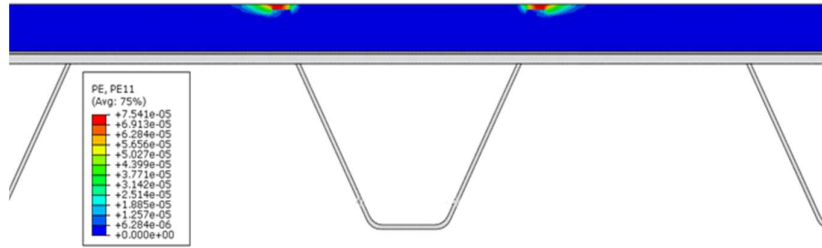


Figure 58: Inelastic strain  $PE_{11}$  from 300 kN load case – 300 kN applied on it

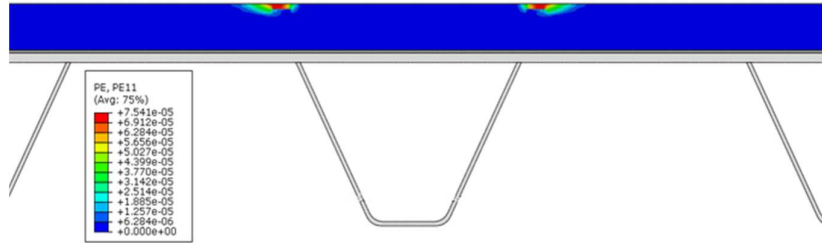


Figure 59: Inelastic strain  $PE_{11}$  from 300 kN load case – unloaded to 0 kN

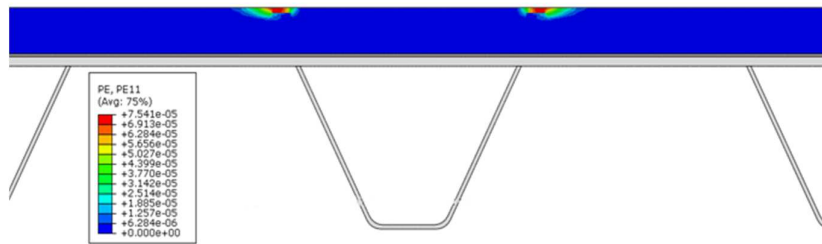


Figure 60: Inelastic strain  $PE_{11}$  from 300 kN load case – reloaded to 50 kN

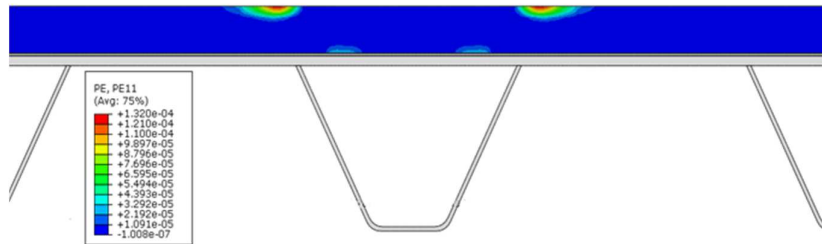


Figure 61: Inelastic strain  $PE_{11}$  from 350 kN load case – 350 kN applied on it

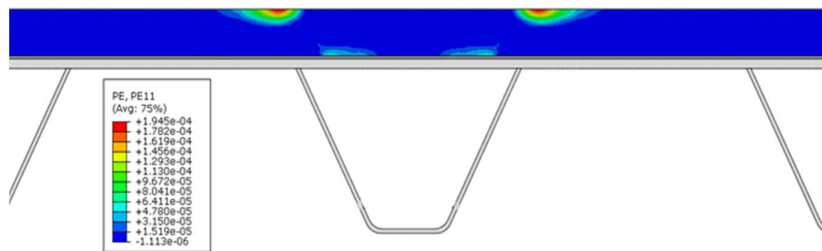
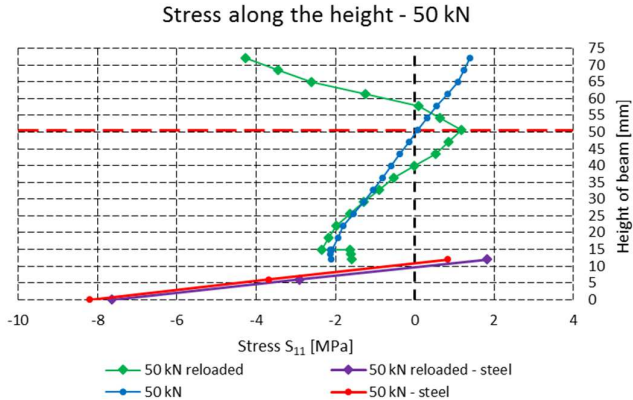


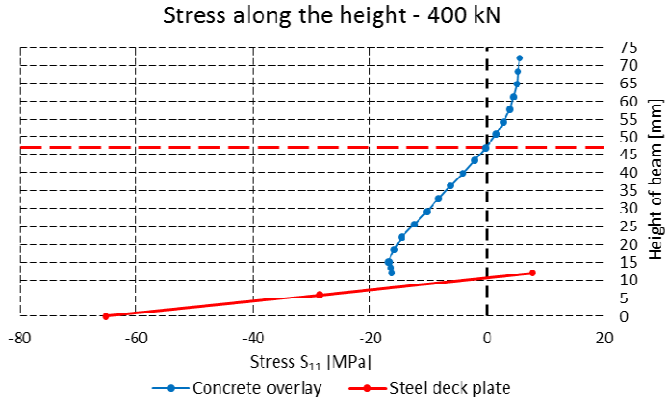
Figure 62: Inelastic strain  $PE_{11}$  from 400 kN load case – 400 kN applied on it



For a better understanding of the stress distribution in the concrete overlay, the stress along the height of overlay is shown in Graph 51 and Graph 52. Graph 51 shows stresses in the overlay with applied 50 kN and compares it with stress curve obtained from reloaded 50 kN. The stress curve from standard 50 kN wheel load is linear, this behaviour changes to nonlinear, because the concrete is cracked and it cannot carry tensile stress in cracked areas. Graph 52 shows nonlinear behaviour of stress distribution, when 400 kN is applied as a wheel load.



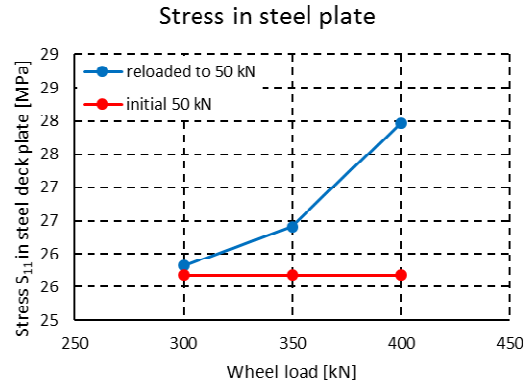
**Graph 51:** Comparison of stress  $S_{11}$  along the height



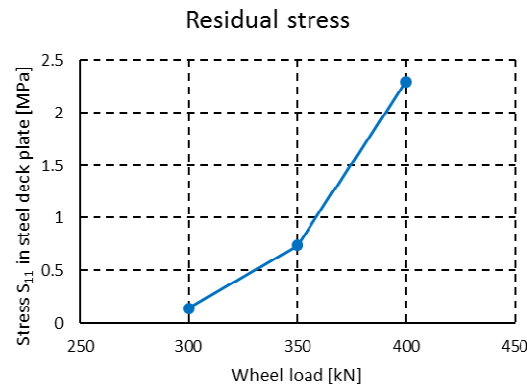
**Graph 52:** Stress  $S_{11}$  along the height – 400 kN applied

Graph 51 also shows difference in stress in the steel deck plate. Stress in the top thread has a higher value in case reloaded again to 50 kN after overloading it to 400 kN. This stress can be called as residual stress, because it stays in the deck plate even, when there is no load applied to it.

Stress in the top thread of the steel deck plate caused by initial 50 kN wheel load has a magnitude 25.6 MPa in all three loaded cases (overloaded to 300 kN, 350 kN and 400 kN). These values are the same, because the 50 kN wheel load does not cause stresses high enough to crack the overlay (stress in concrete overlay is still in elastic area). Stress in the top thread of the steel deck plate caused by reloaded 50 kN wheel load differs for every load case. This residual stress grows higher with higher load magnitude applied as a wheel load. This effect can be found in Graph 53. Residual stress can be calculated as difference between reloaded 50 kN and initial 50 kN wheel load. Residual stress can be found in Graph 54.

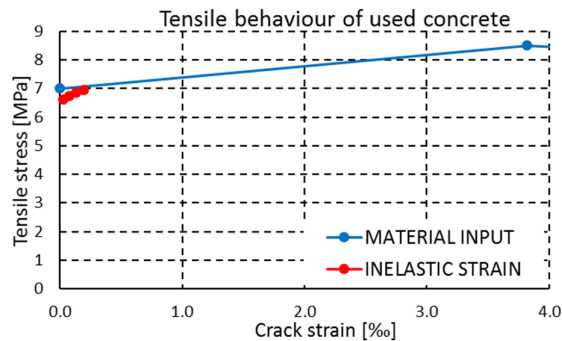


**Graph 53:** Difference of calculated stress for initial 50 kN and reloaded to 50 kN



**Graph 54:** Residual stress in top thread of steel deck plate

The effect of the residual stress in steel deck plate mentioned above in this subsection is caused by inelastic strain of concrete overlay. Inelastic strain starts to appear with 250 kN and gets higher value with increasing load. The values do not change after reloading to 50 kN. The maximum value is + 0.19 ‰ which is still on the hardening branch of stress-strain curve of material used for the overlay (see Graph 18 in subsection 3.2.2.1 of this thesis). Graph 55 shows calculated inelastic strain on the hardening branch of material input into software Abaqus.



**Graph 55:** Calculated  $PE_{11}$  on hardening branch of material stress-strain curve

The fact, that the inelastic strain of the concrete overlay is still on hardening branch of stress-strain diagram, led to changing the input of the REFOR material as it is mentioned in subsection 3.5.3. REFOR material has been changed to behave as a material with

softening branch with tensile strength limit  $f_{ct} = 3.5 \text{ MPa}$ . It was necessary to change maximum wheel load from 400 kN to only 100 kN because of the tensile strength limit of this modified material. Maximum crack strain 0.05‰ ( $5.0 \cdot 10^{-4}$ ), which is close to calculated maximum inelastic strain 400 kN applied on bridge.

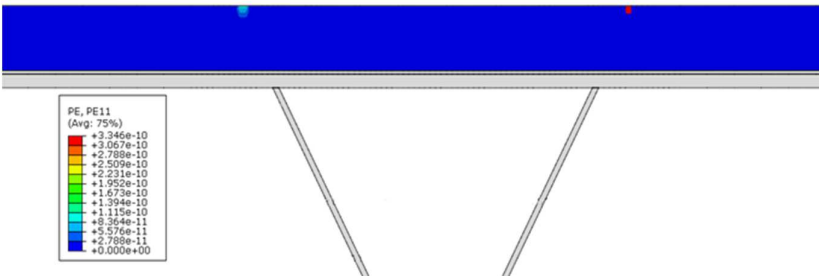


Figure 63: Initial calculated value of inelastic strain  $PE_{11}$

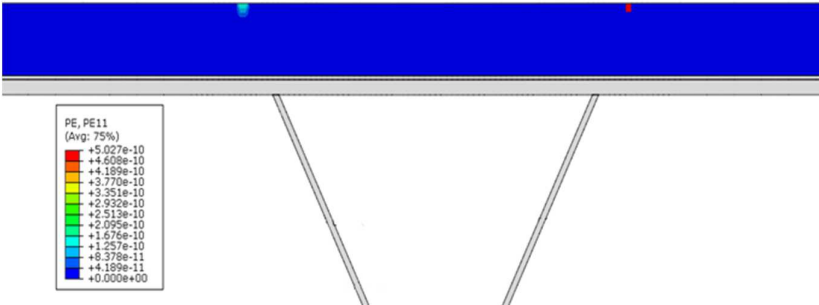


Figure 64: Last calculated value of inelastic strain  $PE_{11}$

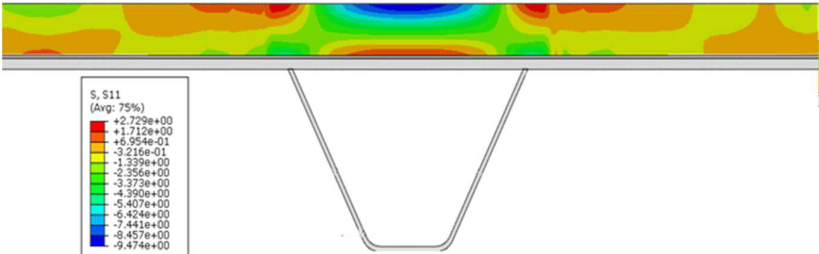


Figure 65: Equivalent stress  $S_{11}$  distribution for last inelastic strain

The calculated inelastic strain in this case has the same place as, where it appeared with the original REFOR material. The values of the inelastic strain of concrete material has a magnitude from  $10^{-11}$  to  $10^{-10}$ . The magnitude is very close to zero. The distribution of the inelastic strain of modified REFOR can be found in Figures 63 and 64, and it is clearly visible that in some elements the calculation of strain failed (red square in Figures 63 and 64). Figure 65 and Figure 64 show distribution of stress in overlay with visible failed area. Failure of calculation is caused probably by the fact, that the used mesh was very coarse for calculation of the strain in overlay.

**4.4. Results from Parameter Study**

The parameter study has been done with a focus on different material behaviour, to see if the material characteristics has an influence on the stress in steel deck plate. This parameter study has been done on simplified numerical model, because on a large model, the calculation took almost 24 Hours.

This simplified numerical model has dimensions 250 mm × 1800 mm and it is modelled with only composite structural parts i.e. steel deck plate, epoxy layer and concrete overlay, other parts of orthotropic structural concept has not been modelled, because this parts add more elements to model. This small model is supported in the middle, where is crossbeam welded to deck plate and in the position, where should be longitudinal ribs to simulate same structural behaviour of large model. These changes, can be found in Figure 66 and Figure 67.



**Figure 66:** Dimensions of simplified numerical model

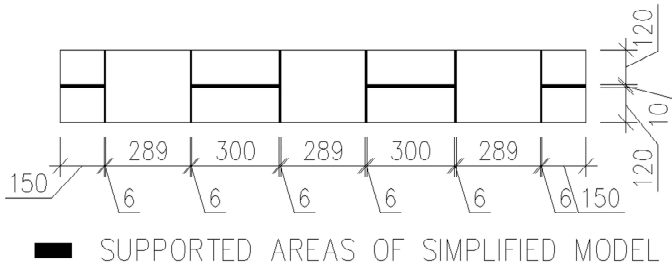


**Figure 67:** Boundary condition of simplified numerical model

Simplified model has been meshed with element type C3D8R - solid 8 node linear 3D brick element with reduced integration. 8 elements were adopted along the height of concrete overlay, one in epoxy layer and two elements in the steel deck plate. Finer mesh has been adopted around the investigated weld area (5 mm length). Mesh properties of simplified model can be found in Figure 68.

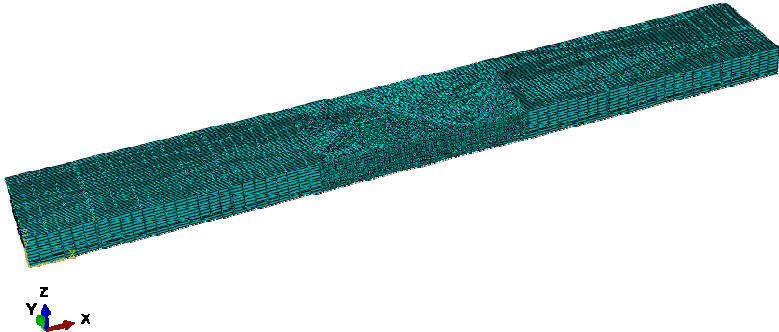
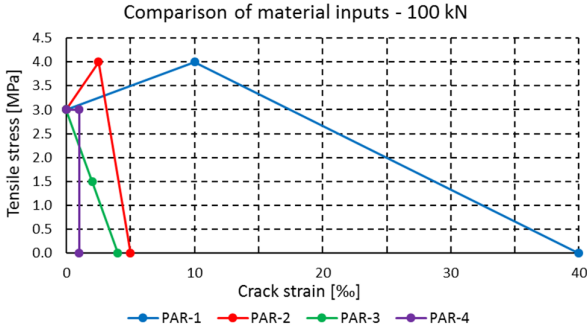


**Figure 68:** Mesh properties of simplified model

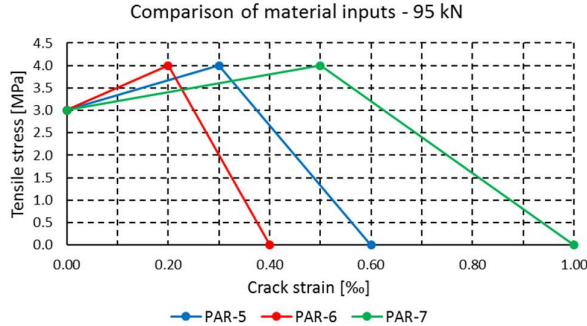
In total, 19 different material inputs were included in this parameter study, to see, if stress is affected by different material inputs. Material input has been separated into four groups by applied wheel load. Wheel load changed depending on material behaviour (strain-hardening, plastic or softening). Different material law has been named as "PAR-" plus number of calculated model (number of used material model). The model was loaded with 100 kN, 95 kN, 75 kN and 50 kN resp. 45 kN. Graphs 56-59

show used material behaviour. Graph 56 shows material input for model loaded with 100 kN and compares other material behaviour to very ductile behaviour of PAR-1, which is very close to behaviour of REFOR material, has lowered tensile strength limit  $f_{ct}$  from 7 MPa to 3 MPa. Other materials have a crack strain of less than 1.0 ‰ (order of magnitude is  $10^{-3}$  as a material input of crack strain behaviour into software Abaqus). This fact of very small values of crack strain, led to changing the applied load in this parameter study to be able obtain accurate results in small computing time. The other reason for doing this parameter study was if it is useful to use very ductile material for the overlay (REFOR) or if it sustainable to use material with very small ductility (less ductile than plain concrete).

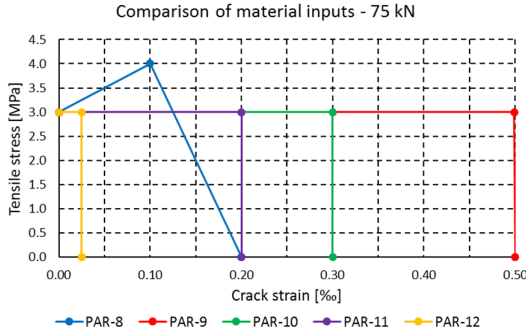
Results were compared in Table 10.



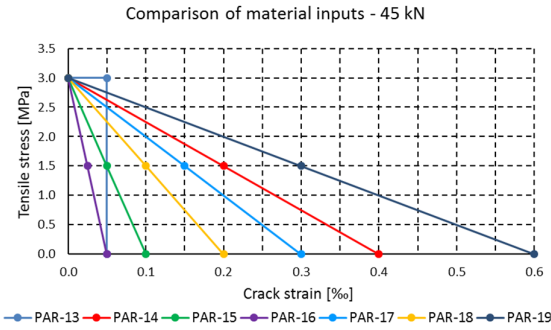
**Graph 56:** Material inputs for cases loaded with 100 kN



**Graph 57:** Material inputs for cases loaded with 95 kN



**Graph 58:** Material inputs for cases loaded with 75 kN



**Graph 59:** Material input in cases loaded with 45 kN

**Table 10:** Results of parameter study

	Wheel load [kN]	Stress in steel deckplate [MPa]	Inelastic strain in concrete [-]	Inelastic strain in concrete [%]
PAR-1	100	27.30	3.66E-04	0.37
PAR-2		27.12	3.40E-04	0.34
PAR-3		35.25	6.49E-03	6.49
PAR-4		27.37	4.31E-04	0.43
PAR-5	95	24.79	2.13E-04	0.21
PAR-6		24.60	1.86E-04	0.19
PAR-7		25.00	2.46E-04	0.25
PAR-8	75	19.20	8.79E-05	0.09
PAR-9		19.12	1.93E-04	0.19
PAR-10		19.12	1.93E-04	0.19
PAR-11		28.27	4.93E-03	4.93
PAR-12		28.70	5.79E-03	5.79
PAR-13	50	12.20	3.83E-05	0.04
PAR-14	45	10.63	NO INELASTIC STRAIN	NO INELASTIC STRAIN
PAR-15		10.63		
PAR-16		15.06		
PAR-17		[-]		
PAR-18		10.63		
PAR-19		14.28		

Table 10 compares stresses in the top thread of the steel deck plate and inelastic strain in concrete overlay. As it is clearly visible in Table 10, some material models significantly differs in stress values (mentioned row are marked with red colour). PAR-3, PAR-16 and PAR-19 has material properties that could be called as a softening and if the results from this models are compared to other models in their results groups, the stress in steel deck plate differs by almost 30%. PAR-11 and PAR-12 has material properties that can be called as a plastic behaviour. This two models differs also in their results group by 30%. PAR-5, PAR-6 and PAR-7 had material properties with post crack-hardening, and all these three results have very similar values of calculated stress and inelastic strain.

## Conclusion

In this thesis we investigated various types of concrete material for overlay as a renovation technique for orthotropic steel bridge decks. The fibre reinforced concrete overlay clearly reduces stress in the investigated weld joint and can be used as an equal replacement for the classical concrete overlay with reinforcement. The results showed, that the stress reducing effect of the overlay depends on Young's modulus of used concrete. This can be found in comparison Graph 32, Graph 33, Graph 48, Graph 49 and Graph 50. The results were identical for materials same E-modulus i.e. CONTEC and REFOR. The standard 50 kN wheel load causes stresses which are in the elastic zone of used concrete and causes no damage to concrete. Models with embedded reinforcement showed no significant influence on the stress in the deck plate. This fact supports the idea of not using the reinforcement at all.

However the overloaded model showed that the damaged overlay has influence on the stress in the deck plate. The residual stress in the deck plate which is caused by cracked overlay gets higher value with increasing magnitude of wheel load. It should be taken into account that 400 kN as one wheel will probably never appear on the deck plate. ČSN EN 19991-2 and its load model LM1 consists of double-axle concentrated loads with magnitude  $Q_k = 300$  kN and it is applied on square area  $400 \times 400$  mm<sup>2</sup>. 400 kN wheel load was only used to crack investigated concrete material which had tensile strength  $f_{ct} = 7$  MPa. The overloaded model showed, that using very ductile material for overlay is not very efficient. Ductile material was not used to its limit, calculated inelastic strain is still on hardening branch and has very small value.

Parameter study on simplified numerical showed that different material input, had major influence on stress in weld joint. It would be very useful to use this knowledge of this parameter study and use it on large model to see how does it behaves in larger scale. It can be also used as a requirement for used concrete mixture or one demand for creating new concrete mixture.

## References

- [1] DE JONG, F. B. P. *Renovation techniques for fatigue cracked orthotropic steel bridge decks*. 2007. PhD Thesis. TU Delft, Delft University of Technology. ISBN 9090214127
- [2] CONNOR, R., FISHER, J., GATTI, W., GOPALARATNAM, V., KOZY, B., LESHKO, B., & PATERSON, D. *Manual for design, construction, and maintenance of orthotropic steel deck bridges*. 2012. (No. FHWA-IF-12-027).
- [3] LEE, M. K., BARR, B. I. G., *An overview of the fatigue behaviour of plain and fibre reinforced concrete*, *Cement & Concrete Composites*, 26, (2004) 299–305.
- [4] KOLSTEIN, M. H. *Fatigue classification of welded joints in orthotropic steel bridge decks*. PhD Thesis. TU Delft, Delft University of Technology, 2007. ISBN 9789090219332.
- [5] EUROCODE, Comité Européen de Normalisation. *Eurocode 3: Design of steel structures - Part 1-1: General rules and rules for buildings*. 2011
- [6] HOBACHER, A. F. *The new IIV recommendations for fatigue assessment of welded joints and components—A comprehensive code recently updated*. 2009. *International Journal of Fatigue*, 31(1), 50-58.
- [7] HOBACHER, A. *Recommendations for Fatigue Design of Welded Joints and Components*. International Institute of Welding, doc. XIII-2151r4-07/XV-1254r4-07. Paris, France, October 2008
- [8] DILSIZ, G. *Levensduurverlenging van vermoeiingsgevoelige orthotrope stalen brugdekken met Engineered Cementitious Composite (ECC)*. 2013. MSc Thesis. TU Delft, Delft University of Technology.
- [9] NAAMAN, A. E. *Engineered steel fibers with optimal properties for reinforcement of cement composites*. 2003. *Journal of advanced concrete technology*, 1.3: 241-252.
- [10] LÖFGREN, I. *Fibre-reinforced Concrete for Industrial Construction—a fracture mechanics approach to material testing and structural analysis*. 2005. PhD Thesis. Chalmers University of Technology.
- [11] WILLE, K.; NAAMAN, A. E. *Fracture energy of UHPFRC under direct tensile loading*. 2010. In: FraMCoS-7 international conference, Jeju, Korea.
- [12] di PRISCO, M. *Fibre reinforced concrete*, 2012. Milano PowerPoint presentation,
- [13] BENCARDINO, F. et al. *Stress-strain behavior of steel fiber-reinforced concrete in compression*. 2008. *Journal of Materials in Civil Engineering*, 20.3: 255-263.
- [14] KESNER, K. E.; BILLINGTON, S. L.; DOUGLAS, K. S. *Cyclic response of highly ductile fiber-reinforced cement-based composites*. 2003 *ACI Materials Journal*, 100.5: 381-390.
- [15] WALTER, R., et al. *Cement based overlay for orthotropic steel bridge decks: A Multi-Scale Modeling Approach*. 2005. PhD Thesis. Technical University of Denmark. Danmarks Tekniske Universitet, Department of Structural Engineering and MaterialsInstitut for Bærende Konstruktioner og Materialer.



- [16] EUROCODE, Comité Européen de Normalisation. EN 14651: *Test method for metallic fibered concrete - Measuring the flexural tensile strength (limit of proportionality (LOP), residual)*. 2005
- [17] ABAQUS, V. 6.14 documentation. Dassault Systemes Simulia Corporation, 2014.
- [18] BEKAERT, J. VANTHOURNOUT, B. *Studie van verschillende types hoogperformante vezelversterkte betonoverlagingen voor bestaande dunne stalen rijvloeren*. Masterproef. Gent, Belgie, 2015.
- [19] PARK, S. H., KIM, D. J., RYU, G. S., & KOH, K. T. *Tensile behaviour of ultra-high performance hybrid fiber reinforced concrete*. 2012. *Cement and Concrete Composites*, 34(2), 172-184.
- [20] KANG, S. T., LEE, Y., PARK, Y. D., & KIM, J. K. *Tensile fracture properties of an Ultra High Performance Fiber Reinforced Concrete (UHPRFC) with steel fiber*. 2010. *Composite Structures*, 92(1), 61-71.
- [21] WILLE, K., NAAMAN, A. E., EL-TAWIL, S., & PARRA-MONTESINIS, G. J. *Ultra-high performance concrete and fiber reinforced concrete: achieving strength and ductility without heat curing*. 2012. *Materials and structures*, 45(3), 309-324.
- [22] CHEN, W-F. DUAN, L. (ed.). *Bridge Engineering Handbook: Construction and Maintenance*. 2014. CRC press,
- [23] DIENG, L., MARCHAND, P., GOMES, F., TESSIER, C., & TOUTLEMONDE, F. *Use of UHPRFC overlay to reduce stresses in orthotropic steel decks*. 2013. *Journal of Constructional Steel Research*, 89, 30-41.
- [24] YANG, J., FISHER, G. *Investigation of the fiber bridging stress-crack opening relationship of fiber reinforced cementitious composites*. 2006. In G. Fischer, & V. C. Li (Eds.), *International RILEM Workshop on High Performance Fiber Reinforced Cementitious Composites in Structural Applications* (pp. 93-105). RILEM Publications SARL.
- [25] XIAO, Z. G., YAMADA, K., YA, S., & ZHAO, X. L. *Stress analyses and fatigue evaluation of rib-to-deck joints in steel orthotropic decks*. 2008. *International Journal of Fatigue*, 30(8), 1387-1397.
- [26] WILLE, K., KIM, D. J., & NAAMAN, A. E. *Strain-hardening UHP-FRC with low fibre contents*. 2011. *Materials and structures*, 44(3), 583-598.
- [27] VANDEWALLE, L., et al. *RILEM TC 162-TDF: test and design methods for steel fibre reinforced concrete:  $\sigma$ - $\epsilon$  design method (final recommendation)*. 2003, *Materials and Structures*, 36.262: 560-567.
- [28] BUITELAAR, P., BRAAM, R., KAPTIJN, N. *Reinforced high performance concrete overlay system for rehabilitation and strengthening of orthotropic steel bridge decks*. 2004. In: *Orthotropic Bridge Conference, Sacramento, USA*. p. 384-401.
- [29] LI, V. C. *On engineered cementitious composites (ECC)*. 2003 *Journal of advanced concrete technology*, 2003, 1.3: 215-230.
- [30] WUEST, J., DENARIÉ E., and BRÜHWILER. E. *Model for predicting the UHPRFC tensile hardening response*. 2008. *Second International Symposium on Ultra High Performance Concrete*. No. MCS-CONF-2008-062. University of Kassel,

- [31] XIAO, Z. G.; YAMADA, K. *A method of determining geometric stress for fatigue strength evaluation of steel welded joints*. 2004. International Journal of Fatigue, 2004, 26.12: 1277-1293.
- [32] SPASOJEVIC, A., et al. *Influence of tensile properties of UHPFRC on size effect in bending*. 2008. In: Ultra High Performance Concrete (UHPC), Second International Symposium on Ultra High Performance Concrete. Ultra-High Performance Concrete (UHPC), Second International Symposium on Ultra High Performance Concrete, p. 303-310.
- [33] FINAZZI, S, et al. *Influence of bending test configuration on cracking behavior of FRC*. 2014. 3<sup>rd</sup> All-Russia (International) Conference on Concrete and Reinforced Concrete.
- [34] NOSHIRAVANI, T., BRÜHWILER, E. *Experimental investigation on reinforced ultra-high-performance fiber-reinforced concrete composite beams subjected to combined bending and shear*. 2013, ACI Structural Journal, 110.2: 251.
- [35] KIM, D. J., et al. *Comparative flexural behaviour of hybrid ultra-high performance fibre reinforced concrete with different macro fibres*. 2011, Construction and Building Materials, 25.11: 4144-4155.
- [36] NAAMAN, A. E.; REINHARDT, H. W. *Proposed classification of HPFRC composites based on their tensile response*. 2006, *Materials and structures*, 39.5: 547-555.
- [37] GRASSL, P., et al. *CDPM2: A damage-plasticity approach to modelling the failure of concrete*. 2013, International Journal of Solids and Structures, 50.24: 3805-3816.
- [38] SHAO, X., et al. *Basic performance of the composite deck system composed of orthotropic steel deck and ultrathin RPC layer*. 2011. Journal of Bridge Engineering, 18.5: 417-428.
- [39] BARNETT, S. J., et al. *Assessment of fibre orientation in ultra high performance fibre reinforced concrete and its effect on flexural strength*. *Materials and Structures*, 2010, 43.7: 1009-1023.
- [40] CEB-FIB - PREPARED BY SPECIAL ACTIVITY GROUP 5. *Fib model code for concrete structures 2010*. Berlin: Ernst, Wilhelm & Sohn, 2013. ISBN 9783433030615.

## List of Abbreviations

CMOD	Crack mouth opening displacement
CONTEC	Used concrete material for overlay
ECC	Engineered Cementitious Composites
E-modulus	Modulus of elasticity
FEA	Finite element analysis
FE	Finite element
FRC	Fibre Reinforced Concrete
FRD	Fibre Reinforced Densit
HPC	High Performance Concrete
HPFRCC	High Performance Fibre Reinforced Cement Composites
IIW	International Institute of Welding
LC	Load Case
LVDT	Linear Variable Differential Transformer
PC	Plain concrete
PVA	Poly-vinyl-alcohol
PAV360	Used concrete material for overlay
REFOR	Used concrete material for overlay
S1%	Volume of steel fibres
S1.6%	Volume of steel fibres
S3%	Volume of steel fibres
SCC	Self-compacting concrete
SLS	Service limit state
UHPRFC	Ultra-high performance fibre-reinforced concrete
ULS	Ultimate limit state

## List of Symbols

$\alpha_t$	Coefficient of the thermal expansion
$\sigma_{fu}$	Tensile strength of fibres
$\sigma_{mu}$	Tensile strength of cementitious matrix
$E_f$	Modulus of elasticity of fibres
$E_m$	Modulus of elasticity of cementitious matrix
$E_d$	Damaged modulus of elasticity of concrete
$E_0$	Initial modulus of elasticity of concrete
$V_f$	Volume of fibres in concrete mixture
$\sigma_{cc}$	Tensile strength limit
$\sigma_{pc}$	Post-crack stress
$E_{cc}$	Modulus of elasticity of concrete
$\varepsilon_{cc}$	Measured elongation (strain) of concrete
$f_t$	Ultimate Tensile strength of the cementitious matrix or concrete
$f_c$	Ultimate Compressive strength of the cementitious matrix or concrete
$G_f$	Fracture energy
$A_{lig}$	New crack area or fracture area
$F$	Force
$\delta$	Crack opening
$\delta_u$	Ultimate Crack opening
$G_{f,A}$	Fracture energy dissipated during strain hardening
$G_{f,B}$	Fracture energy dissipated during softening
$L_g$	Gauge length
$l$	Length
$\Delta l$	Measured elongation
$n$	Number of (micro) cracks
$w$	Stable crack width
$A$	Cross sectional area
$E_f A_f$	Centric stiffness of fibres in cracked cross section
$E_c A_c$	Centric stiffness of uncracked (concrete) cross section
$\sigma_{t,0}$	Failure stress in tension
$\sigma_{c,0}$	Initial yield
$\sigma_{cu}$	First crack in concrete
$d_t$	Damage parameter in tension
$d_c$	Damage parameter in compression
$f_{R,j}$	Residual flexural tensile strength
$F_j$	Load corresponding with CMOD
$l$	Span of tested specimen
$b$	Width of tested specimen
$h_{sp}$	Distance between the notch tip and the top of the specimen
$\varepsilon_{tot}$	Total strain of specimen
$\varepsilon$	Elastic strain

$w_{i1}$	Measured crack opening
$s_{rm}$	Distance between cracks
$y$	Height of the crack
$f_{L,k}$	Fictive flexural strength
$N$	Number of cycles
$\Delta\sigma$	Stress range
$t$	Thickness of investigated steel plate
$\sigma_{hs}$	Hot-spot stress
$\sigma_{0.5t}$	Stress in reference point
$\sigma_{1.5t}$	Stress in reference point
$A_{s,x}$	Total area of reinforcement in transversal direction
$A_{s,y}$	Total area of reinforcement in longitudinal direction
$S_{11}$	Stress in $X$ - direction
$PE_{11}$	Inelastic strain in $X$ - direction

## List of Figures

Figure 1: Main components of orthotropic steel bridge deck .....	12
Figure 2: Types of longitudinal ribs .....	13
Figure 3: Fatigue crack propagation in deck plate .....	15
Figure 4: Typical elliptical surface of fatigue cracks .....	15
Figure 5: Macro section of different to deck plated welds .....	16
Figure 6: Crack in through slice joint .....	16
Figure 7: Fatigue crack trough-crossbeam connection, (trough fitted between crossbeams) .....	17
Figure 8: Fatigue crack trough-crossbeam connection, (floating deck structure) ...	17
Figure 9: Fatigue crack trough-crossbeam connection, (with cut-outs) .....	17
Figure 10: De Jong's sketch of numerical model .....	19
Figure 11: Definition of the hot-spot method .....	20
Figure 12: Hot-spot types .....	20
Figure 13: Position of reference points .....	21
Figure 14: Paths for stress extrapolation at hot-spot.....	21
Figure 15: Dense reinforcement and badly compacted concrete .....	22
Figure 16: Shrinkage of overlay and edge detail .....	22
Figure 17: Difference between reinforced overlay and HPC overlay .....	23
Figure 18: Geometries of fibres used in concrete .....	24
Figure 19: Cross sectional area of fibres used in concrete .....	24
Figure 20: Cross sectional area of fibres used in concrete .....	24
Figure 21: Fibres vs cementitious matrix properties .....	25
Figure 22: Difference between strain hardening/softening of fibre reinforced material .....	26
Figure 23: Difference in cracked plain/fibre concrete .....	28
Figure 24: Definition of energy per unit volume $g_f$ and per unit area .....	29
Figure 25: Definition of fracture energy $G_f$ .....	29
Figure 26: Physical explanation of material behaviour .....	34
Figure 27: Experimental set-up for negative bending test .....	35
Figure 28: Placing of gage and picture of beam .....	35
Figure 29: Experimental results from composite beam tests .....	35
Figure 30: Tree point bending test and detail of CMOD measurement set up .....	36
Figure 31: Simplified model for ULS in uniaxial tension .....	38
Figure 32: Explanation of the calculation of strain .....	39
Figure 33: Cross section of studied bridge deck .....	40
Figure 34: Difference between single and double crossbeam model .....	41
Figure 35: Cross section of deck plate .....	41
Figure 36: Comparison of compressive behaviour .....	44
Figure 37: Boundary conditions of bridge deck model, view in X-axis .....	48
Figure 38: Boundary conditions of bridge deck model, view in Y-axis.....	48
Figure 39: Boundary condition of bridge deck model, view Z-axis.....	48
Figure 40: Load cases .....	49
Figure 41: Positions of load cases on deck plate.....	49
Figure 42: Different types of element in FE software ABAQUS/CAE .....	50

Figure 43: Various types of elements for solid geometry .....	51
Figure 44: Mesh properties of standard and overloaded model.....	51
Figure 45: Mesh properties of overloaded model .....	52
Figure 46: Axonometric view of meshed single crossbeam model.....	52
Figure 47: Axonometric view of meshed double crossbeam model.....	52
Figure 48: Stress $S_{11}$ in concrete overlay from 300 kN load case, 300 kN applied on it.....	66
Figure 49: Stress $S_{11}$ in concrete overlay from 300 kN load case, unloaded to 0 kN .....	66
Figure 50: Stress $S_{11}$ in concrete overlay from 300 kN load case, reloaded to 50 kN .....	66
Figure 51: Stress $S_{11}$ in concrete overlay from 350 kN load case, 350 kN applied on it.....	66
Figure 52: Stress $S_{11}$ in concrete overlay from 350kN load case, unloaded to 0 kN ....	66
Figure 53: Stress $S_{11}$ in concrete overlay from 350 kN load case, reloaded to 50 kN .....	67
Figure 54: Stress $S_{11}$ in concrete overlay from 400 kN load case, 400 kN applied on it.....	67
Figure 55: Stress $S_{11}$ in concrete overlay from 400 kN load case, unloaded to 0 kN.....	67
Figure 56: Stress $S_{11}$ in concrete overlay from 400 kN load case, reloaded to 50 kN .....	67
Figure 57: Inelastic strain $PE_{11}$ from 300 kN load case – 250 kN applied on it.....	67
Figure 58: Inelastic strain $PE_{11}$ from 300 kN load case – 300 kN applied on it.....	68
Figure 59: Inelastic strain $PE_{11}$ from 300 kN load case – unloaded to 0 kN.....	68
Figure 60: Inelastic strain $PE_{11}$ from 300 kN load case – reloaded to 50 kN.....	68
Figure 61: Inelastic strain $PE_{11}$ from 350 kN load case – 350 kN applied on it.....	68
Figure 62: Inelastic strain $PE_{11}$ from 400 kN load case – 400 kN applied on it.....	68
Figure 63: Initial calculated value of inelastic strain $PE_{11}$ .....	71
Figure 64: Last calculated value of inelastic strain $PE_{11}$ .....	71
Figure 65: Equivalent stress $S_{11}$ distribution for last inelastic strain .....	71
Figure 66: Dimensions of simplified numerical model.....	72
Figure 67: Boundary condition of simplified numerical model .....	72
Figure 68: Mesh properties of simplified model .....	72

## List of Graphs

Graph 1: Fatigue strength curves for direct stress ranges .....	14
Graph 2: Effective stress and residual stress applied on structure .....	14
Graph 3: Comparison of stress in X-direction .....	19
Graph 4: Difference in material response to tensile load with steel fibres .....	27
Graph 5: Difference in stress-strain curve for plain and fibre concrete .....	30
Graph 6: Monotonic and cyclic response of UHPFRC .....	30
Graph 7: Comparison of monotone, cyclic and reference stress-strain curve.....	31
Graph 8: Calculation of damaged modulus of elasticity $E_d$ .....	32
Graph 9: Relationship between residual stiffness and compressive stress .....	32
Graph 10: Comparison of monotone, cyclic and semi-cyclic test.....	33
Graph 11: One complete cyclic of cyclic loading .....	33
Graph 12: CMOD test output with marked important points .....	37
Graph 13: Transformation from f- to constitutive law .....	38
Graph 14: Inelastic behaviour of reinforcement steel .....	42
Graph 15: Response of concrete in uniaxial compression .....	43
Graph 16: Comparison of inelastic compressive behaviour .....	45
Graph 17: Response of concrete to uniaxial tension .....	45
Graph 18: Difference of inelastic tensile behaviour .....	46
Graph 19: Material behaviour of modified REFOR material.....	46
Graph 20: Uniaxial cyclic response of concrete .....	47
Graph 21: Loading scheme for overloaded model .....	50
Graph 22: Stress $S_{11}$ on underside of steel deck plate.....	53
Graph 23: Stress $S_{11}$ on inner side of rib wall .....	54
Graph 24: Extrapolated stress $S_{11}$ from steel deck plate without overlay.....	55
Graph 25: Extrapolated stress $S_{11}$ on inner side of steel rib wall without overlay...	55
Graph 26: Extrapolated stress $S_{11}$ from steel deck plate with PAV360 overlay.....	55
Graph 27: Extrapolated stress $S_{11}$ on inner side of steel rib wall with PAV360 overlay .....	56
Graph 28: Extrapolated stress $S_{11}$ from steel deck plate with CONTEC overlay.....	56
Graph 29: Extrapolated stress $S_{11}$ on inner side of steel rib wall with CONTEC overlay .....	56
Graph 30: Extrapolated stress $S_{11}$ from steel deck plate with REFOR overlay.....	57
Graph 31: Extrapolated stress $S_{11}$ on inner side of steel rib wall with REFOR overlay .....	57
Graph 32: Comparison of extrapolated stress $S_{11}$ from underside steel deck plate .....	57
Graph 33: Extrapolated stress $S_{11}$ on inner side of steel rib wall with concrete overlay .....	58
Graph 34: Stress $S_{11}$ on underside of steel deck plate.....	58
Graph 35: Stress $S_{11}$ on underside of steel deck plate.....	59
Graph 36: Extrapolated stress $S_{11}$ on steel deck plate at X = 750 mm without overlay .....	60
Graph 37: Extrapolated stress $S_{11}$ on steel deck plate at X = 755 mm without overlay .....	60



Graph 38: Extrapolated stress $S_{11}$ from inner side of rib wall at $X = 0$ mm without overlay .....	61
Graph 39: Extrapolated stress $S_{11}$ on steel deck plate at $X = 750$ mm with PAV360 overlay .....	61
Graph 40: Extrapolated stress $S_{11}$ on steel deck plate at $X = 755$ mm with PAV360 overlay .....	61
Graph 41: Extrapolated stress $S_{11}$ from inner side of rib wall at $X = 0$ mm with PAV360 overlay.....	62
Graph 42: Extrapolated stress $S_{11}$ on steel deck plate at $X = 750$ mm with CONTEC overlay .....	62
Graph 43: Extrapolated stress $S_{11}$ on steel deck plate at $X = 755$ mm with CONTEC overlay .....	62
Graph 44: Extrapolated stress $S_{11}$ from inner side of rib wall at $X = 0$ mm with CONTEC overlay .....	63
Graph 45: Extrapolated stress $S_{11}$ on steel deck plate at $X = 750$ mm with REFOR overlay .....	63
Graph 46: Extrapolated stress $S_{11}$ on steel deck plate at $X = 755$ mm with REFOR overlay .....	63
Graph 47: Extrapolated stress $S_{11}$ from inner side of rib wall at $X = 0$ mm with REFOR overlay .....	64
Graph 48: Comparison of extrapolated stress $S_{11}$ on steel deck plate at $X = 750$ mm .....	64
Graph 49: Comparison of extrapolated stress $S_{11}$ on steel deck plate at $X = 755$ mm .....	64
Graph 50: Comparison of extrapolated stress $S_{11}$ from inner side of rib wall at $X = 0$ mm .....	65
Graph 51: Comparison of stress $S_{11}$ along the height.....	69
Graph 52: Stress $S_{11}$ along the height – 400 kN applied .....	69
Graph 53: Difference of calculated stress for initial 50 kN and reloaded to 50 kN ..	70
Graph 54: Residual stress in top thread of steel deck plate.....	70
Graph 55: Calculated $PE_{11}$ on hardening branch of material stress-strain curve ....	70
Graph 56: Material inputs for cases loaded with 100 kN.....	73
Graph 57: Material inputs for cases loaded with 95 kN.....	73
Graph 58: Material inputs for cases loaded with 75 kN.....	73
Graph 59: Material input in cases loaded with 45 kN .....	74

## List of Tables

Table 1: Separation of load cycles applied on structure .....	13
Table 2: Renovation techniques .....	18
Table 3: Comparison of different materials used for fibres in concrete mixture ...	25
Table 4: Classification of fibre reinforced concrete based on volume of fibres .....	26
Table 5: Linear elastic behaviour of used materials .....	42
Table 6: Linear elastic material properties of used concrete .....	42
Table 7: Abaqus input files of compressive behaviour .....	44
Table 8: Abaqus input values of tensile behaviour .....	46
Table 9: Input values of modified REFOR material .....	46
Table 10: Results of parameter study .....	74

# CURRICULUM VITAE

## Personal information:

---

Name and Surname: Bc. Petr Miarka  
Address: Ostravska 70, Cesky Tesin, 737 01  
Date of birth: 24. 7. 1991  
E-mail: p.miarka11@gmail.com  
Cell phone number: +420 737 651 041



## Education:

---

September 2014 – February 2017: Brno University of Technology, Faculty of Civil Engineering

Master's program Civil engineering – Building constructions

Specialization: Structural mechanics

Theme of Master's thesis: Numerical study of thin HPC overlays for orthotropic deck plates

Supervisor: doc. Ing. Stanislav Seitel, Ph.D.

Aim of thesis: Analysis of welded joints on orthotropic steel bridge. The aim thesis was to reduce fatigue stress by applying concrete overlay on the top of the deck plate (defence of thesis partly written on ERASMUS+ programme).

September 2015 – June 2016: Ghent University, Belgium

Exchange study stay on ERASMUS+ program,

Writing process: Numerical study of thin HPC overlays for orthotropic deck plates

Supervisors: prof. dr. ir. Wouter De Corte a dr. ir. Arne Jansseune

Aim of thesis: Analysis of welded joints on orthotropic steel bridge. The aim thesis was to reduce fatigue stress by applying concrete overlay on the top of the deck plate in FEM software Abaqus.

September 2010 – June 2014: Brno University of Technology, Faculty of Civil Engineering

Bachelor's program Civil engineering – Building constructions

Specialization: Structural design of concrete structures

Theme of Bachelor's thesis: Reinforced concrete staircase of apartment house - alternatives of structural design with reduction of footfall sound propagation

Supervisor: Ing. Jan Perla

Aim of thesis: Design of staircases in three variation with focus on fabricated structural element which reduces footfall sound propagation in apartment building.

September 2006 - June 2010: Secondary school of Civil Engineering, Havirov

## Work experiences:

---

June 2016 – September 2016

Summer job in company DNADESIGN s.r.o. Execution of concrete staircases (manufacturing and reinforcing form, concrete embedment). Participation on meetings with clients.

### June 2015 – September 2015

Internship in company KPstatika stavby s.r.o. Preparations of construction drawings of steel, timber and concrete structures. Preparation of method for building reconstruction. Participation meetings with clients.

### November 2014 – January 2015

Firesta Brno, preparation of drawing of steel constructions.

## Other knowledge and experiences:

---

### Participation on competitions in field of civil engineering:

Summer semester 2014 – 4<sup>th</sup> place in University's round of EBEC

Summer semester 2013 – 3<sup>rd</sup> place in Faculty's round of EBEC

Participation on SVOČ with bachelor's thesis

### Leisure time activities:

In my free time I am helping in International student club at Brno University of Technology. We help foreign student who came to BUT for internship or exchange study stay with their leisure time activities.

### Language knowledge:

English - B2 - level,

Polish – beginner

Russian – beginner

### Software knowledge:

MS Office (Word, Excel, PowerPoint), Adobe Photoshop, Autodesk Autocad,

Dlubal – RFEM 5.0: FEM software modelling and design according EUROCODES

Nemetschek – Scia: FEM software modelling and design according EUROCODES

Simulia ABAQUS: software for advance FE modelling and design

### Driving licence:

Group B since December 2009

### Soft skills:

I am open minded, friendly person who likes to learn new things every day. I am also hardworking, but I need to receive feedback, so I can learn from my mistakes.

### Hobbies:

Books, cooking, listening to music

Brno 12. 1. 2017

Petr Miarka

## Author's Publications

MIARKA, P., *NUMERICAL STUDY OF THIN HIGH PERFORMANCE CONCRETE OVERLAYS FOR ORTHOTROPIC DECK PLATES*, contribution on Juniorstav 2017 conference, Brno, 2017

Petr Miarka, *Železobetonové schodiště v bytovém domu - varianty konstrukčního řešení s přerušením šíření kročejového hluku*. Brno, 2014. 42 s., 124 s. příl. Bakalářská práce. Vysoké učení technické v Brně, Fakulta stavební, Ústav betonových a zděných konstrukcí. Vedoucí práce Ing. Jan Perla.